Investigations on Sulfated Zirconia Model Systems: from Nanocrystalline Thin Films to Rational Design of Powder Catalysts

Inaugural-Dissertation
to obtain the academic degree
Doctor rerum naturalium (Dr. rer. nat.)

submitted to the Department of Biology, Chemistry and Pharmacy
of Freie Universität Berlin

by

Rhys W. Lloyd
from Bristol

March, 2008

Acknowledgements

I would like to express my gratitude to Prof. Robert Schlögl for his guidance and the opportunity to work on such an interesting project within the department of Inorganic Chemistry at the Fritz Haber Institute. The assessment of this thesis by the Freie Universität Berlin is gratefully acknowledged, in particular the time and effort given by the chair, Prof. Klaus Christmann, and committee members of my doctorial board is appreciated. I would, also, like to thank my supervisors, Dr. Friederike Jentoft and Dr. Wolfgang Ranke, for their advice and assistance. During my time in Berlin I have learnt a great deal from their enlightening teaching.

My sincere thanks to all the members of the department of Inorganic Chemistry, especially those of my group: Functional Characterisation, for creating a friendly atmosphere and an enjoyable place in which to work. I am indebted to all the members of the department that have aided me with my research, including:

- Pradnya Joshi, for assisting with the planning and synthesis of the rationally designed powder sulfated zirconia samples.
- Achim Klein-Hoffmann, for preparing cross sections of the thin films, and Dr. Thomas Hansen and Hermann Sauer, for investigating the cross sections using transmission electron microscopy.
- Gisela Weinberg, for analysing numerous thin film samples via scanning electron microscopy and her valued interpretation of the results.
- The members of the Surface Analysis group, especially Dr. Elaine Vass and Dr. Michael Hävecker, for their help measuring and analysing the data obtained at the Berliner Elektronenspeicherring - Gesellschaft für Synchrotronstrahlung.
- Bernd Steinhauer, for his assistance performing the thermal desorption studies on the thin films.
- Manfred Swoboda, Abed Taha and the Mechanical Workshop of the Fritz Haber Institute for their help designing and the construct of the thin film reactor.
- Edith Kitzelmann and Ming-Hong Looi for performing X-ray diffraction on powder samples and Dr. Frank Girgsdies for fitting the diffractograms.
- Dr. Andreas Furche, for running thermal analyses of the powder samples.

- Gisela Lorenz, for measuring the surface areas of the powder samples.
- Ute Wild, for performing X-ray photoelectron spectroscopy on powder samples.
- Dr. Kristina Chakarova, for measurements performed on the powder samples using diffuse reflectance infra-red Fourier transform spectroscopy.
- Jutta Kröhnert, for constructing a reactor on which the catalytic activity of the powder catalysts could be measured and her general help with technical difficulties.
- Dr. Sabine Wrabetz, for discussion of and providing the powder calorimetry data.

In addition, I would like to thank Prof. F. Aldinger's department at the Max Planck Institute for Metals Research, Stuttgart, for kindly providing the surfactant for forming the self-assembled monolayer and Wacker Siltronic AG for donation of the silicon wafers (100, p-type) used to produce the thin films.

The project funding of this doctorial study as part of the DFG priory program (SPP) 1091 ‘‘Bridging the Pressure and Material Gap in Heterogeneous Catalysis’’, individual project Je 267/1, is gratefully acknowledged. Discussions and input from the fellow members of this priory program; Prof. H. Papp and Dr. C. Breitkopf from the Universität Leipzig; Prof. J. A. Lercher, Dr. R. Olindo and X. Li from the Technische Universität München; Prof. W. Widdra, Dr. K. Meinel and Dr. K.-M. Schindler from the Martin-Luther-University Halle-Wittenberg; Prof. J. Sauer and Dr. A. Hofmann from the Humboldt-Universität zu Berlin; are highly appreciated.

Personal financial support and development programs from the International Max Planck Research School are also gratefully acknowledged.

Furthermore, I would like to thank my friends and family who have encouraged and supported me throughout my studies.

Abstract

Model systems of the alkane skeletal isomerisation catalyst sulfated zirconia were successfully produced via a range of different preparation techniques. The model systems were investigated with various techniques, including thermal desorption, photoelectron, X-ray absorption and IR spectroscopies. Electrically and thermally conducting thin films of sulfated zirconia were prepared on oxidised silicon wafers, in order to allow the application of surface science techniques. Thermal treatment of the films was optimised to chemically mimic the powder process, resulting in films possessing the essential features (including tetragonal phase, nanocrystallinity and sulfur content of ~3 atomic %) of active powder catalysts.

Two distinctly different chemisorption sites were detected on the sulfated zirconia thin films by both ammonia and *n*-butane adsorption studies. Strongly chemisorbed ammonia reacts with certain sulfate species leading to the evolution of SO_2 above 473 K. Low temperature (300-100 K) *n*-butane adsorption-desorption equilibrium isobaric measurements showed adsorption to be promoted over the sulfated zirconia thin films, as compared with oxidised silicon wafers. Strong and weak *n*-butane chemisorption, releasing heats of between 59-40 and 47-34 kJ/mol, corresponds to 5 and 25% of a monolayer coverage, respectively. The total amount of chemisorbed *n*-butane coincides very well with the estimated number of surface sulfate groups. An increase in adsorption heat was observed between coverages of ~5-8% of a monolayer, indicating adsorbate-adsorbate interactions. A bimolecular isomerisation mechanism is thus considered plausible under such coverages. Physisorption on the films generates heats of ~28 kJ/mol, for coverages from 30% up to a complete monolayer. Multilayer adsorption results in the formation of an electrically insulating adsorbate structure.

Carbonaceous deposits were detected on the films after exposure to *n*-butane under reactive conditions (≥ 481 K), thus proving the films have reactive centres. Analysis has shown the deposits to contain unsaturated hydrocarbons, which have a π* resonance typical of butenes; furthermore, sulfate groups are reduced during exposure, thus proving the oxidative dehydrogenating ability of sulfated zirconia. The deposits are also shown to be oxygenated, thus are consistent with the stabilised form of the reactive carbocation intermediates.

Powder sulfated zirconia catalysts were prepared from sulfating agents containing one and two pregrouped sulfur atoms, via a variety of different methods using various sulfur loadings, to test whether disulfate groups are responsible for the catalytic activity of the material. Sulfated zirconias synthesised from two pregrouped sulfur atoms were however found to be less active. Nevertheless, the presence of disulfate groups was found to be a prerequisite for catalytic activity and for materials prepared using the same sulfation method the more active were shown to have higher disulfate concentrations.

It is thus proposed that the more strongly chemisorbing sites, which react with ammonia, correspond to a minority disulfate species. These disulfate sites may oxidatively dehydrogenate *n*-butane, initiating the formation of catalytically active isomerisation centres. The chemical environment of these disulfate groups is envisioned to strongly influence the catalytic reactivity of the active sites they generate.

Zusammenfassung

Um sulfatiertes Zirconiumdioxid, das als Katalysator für die Skelettisomerisierung von Alkanen dient, besser untersuchen zu können, wurden mittels verschiedener Präparationstechniken erfolgreich Modellsysteme hergestellt. Diese wurden u.a. mit thermischer Desorptions-, Photoelektronen-, Röntgenabsorptions- und IR-Spektroskopie analysiert. Dünne elektrisch und thermisch leitfähige Schichten aus sulfatiertem Zirconiumdioxid wurden auf Siliziumscheiben aufgebracht, um Oberflächencharakterisierungsmethoden anwenden zu können. Die thermische Behandlung der Filme wurde so optimiert, daß sie weitgehend der Pulverpräparation entspricht. Dabei entstehen Schichten, die die wesentlichen Merkmale von aktiven Pulverkatalysatoren aufweisen (nanokristalline tetragonale Phase, ~ 3 Atom% S).
Durch Adsorptionsversuche mit Ammoniak und *n*-Butan wurden zwei sich deutlich unterscheidende Bindungsstellen für chemisorbierte Spezies auf den dünnen Filmen entdeckt. Stark chemisorbiertes Ammoniak reagiert mit bestimmten Sulfatspezies, und oberhalb von 473 K wird SO_2 gebildet. Tieftemperaturisobarenmessungen (300-100 K) zeigen stärkere Adsorption von *n*-Butan an dünnen sulfatierten Zirconiumdioxidfilmen als am Siliziumträger. Starke Chemisorption mit einer Adsorptionswärme von 57- 40 kJ/ mol bzw. schwache Chemisorption mit 47- 34 kJ/ mol erfolgt bis zu einem Bedeckungsgrad von 5 bzw. 25% einer Monolage. Die Gesamtmenge des chemisorbierten *n*-Butans entspricht der geschätzten Anzahl von Oberflächensulfatgruppen. Die Adsorptionswärme steigt bei Bedeckungsgraden von ~5-8%, was auf Adsorbat-Adsorbat-Wechselwirkungen hindeutet. Ein bimolekularer Isomerisierungsmechanismus erscheint für derartige Bedeckungsgrade plausibel. Für Bedeckungsgrade von 30% bis zu einer Monolage liefert die Physisorption Adsorptionswärmen von 25 kJ/ mol. Multischichtenadsorption führt zur Bildung einer elektrisch isolierenden Adsorbatstruktur.
Kohlenstoffhaltige Ablagerungen nach Kontakt mit *n*-Butan unter Reaktionsbedingungen (≥ 481 K) beweisen, dass die Filme über reaktive Zentren verfügen. Ungesättigte Kohlenwasserstoffe mit einer π*-Resonanz typisch für Butene sowie die Reduktion von von Oberflächensulfatgruppen belegen die Fähigkeit von sulfatiertem Zirconiumdioxid zur oxidativen Dehydrierung. Sauerstoff-Kohlenstoff-Bindungen sind ein Hinweis auf die Stabilisierung von reaktiven Carbokationenintermediaten durch die Katalysatoroberfläche.
Pulverförmiges sulfatiertes Zirconiumdioxid mit unterschiedlichen Schwefelkonzentrationen wurde nach drei Verfahren präpariert. Hierzu wurden Reagenzien mit ein oder zwei Schwefelatomen verwendet, um zu testen ob die als aktive Zentren vermuteten Disulfatgruppen gezielt hergestellt werden können. Materialien, die aus Vorstufen mit zwei Schwefelatomen hergestellt wurden, waren weniger aktiv. Das Vorhandensein von Disulfatgruppen ist Voraussetzung für katalytische Aktivität. Katalysatoren, welche nach der gleichen Synthesemethode hergestellt wurden, weisen höhere Aktivität bei höherer Disulfatkonzentration auf.
Stärker chemisorbierende Bindungszentren stellen eine Minderheit der Oberflächendisulfatgruppen dar. Diese können *n*-Butan oxidativ dehydrieren, und es bilden sich katalytisch aktive Intermediate. Die chemische Umgebung der Disulfatgruppen hat starken Einfluss auf ihre Reaktivität.

Contents

Abbreviations

θ	Coverage
λ_e	Electron mean free path
A-D	Adsorption-desorption
AFM	Atomic force microscopy
BE	Binding energy
DFT	Density-functional theory
DRIFT(S)	Diffuse reflectance infrared Fourier transform (spectroscopy)
DSC	Differential scanning calorimetry
EDX	Energy dispersive X-ray
FT	Fourier transform
FWHM	Full width at half maximum
l_e	Electron escape depth
LOD	Limit of detection
LOQ	Limit of quantification
MS	Mass spectrometry
m/z	Mass to charge ratio
n.d.	Not detected
NEXAFS	Near edge X-ray absorption fine structure
norm.	Normalised
PE	Photoemission
PSZ	Ammonium peroxydisulfated loaded zirconia
RI	Ring current
rt	Room temperature
SAM	Self assembled monolayer
SEM	Scanning electron microscopy
SZ	Sulfated zirconia
SZ_{com}	Sulfated zirconia prepared from a commercial precursor
SZ_{ev}	Sulfated zirconia prepared by the evaporation technique
SZ_{im}	Sulfated zirconia prepared by the immersion technique

SZ_{iw}	Sulfated zirconia prepared by the incipient wetness technique
T	Temperature
TAP	Temporal analysis of products
TDS	Thermal desorption spectroscopy
(HR)TEM	(High resolution) transmission electron microscopy
TG	Thermogravimetry
TPD	Temperature programmed desorption
TSZ	Ammonium thiosulfate loaded zirconia
UHV	Ultra high vacuum
UP(S)	Ultraviolet photoelectron (spectroscopy)
wt.%	Weight percent
XP(S)	X-ray photoelectron (spectroscopy)
XRD	X-ray diffraction
Z_{com}	Zirconia prepared from a commercial zirconium hydroxide

1. Introduction

1.1 Catalytic Isomerisation of Alkanes

Hydrocarbon isomerisation is widely applied industrially for the production of both fuels and petrochemicals.[1] Skeletal isomerisation of straight chain alkanes increases their octane number and hence, also, their commercial value. Octane ratings are indicative of the antiknock quality of a given fuel or component. The tightened regulation of petrol over the past two decades, especially the elimination of tetraethyl lead as well as legislation restricting both benzene and sulfur content, has resulted in the increased importance of branched light alkanes for the production of clean-burning, high performance fuels.

Alkane isomerisation is an equilibrium limited reaction, with the more highly branched isomers generally favoured at lower temperatures. The thermodynamic equilibrium position for the butane skeletal isomers is shown in Figure 1-1.[2]

Traditionally alkane isomerisation was catalysed by strong liquid acids; HF/SbF_5, RSO_3H/SbF_5, CF_3SO_3H and HSO_3F are all active homogeneous isomerisation catalysts.[3] Homogeneous catalysts, however, suffer the following disadvantages: the corrosive nature of the catalysts gives rise to acidic and salty waste waters which cause handling and disposal problems, it can be difficult to separate the catalyst from the product and homogeneous processes often use stoichiometric amounts of catalysts as they are not as selective;[4] thus they are not desirable for large scale chemical processes.

The need for environmentally friendly production within the chemical industry is universally acknowledged, thus the use of heterogeneous catalysts (which have the potential to be recycled and avoid the aforementioned disadvantages) are an attractive alternative.[5,6]

Chlorided alumina based catalysts currently have the highest isomerisation activity and yield available.[7,8] However, they need a constant organic chloride co-feed, they cannot be regenerated and are sensitive to contaminants such as water, carbon oxides and oxygenates. Zeolitic isomerisation catalysts are able to be regenerated and relatively contaminant tolerant. Although, zeolitic catalysts are only active at much higher temperatures than chlorided alumina catalysts, thus the maximum conversion is limited by the unfavourable equilibrium position. Yields are also lower for the zeolitic catalysts

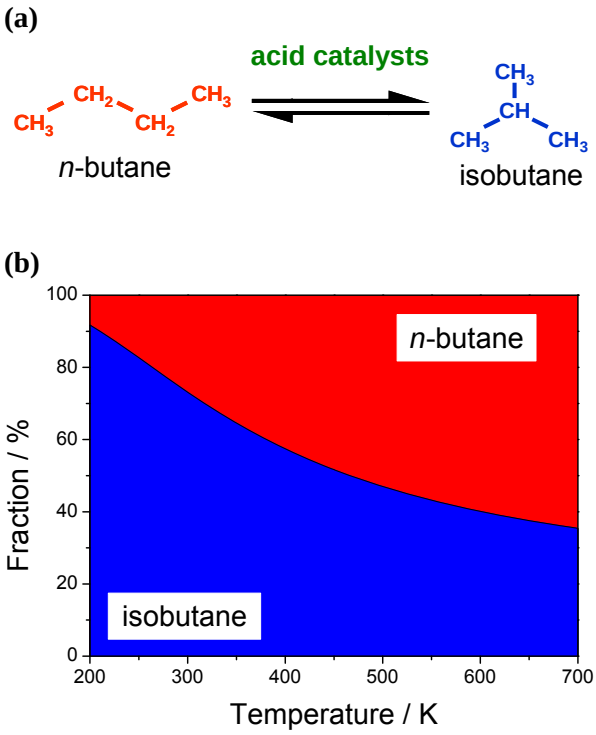

Figure 1-1: (a) Chemical equation for the conversion of *n*-butane to isobutane over acid catalysts. (b) Equilibrium position for *n*-butane/isobutane isomers as a function of temperature (temperature dependence of the reaction enthalpy was neglected).[2]

than the chlorided alumina catalysts as they are less selective. The development of sulfated zirconia based catalysts, such as the Par-Isom™ process from UOP,[9] offer a promising alternative to the aforementioned catalysts (see Figure 1-2a). Sulfated zirconia based catalysts are active at lower temperatures than zeolitic catalysts (thus under more favourable equilibrium conditions); they are also water tolerant, can be regenerated and do not require a chlorided co-feed or caustic scrubbing unlike the chlorided alumina catalyst. In 2002 UOP had licensed 8 Par-Isom™ units worldwide utilizing sulfated zirconia based catalysts.[10] The latest commercial isomerisation catalyst from UOP, the PI-242™, has a performance near to that of the standard industrial chlorided-alumina based process but with the aforementioned advantages of a sulfated zirconia based process.[9] The relative stability of the PI-242™ thus makes initial start up costs for operating a plant much lower than if a chlorided-alumina based process was used. The PI-242™ is thus economically viable industrially as low cost isomerisation catalysts (see Figure 1-2b).

1.2 Sulfated Zirconia

The first reported discovery of sulfated zirconia (SZ) was in 1962 by Holm and Bailey,[11] who found platinum doped sulfated zirconia to be an active isomerisation catalyst. However, it was not until Hino and Arata reported in 1979 and 1980 the isomerisation of *n*-butane at room temperature using sulfated zirconia that an interest by the wider scientific community was initiated.[12,13] Hino and Arata described sulfated zirconia to be

(a)

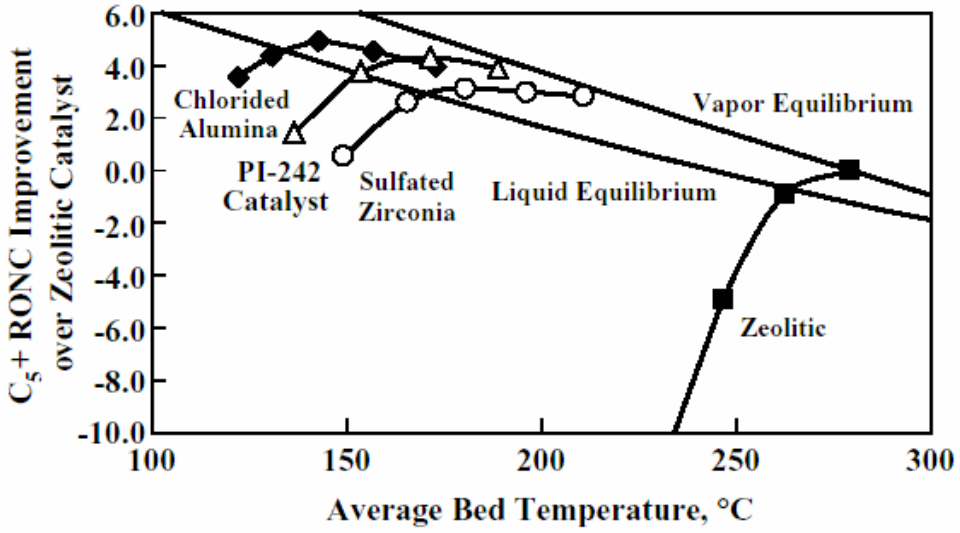

(b)

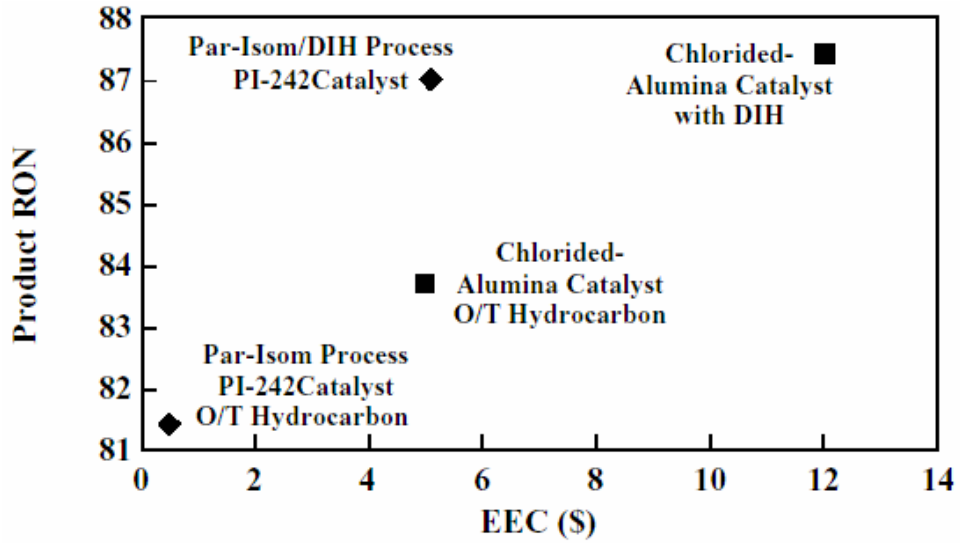

Figure 1-2 (a) Relative product octane comparison (RONC) to a zeolitic catalyst vs. temperature, based on pilot plant testing using a feed typical of commercial operating conditions. (b) Equipment erection cost (EEC) for a new plant vs. product relative octane number (RON). Hydrocarbon once through (O/T) and recycle design using a de-isohexanizer column (DIH) compared.[9]

superacidic (more acidic than 100% H_2SO_4) based on its ability to isomerise *n*-butane at low temperatures and acidity measurements using Hammett indicators.

Sulfated zirconia can be considered as zirconium dioxide (zirconia) doped with sulfate. Various optimum sulfur contents have been reported, including: 170 μg/m^2 (3 S atoms/nm),[14] 1-2 weight (wt.)% S,[15] or 2.6 wt.% S.[16] Zirconia occurs in three main polymorphs: monoclinic, tetragonal and cubic. The room temperature stable monoclinic phase transforms into the tetragonal phase at 1443 K, which transforms into the cubic

phase at 2643 K.[17] The metastable tetragonal and cubic phases can be stabilised at room temperature by the addition of various dopants (including sulfate)[18] and also crystallite size effects (by < 30 nm sized crystals).[19-22] Cubic and tetragonal sulfated zirconias are active isomerisation catalysts, whereas monoclinic sulfated zirconia has been reported to be inactive,[23] or 4-5 times less active than tetragonal zirconia.[24] For mixed monoclinic-tetragonal phase materials the isomerisation conversion has been shown to be proportional to the fraction of the tetragonal phase, thus indicating the activity of the monoclinic phase to be insignificant by comparison.[25,26] However, the zirconia phase is not the only prerequisite for an active catalyst, many other factors are involved.[27]

1.2.1 Preparation

There are many different methods to prepare sulfated zirconia, the majority of these routes can be generalised as follows:[28] (1) Precipitation via hydrolysis of zirconium salt solutions followed by sulfation. Typical salts used are $ZrOCl_2$ or $ZrO(NO_3)_2$ and possible sulfation agents include H_2SO_4, $(NH_4)_2SO_4$ and $(NH_4)_2S_2O_8$ (2) Sol-gel synthesis from organometallic zirconium compounds. Sulfuric acid can be used both as the sulfating agent and to initiate the gelation. (3) Thermal decomposition of zirconium sulfate.

Besides these main preparation routes, various uncommon methods have been reported and reviewed by Afanasiev *et al.*.[29] Sulfated zirconium hydroxides are also commercially available from suppliers such as MEL chemicals[30] and Sigma-Aldrich.[31]

Normally sulfation is followed by calcination to produce a crystalline oxide. Initially it was believed that only sulfation prior to calcination results in highly active catalytic materials;[12] however, recently sulfation of crystalline zirconia has been shown to produce active materials.[26] The preparation route is extremely important in the determination of physical properties of the produced sulfated zirconia, such as its surface area; which is inherently related to catalytic activity.[16,32]

Doping of sulfated zirconia with various main group metals (such as Al[33] and Ga[34]) and transition metals (such as Pt,[35] Mn and Fe[36]) has been shown to promote the isomerisation activity of the catalyst. How these materials participate in the alkane isomerisation is a subject of much debate and hence they are considered beyond the scope of this thesis.

1.2.2 Acidic properties

Sulfated zirconia catalysts were initially believed to be superacidic due to their ability to isomerise *n*-butane even at room temperature (which is normally only possible by liquid superacids) and acidity measurements using Hammett indicators.[12,13] There are, however, a number of drawbacks regarding the indicator technique including the assumptions that equilibrium is achieved, the active site is an isolated acid and the end point has been detected.

Direct correlations between the catalytic activities of sulfated zirconia and its acidity are not consistent across the literature.[37] The techniques used to evaluate the acidity of sulfated zirconia often suffer from experimental problems, such as reaction rather than desorption during temperature programmed methods. More recent investigations have revealed the acidity of sulfated zirconia not to be stronger than that of sulfuric acid using NMR[38], UV-Vis[39] and IR spectroscopies[40] or theoretical calculations.[41]

Investigations into the type of sites have been made using numerous probes including pyridine and carbon monoxide; although to date no consistent theories have emerged to link the catalytic activity of sulfated zirconia to either its Brønsted or Lewis acidic sites. Characterisation of solid acid-base catalysts remains a challenge as the determination of acid sites depends on the choice of appropriate probe molecules.

1.2.3 Sulfate structure

It has been shown that only the presence of sulfur in the oxidation state +6 results in active metal oxide isomerisation catalysts.[42-45] Normally it is assumed that the sulfate is located at the surface of the zirconia crystals, there is however no proof that this applies to all of the sulfur present.[46]

Numerous sulfate structures have been published, the majority of which are proposed with the presence of strong Brønsted or Lewis acid sites in mind.[46] Structural models have been published with the sulfate connecting to zirconia via three oxygen bridges (tridentate),[47,48] two oxygen bridges (bidentate) either chelating to one[49-51] or bridging two Zr cations[52-54] (Figure 1-3) and even via one oxygen bridge (monodentate) corresponding to adsorbed SO_3.[55] At high coverage the detection of tetradentate disulfate (pyrosulfate, $S_2O_7^{2-}$)[56] species has also been reported.[47,57] Unless sulfated zirconia is completely dehydrated, hydrated sulfate states will be present;[40] hydroxyl groups may be

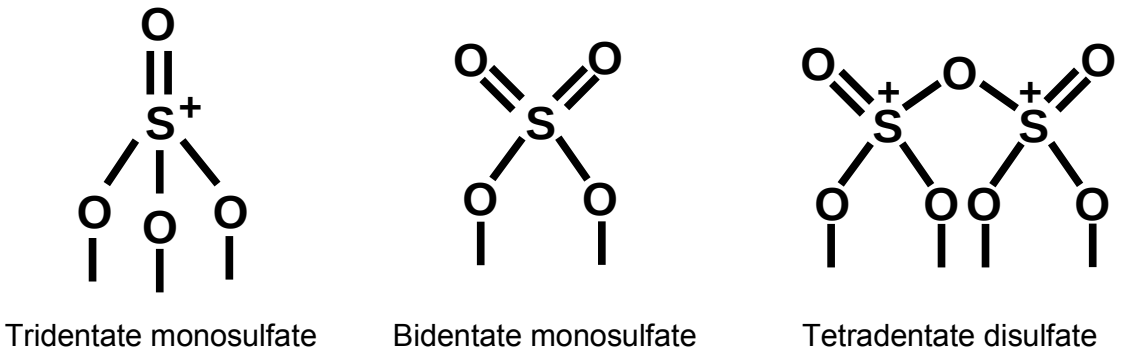

Figure 1-3: Proposed dehydrated sulfate structures.

attached to either S or Zr,[40,58-60] or bridging S and Zr.[32,61] From the large number of models proposed it can be assumed that there is no single sulfate structure but a number of different coexisting interchangeable species, which depend on various conditions such as the coverage, degree of hydration, pretreatment and measurement atmosphere.

Recent experimental and theoretical findings[62,63] have shown that active catalysts possess an IR band at ~1404 cm^{-1}, which is ascribed to the S=O bond stretching vibrations in disulfate or adsorbed SO_3 molecules.

1.2.4 Catalytic properties

Prior to reaction, sulfated zirconia must be activated in order to remove excess water from the material. The catalyst should not, however, be completely dehydrated. Decreasing the water content has been shown to result in a decrease in Brønsted acidity and an increase in Lewis acidity.[64] Various optimal activation temperatures have been reported including: 523-573 K,[64] 573 K,[65] 590 K,[66] 673 K,[67,65] 723 K,[68] and 923 K.[69] The range of temperatures may be due to the differing materials; however, other conditions such as the gas atmosphere, holding time, flow and heating rates may have an influence.

The catalytic performance of sulfated zirconia for the isomerisation of alkanes has typically one of two different profiles depending on the conditions: (a) an induction period followed by a slow deactivation or, usually at higher initial conversions, (b) a shorter induction period, followed by a rapid initial deactivation, then a slow deactivation. During the initiation period active sites are formed on the catalyst, hence the activated catalyst can be considered as a "precatalyst" which transforms into the active species only upon exposure to the reactant. This indicates the importance of investigating

the interaction between sulfated zirconia and the reactant. A number of causes of the deactivation have been proposed: (i) coke formation,[15,66,70-82] which other authors have dismissed,[83] (ii) reduction of sulfate[83] and sulfur loss as H_2S,[77] (iii) reduction of Zr^{4+},[71] (iv) tetragonal to monoclinic zirconia phase transformation[75,84] and (v) poisoning by water.[73]

1.2.5 Isomerisation mechanism

The isomerisation of alkanes on anion modified oxides such as sulfated zirconia is believed to proceed via carbocation-like reactive intermediates;[85] but the formation of such surface species is a subject of much debate (Figure 1-4). It was initially suggested that protolytic activation of a C-H bond via formation of a carbonium ion with a pentacoordinated C, which releases H_2 to form a carbenium ion.[86] This mechanism is in direct analogy to the isomersation of alkanes using liquid superacids, it has thus been criticised as experimental and theoretical studies have shown sulfated zirconia not to act as a superacid (see section 1.2.3). Activation via direct hydride abstraction by Lewis acid sites has also been proposed,[87,88] although no conclusive evidence has been produced to corroborate such a mechanism. Tabora and Davis[89] proposed that alkene impurities in the hydrocarbon feed could yield carbenium ions via protonation on Brønsted acid sites. Yet the presence of catalytic activity using an alkene free feed (although initially a much lower activity is observed) implies that *in situ* generation of alkenes, via oxidation of the alkane by sulfate groups, is possible.[90,91]

Recently, during the course of this work, evidence supporting the oxidative dehydrogenation mechanism has been published. Li *et al.*[63] reported detecting the three products of the oxidative dehydrogenation mechanism either during or after reaction. Butene was detected after *n*-butane temperature programmed reaction spectroscopy; the reduction of sulfate was shown by thermally desorbing the various sulfur species from the spent catalyst followed by ion chromatography; and the formation of water was proven using *in situ* IR spectroscopy.

Two pathways have been proposed for the skeletal isomerisation of the carbocationic intermediate: a monomolecular (intramolecular) and a bimolecular (intermolecular) mechanism. The monomolecular route proceeds via the formation of a cyclopropane complex, which for *n*-butane would mean the generation of a potentially highly unstable

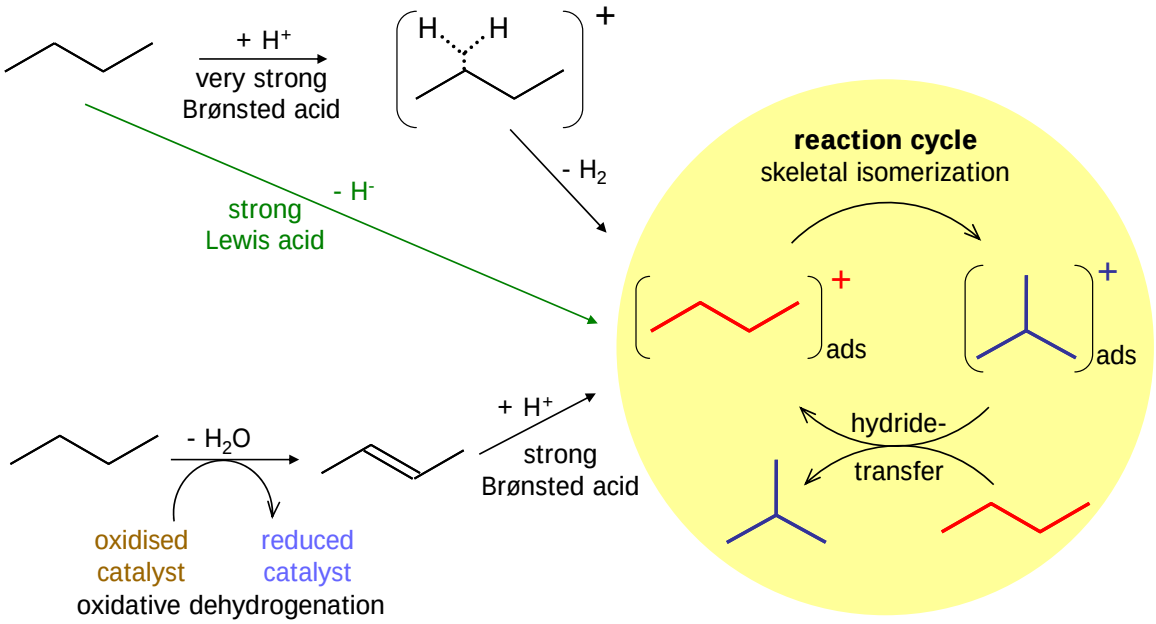

Figure 1-4: Proposed reaction mechanisms.

primary carbenium ion, although such a species could be stabilised on the surface in the form of an alkoxide. The bimolecular mechanism proceeds via the formation of a C_8 carbocation followed by β scission. ^{13}C labelling and kinetic studies have produced evidence supporting both mechanisms.[92-95] Proposals of the mechanism changing based on conversion, temperature and time on stream have also been reported.[96,97]

1.3 Application of Surface Science Techniques to Oxide Catalysts

The precise nature of the active isomerisation sites on sulfated zirconia is still a subject of debate. There has been a huge advance in the development of surface sensitive techniques over the past several decades. However, the application of these techniques to "real" powder oxide catalysts, such as sulfated zirconia, is often not possible or limited; as their porous structures give rise to diffusion limitations and their electrically and thermally insulating nature can cause charge accumulation and temperature gradients. In order to overcome these problems it is possible to use model systems.

Thin single crystalline films grown on conducting substrates have been successfully employed leading to a greater understanding of oxide systems on an atomic level.[98,99] The drawback of these systems are due to their oversimplification, for example the lack of

defects and support interaction, extrapolating to "real" powder catalysts has had limited success. Alternatively, particles supported on flat model supports have also been investigated.[100,101] By depositing a thin oxide or carbon film on an inert conducting substrate serious charging accumulation can be avoided, even if the film is an insulator. The catalytic material can thus be deposited on this support. Such systems are inherently more complex than the flat continuous single crystalline films.

Various methods exist for depositing oxide films or particles on flat substrates, including: evaporation of metals followed by oxidation, chemical vapor deposition (vacuum dosing of volatile organometallic precursors), wet chemical impregnation (such as spin or dip coating of organometallics) or microfabrication via lithography. The resulting model systems allow the application of surface spectroscopies.

1.3.1 Sulfated zirconia thin solid films

The specific chemical and physical properties of zirconia films have been extensively studied due to their promising technological applications; for example as wave guides when deposited on glass substrates,[102] thermal barrier coatings[103] and protective coatings from abrasion, wear and wet corrosion.[104] Numerous different methods for the synthesis of zirconia films have been published, therefore only zirconia films incorporating sulfate are commented on below.

Anodic oxide films have been prepared electrochemically on zirconium rods in sulfate containing electrolytes by various groups.[105-114] Zirconium, unlike most metals, is known to incorporate anions from solutions during anodic oxidation.[107,115-117] Rogers *et al.*[107] showed the sulfur content of anodic zirconia films to vary linearly from approximately 5 to 35×10^{20} atoms/cm^3 with increasing the ionic current density. Meisterjahn *et al.*[108] reported a linear film growth of 2.6 nm/V (up to 9 V) on an initial oxide thickness of 4-6 nm. Pauporte and Finne[114] were able to grow dense 300-340 nm anodic zirconia films.

De Guire and co-workers[118-120] developed a method to prepare sulfated zirconia films by chemical deposition of zirconium sulfate from an aqueous acid stabilised medium on sulfonic acid terminated self-assembled monolayers (SAMs) attached to oxidised silicon wafers. Surface morphology studies of such zirconia films found in addition to the film, particles of 200 nm and larger embedded in the film.[121,122] Further development to prevention of homogenous deposition, by lowering of the film deposition temperature,

resulted in smooth, non-porous, continuous sulfated zirconia thin films.[123,124] transmission electron microscopy (TEM) investigations have shown annealing the films to produce tetragonal sulfated zirconia.[125-127] More details regarding the preparation and thermal treatment of these films are given in Chapter 2. Investigations of the stability of the sulfated zirconia precursor solution have been performed,[128] as well as on the forces between the SAMs and zirconia particles in solution.[129] Mechanical properties of sulfated zirconia films prepared from similar aqueous depositions on SAM covered substrates have also been studied.[130-132]

Rizzato *et al.*[133] prepared sulfated zirconia films on borosilicate glass surfaces by sol-gel dip coating. Layer thickness was shown to increase with increasing withdrawal speed (from ~25 to 100 nm) and decreases with thermal treatment. At temperatures below 623 K the films were shown to have a pore free structure, which consists of an inner layer of $Zr_{18}O_4(OH)_{36}(SO_4)_9(Cl)_6$ and a thin (~2 nm) superficial layer of $Zr_{18}O_4(OH)_{38.8}(SO_4)_{12.6}{\cdot}33H_2O$.

Lin *et al.*[134] reported the direct liquid phase deposition of sulfated zirconia films on silicon wafers via the hydrolysis of zirconium sulfate with varying concentrations of ammonium peroxydisulfate (persulfate, $S_2O_8^{2-}$).[56] The ammonium peroxydisulfate suppressed the zirconium precipitation and improved the film growth via heterogeneous nucleation on the silicon. Film thicknesses of up to 200 nm were obtained. Thermal treatment of the films at 873 K resulted in the formation of the tetragonal phase.

Meinel *et al.*[135] prepared single-crystalline cubic sulfated zirconia films by reactive deposited of Zr onto Pt(111) in an O_2 atmosphere, followed by exposure to a SO_3 atmosphere. During sulfation a ($\sqrt{3}$ x $\sqrt{3}$)R30° structure develops, which is stable to 700 K.

1.4 Objectives and Strategy

The main aim of this thesis is to investigate the isomerisation sites on sulfated zirconia by the application of surface science techniques, which is made possible by the use of a model thin film system. Fischer and co-workers[123,124] described the preparation of nanocrystalline thin films that are potentially suitable models for powder sulfated zirconia catalysts. The thinness of such films permits thermal and electrical conductivity,

the homogenous flat surface of the films prevents diffusion and simplifies the system, while their nanocrystalline nature permits the chemical complexity and existence of defects to yield catalytically relevant activity; hence films of this type can be considered to act as a bridge between the materials gap in catalysis, which exists between "real" powder catalysts and "ideal" single crystalline materials.

The main goals of the thin film investigations in this thesis are to:

(i) Produce model sulfated zirconia thin films based on the process described by Fischer and co-workers.[123,124]

(ii) Investigate the role of the thermal treatment of the films.

(iii) Characterise the (acidic) surface sites via adsorption of probe molecules.

(iv) Validate the model system via proof of its catalytic reactivity.

During the course of this work, reports proposing the active calcined sulfate structure to be that of disulfate were published.[62,63] Active catalysts were shown to develop an IR band at ~1404 cm^{-1}, which theoretical studies have shown can only arise from disulfate or adsorbed SO_3 molecules. Thus as a complementary study to the thin films investigations in this thesis, the rational design of a disulfated zirconia powder catalyst has been attempted. The goals of this sub-project are to:

(i) Synthesise sulfated zirconia powders from sulfating agents containing two pregrouped sulfur atoms and an analogous mono-sulfur precursor.

(ii) Compare their catalytic activities.

(iii) Attempt to relate any catalytic differences observed to the proposed disulfate IR band at ~1404 cm^{-1}.

The two strategies of this thesis are designed to test recent proposals of the scientific community and increase the understanding with regards to the surface chemistry of sulfated zirconia catalysts. In order to improve our fundamental knowledge of how sulfated zirconia catalysts work only un-promoted catalysts and the simplest skeletal isomerisation test reaction (*n*-butane to isobutane) have been investigated.

2. Synthesis and Thermal Treatment of Sulfated Zirconia Thin Films

2.1 Introduction

2.1.1 Biomimetic synthesis of oxide thin films

The production of oxide thin films by the so-called biomimetic processing was pioneered by the work of Bunker and co-workers.[136] The main principle of such a preparation is to use a self-assembled monolayer (SAM) to mediate film deposition from an aqueous medium at low temperatures; thus mimicking biological growth of ceramics. Immersion of a SAM covered substrate into a deposition medium, consisting of a dissolved metal salt, results in the formation of a film consisting of an oxide or a potential oxide precursor (such as a hydroxide, sulfate or carbonate depending on the anions present). Two different mechanisms for film deposition are discussed in the literature:[137,138] (i) cluster growth of particles in the liquid phase (homogeneous) followed by adsorption on the SAM and coagulation to form a film and (ii) ion by ion, via successive adsorption of anions and cations on the substrate (heterogeneous nucleation). Deposition conditions can dictate which deposition mechanism is observed. The two mechanisms may also occur simultaneously.[137] Successful biomimetic syntheses promote heterogeneous nucleation and suppress homogeneous nucleation.[136]

2.1.2 Self-assembled monolayers

SAMs are molecular assemblies that are spontaneously formed on an appropriate substrate when immersed into a solution of active surfactant in an organic solvent.[139,140] Various reviews have reported on their synthesis, structure and properties.[141-143] There are a number of different ways of preparing SAMs, these include: organosilicates on hydroxlyated surfaces (e.g. SiO_2 on Si); alkanethiols on gold, silver and copper; dialkyl sulfides on gold; dialkyl disulfides on gold; alcohols and amines on platinum; and carboxylic acids on aluminum oxide and silver.[144]

SAMs can be considered to consist of three parts: a head group, an alkyl body -(CH_2)- and a tail group. The head group binds to the substrate via chemisorption. This is an exothermic process (typically in the order of 10s kJ/mol) and results in the apparent pinning of the SAM to a specific site on the substrate. Although, as a result of the strong molecular interaction with the substrate the head groups try to occupy every available binding site on the surface, during this process they push together molecules that are

already adsorbed. In the case of trichorosilyl head groups cross linking also occurs, increasing the stability of the SAM.

The close packing of the alkyl chains gives rise to short range van der Waals forces (typically up to 40 kJ/mol). A minimum chain length of ~9 carbon atoms is necessary to stabilise the formation of a SAM. Chain lengths above ~20 carbon atoms result in solubility problems. The highest degree of ordering and stability has been reported for surfactant molecules with carbon chain length of 16 atoms. In the case of trichlorosilyl head groups, the chemisorption, cross linking and van der Waals forces can result in the SAM being stable to prolonged exposure in pHs ranging from strongly acidic to mildly basic, at temperatures up to 313 K.

The tail or surface group of the SAM can be chosen from a number of species, including: sulfonate, thioacetate, hydroxyl and methyl. Sulfonate tail groups are very effective in initiating and sustaining the formation of oxide thin films when immersed in an appropriate precursor solution. However, sulfonate tail groups cannot be used in combination with trichloromethyl head groups, as they both have similar propensities to react with substrate hydroxyl groups. It is however possible to transform the tail group *in situ* after deposition of the SAM for the generation of specific reactive tail groups, for example the oxidation of thioacetate to sulfonate.

2.1.3 Aqueous zirconium sulfate solutions

The solution chemistry of zirconium sulfate is complex because sulfate not only strongly complexes with zirconium[145,146] but is a potential bridging ligand and promotes polymerization.[147,148] Anion[149-151] mixed hydroxo sulfato complexes,[148] also of polynuclear type, are formed in sulfate solutions. Zirconium sulfate solutions are unstable with regards to hydrolysis and precipitation. Heating promotes hydrolysis and hence precipitation. The large number of possible sulfates, particularly basic sulfates, of various constitutions that are precipitated from zirconium sulfate solutions suggest that many complexes of different constitutions may exist in solution. The chemistry of zirconium sulfate solutions may be ruled by complicated equilibria. The time frame for changes in these solutions indicates the equilibration is slow. Hauser[152] observed precipitation in 0.5 M zirconium sulfate solutions only after 2 weeks at 312.5 K. Matijević[147] delayed the onset of precipitation of 0.2 mM zirconium sulfate solutions by 10 h, 2 or 4 days using 1,

2 or 4 mM nitric acid solutions, respectively. Cölfen *et al.*[128] showed that for solutions containing low zirconium sulfate concentrations (2 or 4 mM) and high acid concentrations (0.4 or 0.6 M HCl) switching between relatively moderate temperatures of 323 to 343 K results in a change from long-term metastable (more than 96 hours) to rapidly precipitating (30 minutes) conditions.

2.1.4 SAM mediated sulfated zirconia thin film growth

De Guire and co-workers[118-120] showed that zirconium containing films could be grown on oxidized silicon wafers via SAM mediated aqueous deposition. They demonstrated that SAMs formed from the following precursors promoted film growth: trichlorosilylhexadecane thioacetate, hexadecyl trichlorosilane and octadecyl trichlorosilane. The SAMs formed from trichlorosilylhexadecane thioacetate and hexadecyl trichlorosilane needed to be converted to sulfonate terminated SAMs via exposure to gaseous SO_3 or immersion in a saturated aqueous solution of $KHSO_5 \cdot KHSO_4 \cdot K_2SO_4$, respectively. In the absence of a SAM no film growth was observed, as shown by XPS measurements. The films were grown from aqueous solutions of either 4 mM zirconium sulfate in 0.4 M HCl or 10 mM zirconium sulfate in 0.6 M HCl, at 343 K, during single depositions between 0.5 and 24 hours or four successive 1 hour immersions in freshly prepared solutions. After approximately 30 minutes at 373 K a visible cloudiness was observed in the deposition medium, indicating bulk (homogeneous) precipitation. Cross section TEM measurements revealed, prior to bulk precipitation films of only 3 nm thickness could be grown; following bulk deposition films could be grown up to a maximum of 40 or 125 nm, during one immersion, in 4 or 10 mM zirconium sulfate solutions, respectively. The successive 1 hour immersions in freshly prepared deposition medium produced a film of 180 nm. Films grown on the sulfate free SAM (formed from octadecyl trichlorosilane) were shown to contain sulfate by XPS measurements. The films grown on sulfonate terminated SAMs were found to be adherent to the substrate using a tape peel test, this was not the case for those grown on the SAM formed from octadecyl trichlorosilane. Atomic force microscopy (AFM) and scanning electron microscopy (SEM) topography studies[121,122] found that in addition to film formation, particles of typically 0.5-1 μm in diameter (SEM and AFM) and 30-50 nm in depth (AFM) are embedded in the films.

Fischer and co-workers[123,124] found by lowering the film deposition temperature from 343 K to 323 K that the presence of particles in the film could be avoided; thus resulting in smooth, non-porous, continuous sulfated zirconia thin films. Roddatis *et al.*[126,127] showed by cross sectional TEM measurements the growth rate of the films deposited between 2-96 hours to be constant, at ~1 nm/h. The deposited films were also shown, by high resolution (HR)TEM, to be initially amorphous; however, electron beam irradiation was shown to induce the formation of 5-10 nm tetragonal crystals.

Wang *et al.*[130,131] have also prepared films from 0.4 mM zirconium sulfate on sulfonated SAM of 3-mercaptopropyl trimethoxysilane at both 343 and 323 K in 0.4 M HCl. After 6 hours deposition at 343 K a film of 68 nm with ~300 nm quadratic-looking features was observed. At 323 K, however, much smoother films were produced, the film growth rate was shown to be ~1 nm/h between 20-100 hours.

More recently Zhang *et al.*[132] prepared films from 0.01 M zirconium sulfate solutions containing 0.4-0.1 M HCl at temperatures of 343-363 K for 0.5-24 hours, on a SAM formed from diethylphosphatoethyltriethoxysilane and hydrolysed in HCl. In addition films were also formed hydrothermally in an acid digestion bomb at 408 K for 24 hours, during which the pressure was about 5 atm.

2.1.5 Thermal treatment of heterogeneously deposited sulfated zirconia thin films

Fischer and co-workers[123,124] also investigated the effects of thermal treatment in either argon or synthetic air at 773 K on heterogeneously deposited films. AFM and SEM investigations show the films surfaces to be smooth and free from cracks after treatment in both atmospheres.

Roddatis *et al,*[126,127] studied, using HRTEM, heterogeneously deposited films thermally treated at various temperatures in argon. Fourier transform analysis of selected areas of the HRTEM images showed that below 798 K the structure does not change from the amorphous state, whereas at 823 K crystallisation of the zirconia to the tetragonal state occurs and above 873 K a small amount of monoclinic zirconia is seen. HRTEM images show that the 823 K treatment produces a continuous polycrystalline zirconia film, thinner than the as-deposited film by 60–70%, with 10–50 nm grain sizes.

2.1.6 Aims

To allow the application of surface science techniques to sulfated zirconia, thin films as described by A. Fischer[123,124] will be produced. The chemical and physical properties of the films will be studied in order to ensure that the films are a suitable chemical model system for sulfated zirconia, conducting and non-porous. If the film synthesis is not successful, further efforts will be made to modify the system and its synthesis.

Thermal treatment of the films produced will be investigated in both an inert and an oxidising atmosphere with equivalent temperature programs; in order to study both the chemical and physical effects of the SAM decomposition and film crystallization.

In order to further bridge the materials gap with "real" powder catalysts of varying compositions, synthesis of an analogous powder catalyst was attempted. The analogous powder was produced from the same precursor material as the thin films, thus mimicking their preparation; however a higher deposition temperature was used in order to allow precipitation of the powder.

2.2 Experimental

2.2.1 Film synthesis

2.2.1.1 Substrate preparation

Single crystal silicon (100) 1 cm^2 wafers were used as the substrate, either p-type, 10 mOhm.cm, 750 μm thick polished on both sides or n-type, 4.2 Ohm.cm, 1.3 mm thick with a groove drilled into the side for thermocouple placement, polished on one side. The silicon wafers were cleaned using laboratory tissues and solvents (sequentially chloroform, acetone, ethanol and water). Millipore® filtered water was used for all preparation steps. The silicon wafers were then treated in Standard Clean 1 (SC1)[153]: 1 part 27% ammonia, 1 part 30% hydrogen peroxide to 5 parts water at 343 K for 1 h, followed by Standard Clean 2 (SC2)[153]: 1 part 32% hydrochloric acid, 1 part 30% hydrogen peroxide to 5 parts water also at 343 K for 1 h. Oxidation of the wafers was performed in “piranha” solution (3 parts 30% hydrogen peroxide to 5 parts conc. sulfuric acid) at 353 K for 1 h. On removal the wafers were rinsed with water and dried in an argon stream.

2.2.1.2 Self assembled monolayer deposition and functionalisation

To deposit the SAM, the wafers were immersed in a solution of 50 µl of 1-thioacetato-16-(trichlorosilyl)hexadecane in 5 ml of bicyclohexyl for 5 h under an argon atmosphere using a glove bag. The hydrophobic terminal thioacetate group of the SAM was then oxidized in a saturated aqueous solution of $KHSO_5 \cdot KHSO_4 \cdot K_2SO_4$ for 5 hours.

2.2.1.3 Deposition of the sulfated zirconia precursor film

After oxidation the wafers were rinsed with water and transferred immediately into the deposition medium, an aqueous solution of 4 mM zirconium (IV) sulfate tetrahydrate in 0.4 M hydrochloric acid. The temperature of the deposition medium was ramped slowly (~1 K/min) to 323 K, in individual deposition tubes using a water bath. Films were deposited over time periods of 24-96 h in order to prepare films of various thicknesses to suit the different characterisation techniques employed; thinner films to maximise the conductivity of the samples and thicker to minimise substrate contributions. On removal from the deposition medium the films were rinsed with water and blown dry using argon.

2.2.1.4 Thermal treatment of the thin films

Thermal treatment of the films was performed in an inert atmosphere (pyrolysis), either argon or nitrogen (to avoid potential heat damage to the film from combustion of the SAM) or in air (calcination, to mimic the powder preparation). The films were heated to 823 K in 125 ml/min of the chosen atmosphere for 2 h, ramping the temperature up and down at 5 K/min.

2.2.2 Synthesis of an analogous sulfated zirconia powder

2.2.2.1 Precipitation of the powder

Analogous aqueous solutions to those used to deposit the sulfated zirconia precursor films, of 4 mM zirconium (IV) sulfate tetrahydrate in 0.4 M hydrochloric acid, were heated to 343 K in order to initiate bulk precipitation. After either 76 or 96 h at 343 K the precipitate was filtered, rinsed with water and dried in air.

2.2.2.2 Thermal treatment of the precipitate

Batches of the precipitated powder were heated to 823 K for 2 h in 125 ml/min of nitrogen or in 125 ml/min of synthetic air to the following temperatures: 873, 898, 923, 948, 973 and 998 K for 3 h. In all cases the oven temperature was ramped up and down at 5 K/min.

2.2.3 Characterisation techniques

2.2.3.1 XPS

The surface chemical composition of the films was investigated by X-ray photoelectron spectroscopy (XPS) using the Mg Kα excitation (hν = 1256.3 eV) with a pass energy of 30 eV. A Shirley background was subtracted and binding energies were corrected to Zr $3d_{5/2}$ = 182.2 eV of ZrO_2.[154] Atomic sensitivity factors for Zr 3d, O 1s, and S 2s were taken from reference 155.

2.2.3.2 SEM

Topographical imaging of the films was performed using a Hitachi S-4100 scanning electron microscope (SEM) with a Thermo Noran System SIX energy dispersive X-ray detector (EDX). The SEM was operated at 5 kV using a working distance of 9 mm for imaging and 15 mm for EDX measurements.

2.2.3.3 TEM

Cross section high resolution transmission electron microscopy (HRTEM) was performed on 24 and 48 h deposited calcined films. The samples were prepared by first cutting the wafers and gluing them together, film surface to film surface, then mechanically polishing and dimpling them down to 5-10 μm, followed by ion milling with a Gatan precision ion polishing system operated at 3.5 kV using Ar^+ ions. In order to minimise heating of the samples a single unfocused ion beam was used and the samples were rotated.

Analysis was performed using a Philips CM200 electron microscope with a field emission gun operated at 200 kV, additionally featuring a Tridiem Gatan imaging filter and a Genesis 4000 energy-dispersive X-ray spectrometer. The microscope has a maximum resolution of 0.18 nm. Fast Fourier transformation was employed to analyse the structure of small areas or individual grains.

2.2.3.4 XRD

The X-ray diffraction (XRD) measurements were performed using a STOE STADI P transmission diffractometer equipped with a primary focusing Ge monochromator (Cu $K\alpha_1$ radiation) and a position sensitive detector. The powders were mounted between two layers of X-ray amorphous polyacetate (Mylar) foil, using a small amount of X-ray

amorphous grease to hold the powder in place. The foils were clamped into a ring shaped holder which rotates during the measurement.

Fittings of the diffractograms were performed with the program Topas v.3.0 (Bruker AXS), using the Rietveld method, to give a monoclinic to tetragonal ratio. The calculations of the theoretical peak intensities for monoclinic and tetragonal zirconia were based on ICSD[156] entries 89426 and 97004, respectively.

2.3 Results

2.3.1 As deposited films

XPS measurements of the as deposited films (Figure 2-1) show signals arising from zirconium, oxygen, sulfur, carbon and silicon. Signals from the silicon substrate decrease with increasing deposition time. Two maxima of the Si 2p were detected, one at Si $2p_{3/2}$ = 99.7 eV consistent with Si(100) and the other at Si $2p_{(3/2+1/2)}$ = 103.7 eV, in accordance with oxidised silicon.[154] Signals arising from the zirconia film were shifted towards higher binding energies because of charging, an offset of around 2.2 eV was observed. Thus the maximum of the S 2p (S $2p_{3/2+1/2}$) signal was detected at 168.4 eV, indicating a sulfur oxidation state of +6. The O 1s signal is composed of at least two peaks, the lower binding energy peak at around 529.4 eV relates to oxide anions and the higher binding energy peak at ca. 531.1 eV corresponds to sulfate and hydroxide species. Assuming the charging correction is also valid for the carbon signal, the C 1s peak has a maximum at ~284.0 eV, which is similar to the reported value of "chain" carbon[157] as would be expected from the SAM.

SEM images (not shown) reveal the surface of the as deposited films to be continuous, mainly smooth and homogeneous. However, spherically shaped particles of up to 1-2 μm are observed on the film surface. EDX analyses reveal these particles to consist of zirconium, oxygen and sulfur.

2.3.2 Thermal treatment of films

XP spectra of the films after the different thermal treatments show the loss of sulfur, as is apparent from both the S 2p and S 2s (Figures 2-1a and b) regions as well as from the O 1s signal (Figure 2-1c). The higher binding energy component of the O 1s signal (relating to hydroxyl and sulfate groups) is reduced after both thermal treatments, but

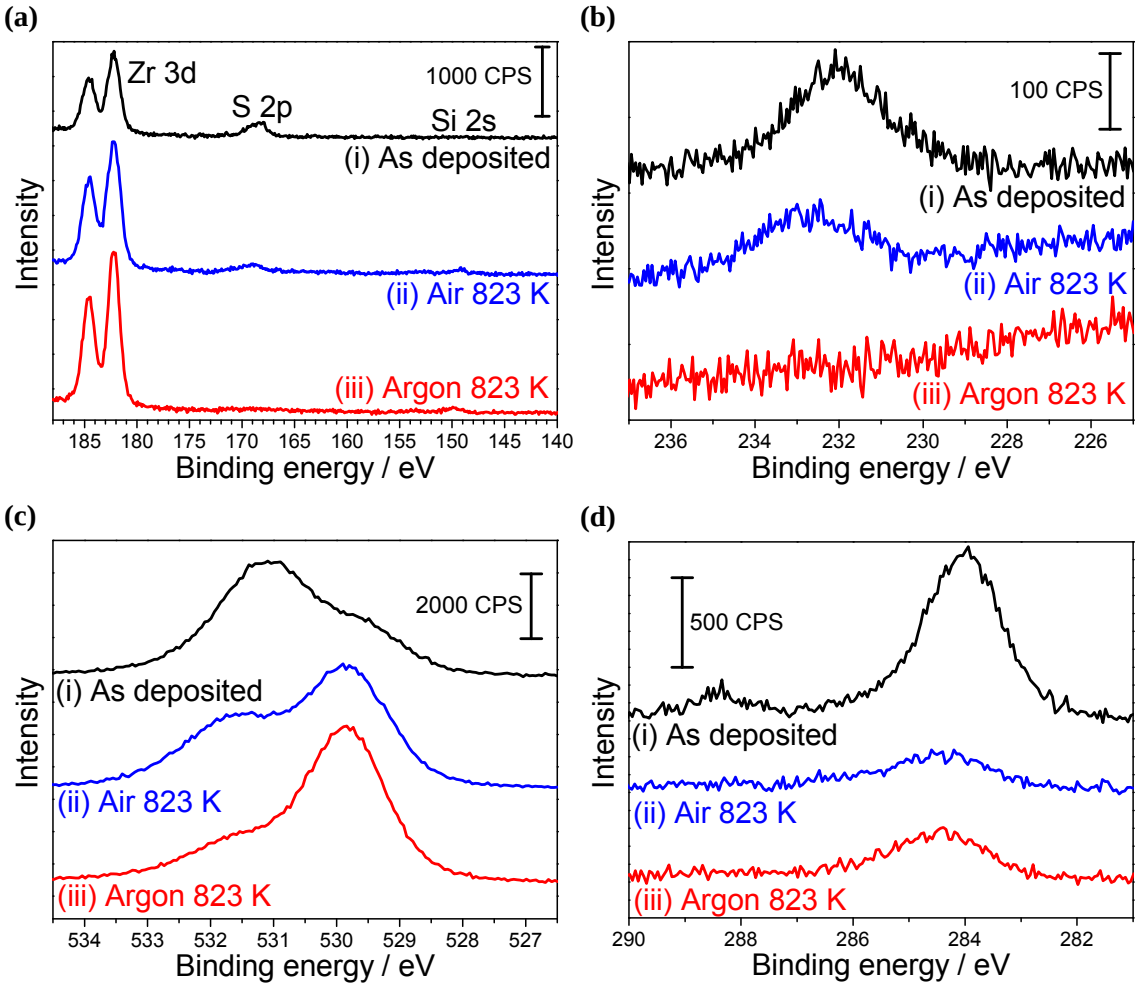

Figure 2-1: XP Spectra of the (a) Zr 3d, S 2p, Si 2s and Si 2p (b) S 2s (c) O 1s and (d) C 1s regions of sulfated zirconia thin films (i) as deposited and after thermal treatment at 823 K in (ii) argon and (iii) synthetic air.

Table 2-1: Elemental compositions calculated from XPS data of as deposited and thermally treated sulfated zirconia films deposited over 48 h. Samples compared to a typical active tetragonal powder sulfated zirconia sample.[162] n.d. = not detected.

Atomic %	Zr	O	S
As deposited	18.6	73.5	7.9
Argon 823 K	30.0	70.0	n.d.
Air 823 K	25.8	71.1	3.2
Calcined powder	27	68	5

more significantly for the treatment in argon. After thermal treatment of the films in argon no sulfur is detectable in the S 2p or S 2s regions. Thermal treatment of the films in

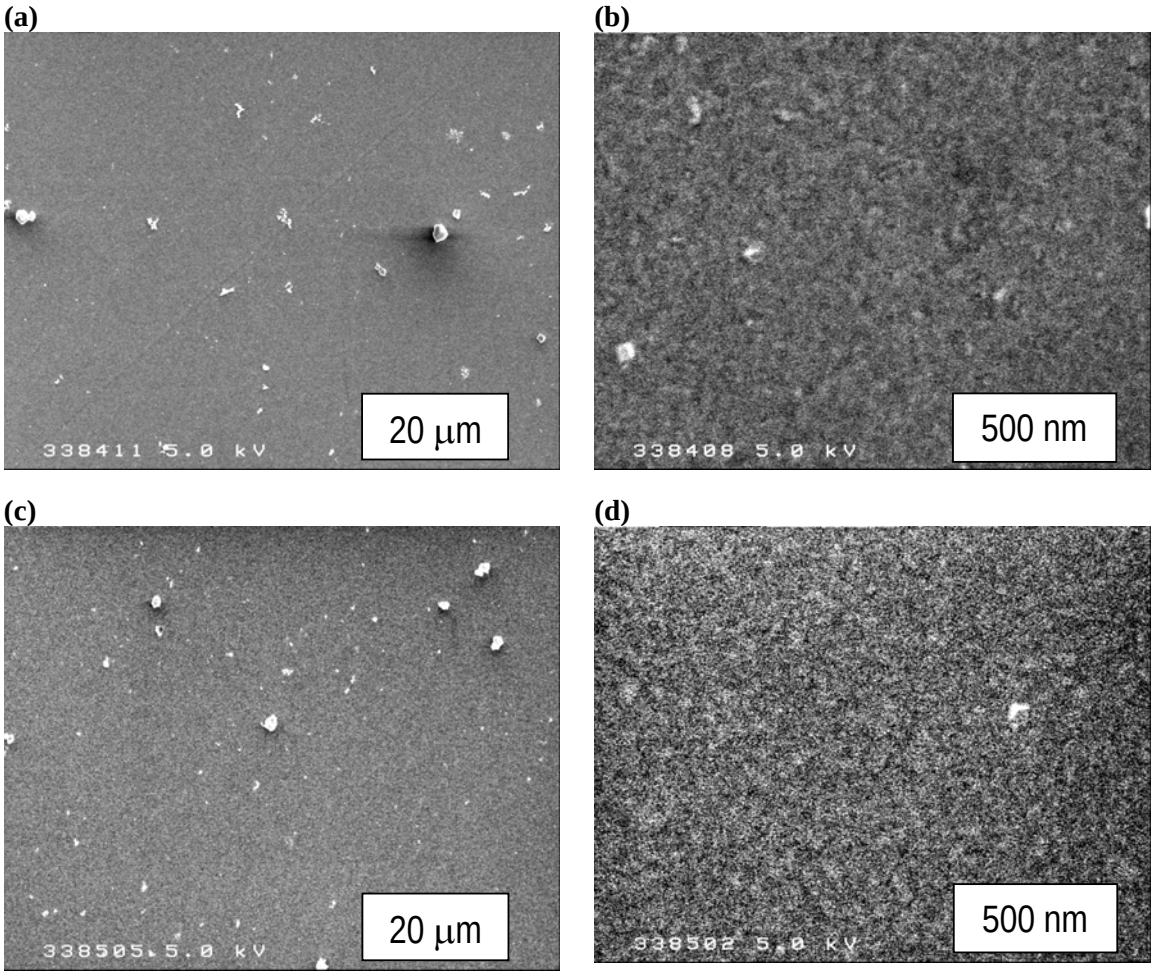

Figure 2-2: SEM images of sulfated zirconia thin films after thermal treatment at 823 K in (a&b) argon and (c&d) synthetic air.

Table 2-2: Elemental compositions of sulfated zirconia thin films and particles on the films after differing thermal treatments, as measured by EDX.

Atomic %		Zr	O	S
Argon 823 K	overview	13.0	87.0	n.d.
	particles	15.7	80.0	4.3
Air 823 K	overview	14.4	79.9	5.7
	particles	14.7	80.2	5.1

synthetic air retards the loss of sulfur and thus elemental compositions of the films are comparable to a typical active powder catalyst (Table 2-1). In addition to the loss of sulfur, the C 1s signal is reduced and shifts to 284.6 eV, consistent with the decomposition of the SAM and the main source of carbon being either atmospheric contamination (adventitious) or SAM decomposition products. The silicon substrate

peaks are more prominent after thermal treatment, indicating a decrease in layer thickness. Estimation of the thickness of the air-treated films from the intensity of the Si 2p signal (using an electron mean free path taken from reference 158) yields values of 2–12 nm, increasing linearly with deposition time (see Figure 2-4).

SEM images (Figure 2-2) show the films after the thermal treatments to remain smooth, homogeneous and crack free. The particles on top of the films remain unchanged; no differences in average size of the particles or in the quality of the film surrounding the particles are noticed after the differing treatments or from comparisons with the as deposited films. EDX analysis of the films overall elemental composition (Table 2-2), results in similar values to those calculated from XPS measurements; no sulfur was detected in the argon-treated film and slightly lower sulfur content compared to the as deposited film for the air-treated film. Focusing of the incident electron beam for EDX analysis on the particles shows that their compositions differ from that film for the argon-treated sample, in that they contain sulfur. The particles on the air-treated films, however, have similar compositions to the films. Elemental compositions of the overall surface and particles of the air-treated films by EDX analysis are comparable to a typical powder catalyst.

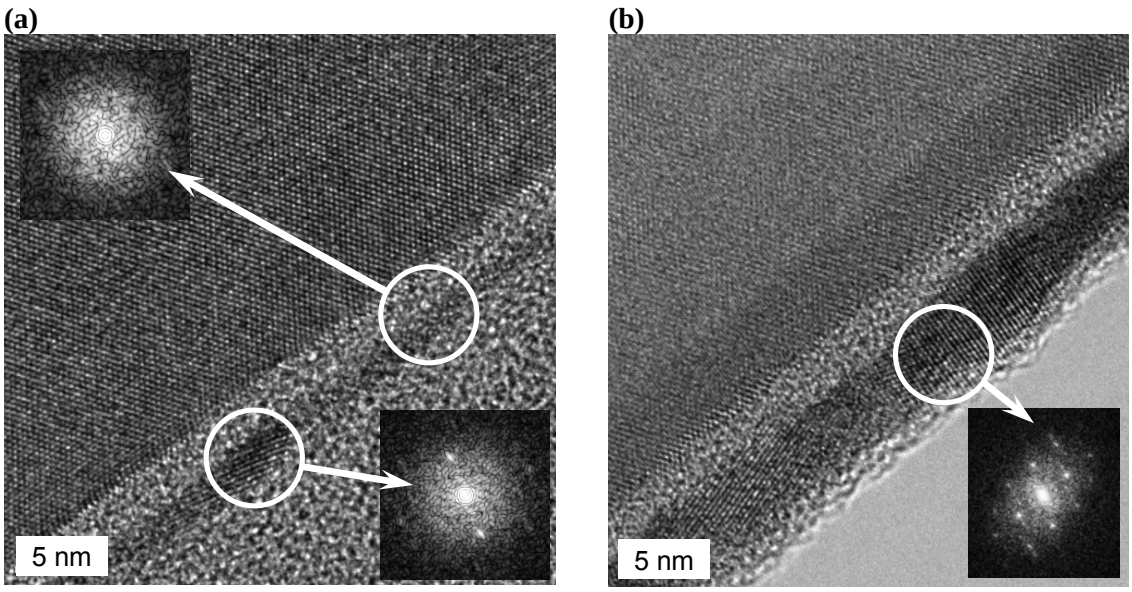

Figure 2-3: HRTEM cross section images (and Fourier transforms of selected areas inset) of calcined sulfated zirconia thin films after (a) 24 h and (b) 48 h depositions.

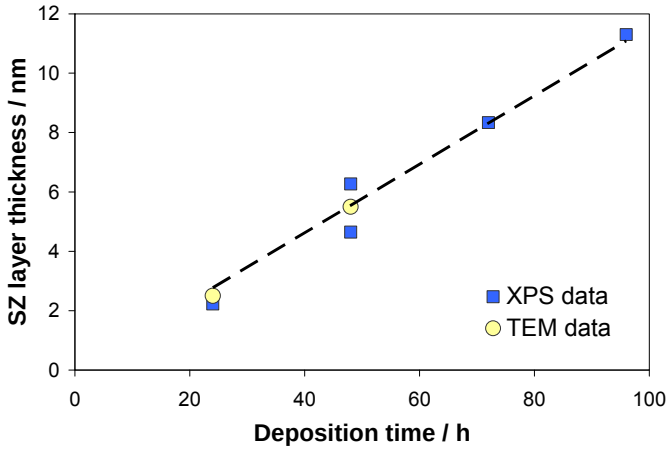

Figure 2-4: Sulfated zirconia film thickness after various deposition times calculated from TEM and XPS results.

Cross sectional HRTEM images of air-treated films deposited over 24 and 48 hours are shown in Figure 2-3. TEM analyses reveal both films to be continuous, with average thicknesses of 2.5 (24 h deposition) and 5.5 nm (48 h deposition). The film thickness of the 24 h deposited film varies from 1 to 5 nm. The 48 h film is, however, of relatively homogeneous thicknesses (within 1 nm). HRTEM images show the 24 h film to be mainly amorphous with some crystals in the thicker areas of the film; crystals of between 1-10 nm parallel to the film are detected. The 48 h film is shown to be fully crystalline with crystals from 5 up to 30 nm detected. Fourier transform analyses of selected areas of the HRTEM images reveal the structures of the crystalline layers from both films to be consistent with the tetragonal phase. Minor amounts of the cubic phase cannot be excluded; however, no monoclinic phase was present in the areas of film examined.

2.3.3 Analogous sulfated zirconia powder

X-ray diffractograms for the films' starting material (zirconium sulfate), the precipitate from the deposition medium at 343 K and after various thermal treatments are shown in Figure 2-5. Comparing the diffractogram of the commercial zirconium sulfate to that of the precipitate it is clear to see the two samples have the same crystalline phase. Heating the precipitate, to

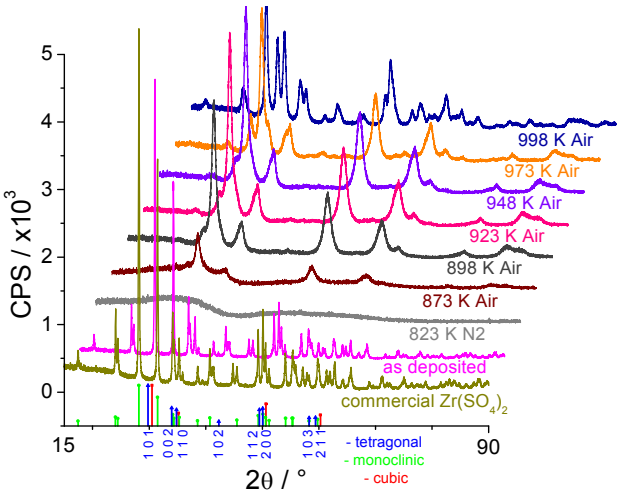

Figure 2-5: X-ray diffractograms of commercial zirconium sulfate (the deposition medium starting material), the deposition medium precipitate at 343 K (as deposited) and after various thermal treatments.

823 K for 2 hours in nitrogen, results in the formation of an XRD amorphous material. Increasing the temperature (873-973 K), holding time (to 3 hours) and changing the gas to synthetic air (typical conditions for calcining sulfated zirconia powders),[28] results in the formation of predominantly tetragonal powder. However, a fraction of monoclinic phase is always present (see Table 2-3). The sample treated at 898 K has the lowest fraction of monoclinic phase. Treatment of the precipitate at 998 K results in a mainly monoclinic phase powder.

Table 2-3: Phase compositions of the deposition medium precipitate after thermal treatment in synthetic air at various temperatures.

Temperature / K	% Tetragonal	% Monoclinic
898	85	15
923	80	20
948	78	22
973	69	31
998	24	76

2.4 Discussion

The appearance of particles on the films in the SEM measurements indicated that homogeneous nucleation is occurring in the deposition medium, despite using conditions identical to methods reported to result only in heterogeneous nucleation.[123,124,131] Various parameters were investigated (results not shown) in order to avoid homogeneous nucleation including: the order in which the deposition medium is prepared and diluted; reducing the deposition temperature to 313 K; increasing the acid concentration to 0.5 and 0.6 M; decreasing the zirconium sulfate concentration to 2 mM; filtering, centrifugation and ultra-sonification of the deposition medium prior to immersion of the wafers; purchasing new raw materials of different production batches; changing the water purification method from doubly distilled to Millipore deionised; utilizing a water or oil bath to heat the deposition medium; heating the deposition medium at various rates. None of these measures completely prevented formation of particles. The following method parameters were changed from the original method used[123,124] to produce the films reported on here: cleaning of the silicon wafers in acid (SC1) and basic (SC2) solutions were extended to 1 hour and using Millipore water for all preparation steps in order to reduce contamination; oxidation of the silicon wafer in piranha solution was extended to 1 hour in order to ensure that a complete, thick, homogeneous layer of silicon oxide is

formed; heating of the deposition medium was performed at a constant rate of 1 K/min in order to reduce homogeneous nucleation and hence the occurrence of particles on the films.

Homogeneous nucleation not only results in the formation of particles on the film surface, but in the formation of thinner films per deposition time as compared to those reported from heterogeneously nucleated growth only; as indicated from XPS substrate peaks and TEM images. This effect can be explained by the precipitation of particles via homogeneous nucleation reducing the concentration of zirconium sulfate in solution, thus the rate of heterogeneous nucleation is decreased. The thickness of the calcined films is shown to increase linearly with time and particles were observed on the films regardless of deposition time, thus indicating that the homogeneous precipitation occurs during the initial stages of film deposition.

Topographical studies showed the majority of the films surface to be free of particles and smooth. No influence of the particles was detected using XPS (differential charging not observed, as compared with previously published results).[123,124] The elemental composition of the both the films and particles adhering to the films, after thermal treatment in synthetic air, were shown to be equivalent and similar to an active powder sample. Therefore, despite the presence of particles adhering to their surfaces, the produced films are considered a suitable model for surface science studies.

Thermal treatment of the films in an inert gas (argon) results in loss of sulfur whereas in air the majority of sulfate is retained, which is explainable by its decomposition pathway into SO_2 (g) + ½ O_2 (g).[159] Therefore, films thermally treated in air were used for further investigations. Structural studies of the air-treated films show that very thin films do not crystallise. In order to form a fully crystalline material films of approximately 5 nm thickness are required. In subsequent chapters of this thesis calcined films deposited over 48 h were used when possible; however initial experiments were performed without the knowledge that films from shorter deposition times resulted in films of generally amorphous character. Given that the thinner films still have some tetragonal areas experiments performed on these samples are not regarded as meaningless, although the interpretation of such experiments must consider the low tetragonal fraction of the films.

Thermal treatment of analogous powders precipitated from the deposition medium at 343 K did not result in the formation of a fully tetragonal material, despite using various temperatures and conditions typical for calcining sulfated zirconia powders. Bulk precipitation of the deposition medium at 343 K does not change the crystalline phase from that of the orthorhombic zirconium sulfate tetrahydrate starting material.[160] Deposition of the thin films on the other hand results in the formation of an amorphous phase (as evident from results not shown and previous studies).[126,127] Thus the deposition mechanism, homogeneous versus heterogeneous, affects the crystalline phase formed. In addition the tetragonal phase is stabilised by the formation of small crystals (< 30 nm sized crystals),[19-22] which are formed on the 48 h deposited thin films after thermal treatment. The 48 h films were thus found to have tetragonal crystals equivalent in size to those of active sulfated zirconia powders.[23] However, the tendency of very thin films not to form the tetragonal phase may also be explained by the surface energy stabilisation of the amorphous zirconia.[161]

The bulk precipitation from the deposition medium is judged not to result in a realistic link between the sulfated zirconia thin films and powdered sulfated zirconias (given the different crystalline phases present). Therefore the produced thin films have been compared to tetragonal sulfated zirconia powders prepared by calcining either material prepared using a standard precipitation technique[162] (as used for XPS comparisons in this chapter) or a commercially available (from MelCat) sulfated zirconium hydroxide material.

2.5 Conclusions

Thin films containing zirconium, oxygen and sulfur were successfully synthesised using a biomimetic route outlined in the literature. Homogeneous nucleation of the deposition medium was suppressed but not completely avoided, resulting in particles on the films surface. The presence of such particles is adjudged not to interfere with surface science studies of the films.

Thermal treatment of the films was optimised in air to form a tetragonal film of continuous thickness with a comparable composition to a typical active powder catalyst. The deposition mechanism and the dimensions of the formed films appear to play crucial

roles in formation of the tetragonal phase. Homogeneous deposition results in a powder material that is XRD amorphous after thermal treatment at low temperatures or a mixture of tetragonal and monoclinic after high temperature treatment. If the films are too thin the layer will not crystallise.

3. Thermal Desorption Spectroscopic Studies on Sulfated Zirconia Thin Films

3.1 Introduction

3.1.1 Temperature programmed desorption from sulfated zirconia powders

Numerous temperature programmed desorption investigations have been carried out on sulfated zirconia using various probe molecules, including: pyridine,[163-170] 2,6-dimethylpyridine,[165] ammonia,[165,168,171-196] benzene[164,172,197-199] and substituted derivatives,[197,199] isopropylamine,[199,200] *n*-butylamine,[201] acetonitrile,[202] carbon dioxide,[179] nitrogen monoxide,[188,203] *n*-butane,[27,63] 1-butene,[204] argon[205] and hydrogen.[206] The majority of desorption studies use basic probe molecules (such as pyridine and ammonia) to determine the strength (either relative or absolute) and total number of acidic sites. However, studies have shown the thermal treatment of sulfated zirconia after exposure to such bases to result not just in desorption of the probe molecule but, also, its decomposition.[164,166,167,171] Furthermore, pyridine adsorption has been shown to reduce the sulfate stability.[164,166,167] Thus sulfated zirconia reacts with such bases and hence a qualitative measure of the acidic strength is not possible. Some papers argue that the sites on which the probe molecule is decomposed must be strong acids and quantification of the total number of acidic sites is still possible from evaluation of the amount of desorbing probe and its decomposition products.[171,179] However, with unspecific analytical methods of detection (such as thermal conductivity detectors) it is not possible to differentiate between the probe molecule plus its decomposition products and the decomposition of sulfated zirconia.

Investigations have been performed using weak bases (such as benzene, substituted benzenes, acetonitrile and amines) in order to avoid decomposition, because of their weaker interaction. Such probes only interact with the strongest adsorption sites. In many cases, however, decomposition products (typically including CO_2 and SO_2) have, also, been observed.[164,198-202] Sulfated zirconia has been shown to interact even with argon (up to ~170 K).[205] Furthermore, the probe molecules used may adsorb on zirconia itself.[165,177,178,186,188,189,192,207-211]

Thermal desorption investigations after exposing sulfated zirconia to 1-butene at 323 K, monitored by GC-MS, have shown the probe molecule to oligomerize on the surface.[204] Recent studies exposing an active sulfated zirconia isomerisation catalysts to *n*-butane at

323 K followed by temperature programmed desorption detect higher MS signals for the desorption of butene than butane.[27,63] Whereas for a relatively inactive sulfated zirconia material, butane and butene desorption were not detected. The generation of catalytic sites on the active material was thus ascribed to its dehydrogenation functionality.

3.1.2 Temperature dependent desorption from sulfated zirconia thin films

The adsorption of ammonia on nanocrystalline sulfated zirconia thin films has been previously investigated using XPS.[123] XP spectra of the N 1s signal after exposure to 10000 L of ammonia at room temperature show two peaks at 402.1 and 400.0 eV. Heating to 473 K results in a significant decrease of the higher binding energy peak while the lower binding energy species remains relatively unaffected, indicating a weakly and a strongly bound adsorbate species.

3.1.3 Motivation

Temperature programmed desorption has been applied to the sulfated zirconia thin films in order to take advantage of their non-porous nature and thermal conductivity. These properties should improve the detection resolution of the desorbing species and hence, also, the quantification of the number and strength of different adsorption sites. The interaction of both the reactant (*n*-butane) and a basic probe (ammonia) have been studied to allow identification of both catalytically relevant and acidic sites.

3.2 Experimental

3.2.1 Apparatus

Thermal desorption spectroscopy was performed on samples mounted on a sapphire holder and heated via electron bombardment.[212] The samples were secured to the sapphire holder and grounded via a stainless steel clip, which also held a K type thermocouple in contact with the surface of the sample. Activation and thermal desorption spectroscopy were performed in a chamber with a base pressure in the order of 10^{-9} hPa, in which a differentially pumped mass spectrometer was placed within 1 mm of the sample surface. The recorded mass to charge ratios (m/z) are shown in Table 3.1. Exposure to the probe molecules was performed in a separate preparation chamber, at room temperature, and then the samples were transferred into the main chamber under vacuum.

Table 3-1: Recorded mass fragments and potential parent molecules, relative abundances taken from reference 213.

m/z ratio	Possible fragments	Possible parent molecules (relative abundance)
2	H_2^+, He^+	
12	C^+	*n*-butane (0.1), isobutane (0.1)
14	CH_2^+, N^+, CO^{++}	ammonia (2), *n*-butane (1), isobutane (1)
15	CH_3^+, NH^+	ammonia (8), isobutane (7), *n*-butane (6), 1-butene (2)
16	O+, NH_2^+, CH_4^+	ammonia (80), water (0.9), isobutane (0.2), *n*-butane (0.1), 1-butene (0.1)
17	NH_3^+, OH^+	ammonia (100), water (21)
18	H_2O^+	water (100), ammonia (0.4)
26	$C_2H_2^+$	1-butene (8), *n*-butane (6), isobutane (2)
27	$C_2H_3^+$	*n*-butane (39), isobutane (28), 1-butene (25)
28	N_2^+, CO^+, $C_2H_4^+$	*n*-butane (32), 1-butene (27), isobutane (3)
29	$C_2H_5^+$	*n*-butane (43), 1-butene (13), isobutane (6)
32	O_2^+, S^+	
39	$C_3H_3^+$	1-butene (34), isobutane (17), *n*-butane (14)
41	$C_3H_5^+$	1-butene (100), isobutane (38), *n*-butane (29)
42	$C_3H_6^+$	isobutane (32), *n*-butane (12), 1-butene (3)
43	$C_3H_7^+$	*n*-butane (100), isobutane (100), 1-butene (0.1)
56	$C_4H_8^+$	1-butene (39), *n*-butane (1), isobutane (0.4)
58	$C_4H_{10}^+$	*n*-butane (12), isobutane (3), 1-butene (0.1)
60	SiO_2^+	
64	SO_2^+	
80	SO_3^+	

3.2.2 *n*-Butane thermal desorption spectroscopy

n-Butane thermal desorption spectroscopy was performed on a calcined 24 hour deposited sulfated zirconia film. Activation of the film was performed under vacuum at 814 K with a heating rate of 18 K/min. The activated film was exposure to 5 hPa and $5x10^{-2}$ hPa *n*-butane for 15 minutes and 12.9 hPa for 1 hour, each followed by desorption using an 18 K/min ramp, and 5.2 hPa for 15 minutes followed by desorption using a 36 K/min ramp. For comparison an oxidised silicon wafer activated under vacuum at 723 K with a heating ramp of 18 K/min was used. The wafer was exposed to 6.6 hPa *n*-butane for 15 minutes and 4.9 hPa for 1 hour, both followed by desorption using an 18 K/min ramp.

3.2.3 Ammonia thermal desorption spectroscopy

Ammonia thermal desorption spectroscopy was performed also on a calcined 24 h deposited sulfated zirconia film. The film was activated at 723 K under vacuum with a

heating rate of 18 K/min. After activation a background signal due to heating of the sample without prior adsorption was performed using also an 18 K/min ramp. The film was exposed to 49 hPa ammonia for 30 minutes and 520 hPa ammonia for 1 hour, each followed by thermal desorption at 18 K/min.

3.3 Results

3.3.1 *n*-Butane thermal desorption spectroscopy

Desorption spectra displaying the most abundant hydrocarbon fragment $C_3H_7^+$ (m/z =43) after *n*-butane exposures are shown in Figures 3-1 and 3-2. Figure 3-1 indicates that there is an increased amount of hydrocarbon desorbing from the sulfated zirconia thin film in comparison to the oxidised silicon wafer. Desorption profiles from the sulfated zirconia film and the oxidised wafer are fairly similar in shape, a broad peak is detected from 323 K to 623 K centred around 423 K. There does, however, appear to be a minimum in the sulfated zirconia desorption profiles, at ~440 K after 15 minutes exposure or ~425 K after 1 hour exposure to *n*-butane, indicating the desorption from at least two different types of adsorption sites.

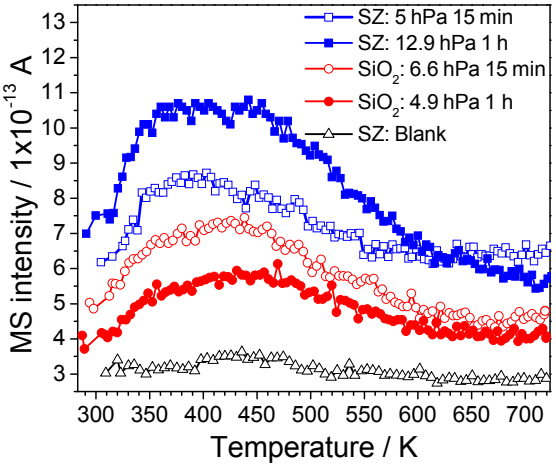

Figure 3-1: *n*-Butane desorption (hydrocarbon fragment m/z 43 shown) from an oxidised silicon wafer (circles) and a sulfated zirconia thin film (squares) after *n*-butane exposure at room temperature for 15 minutes (hollow) or 1 hour (filled). Blank sulfated zirconia thin film measurement, without *n*-butane exposure, also shown (triangles).

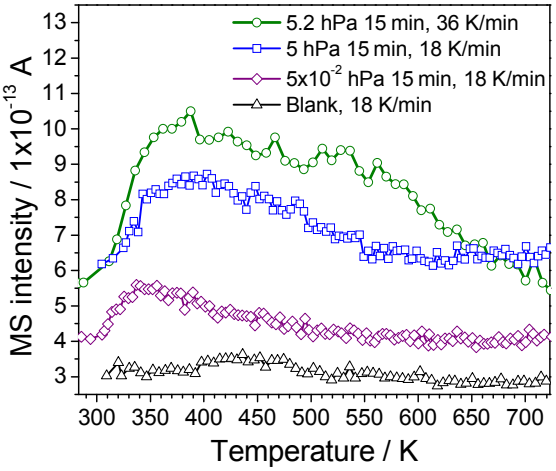

Figure 3-2: *n*-Butane desorption (hydrocarbon fragment m/z 43 shown) from a sulfated zirconia thin film after exposure to $5x10^{-2}$ hPa (diamonds) and 5 hPa *n*-butane using a heating rate of 18 K/min (squares) or 36 K/min (circles), exposures for 15 minutes at room temperature. Blank sulfated zirconia thin film measurement, without *n*-butane exposure, also shown (triangles).

The amount of hydrocarbon desorbing from the sulfated zirconia film is greater after the 1 hour exposure than the 15 minutes exposure. The reverse is true for the oxidised silicon wafer. However, the desorbed amount correlates with slight increases in *n*-butane pressure during dosing, from 4.9 to 6.6 hPa for the oxidised silicon wafer and 5 to 12.9 hPa for the sulfated zirconia thin film. The dependence of dosing pressure on the desorbed amount can be more clearly seen in Figure 3-2, decreasing the exposure pressure from 5 hPa to $5x10^{-2}$ hPa results in a significant signal decrease and the peak shifts to lower temperatures. Increasing the heating rate (from 18 K/min to 36 K/min) results in desorption being additionally observed at slightly higher temperatures (Figure 3-2).

Ratios of fragments m/z 41:43, as determined by integrating the desorption signals between room temperature and 673 K using linear backgrounds, are displayed in Table 3-2. The higher ratio seen for the initial measurement performed on the sulfated zirconia thin film (after dosing at 5 hPa *n*-butane for 15 minutes) can be interpreted as a relative increase in the desorption of unsaturated hydrocarbons. The consecutive measurement (after dosing at 12.9 hPa *n*-butane for 1 hour) and all measurements thereafter (not shown) on the sulfated zirconia thin film do not show ratios that differ significantly from those obtained during desorption measurements using the oxidised silicon wafer.

Table 3-2: Fragmentation ratios for thermal desorption of *n*-butane from a Si wafer and SZ thin film, compared to *n*-butane and 1-butene ratios taken from reference 213.

	41:43
SZ film 5 hPa 15 min	0.66
SZ film 12.9 hPa 1 h	0.50
Si wafer 6.6 hPa 15 min	0.44
Si wafer 4.9 hPa 1 h	0.57
n-butane (NIST)	0.29
1-butene (NIST)	1000

3.3.2 Ammonia thermal desorption spectroscopy

Figure 3-3a, shows the desorption of ammonia (as indicated by the MS fragment NH) from a sulfated zirconia thin film. No significant desorption peaks are observed from the "blank" non-exposed surface. For the 49 hPa, 15 minutes exposure a broad peak from 373 to 423 K and a sharp peak centred at ca. 637 K are detected. Increasing the exposure pressure and time to 520 hPa and 1 hour results in considerable broadening of the high temperature peak, so much so that it appears as a continuous increase in desorption from ca. 353 K until ca. 710 K. There is still an additional peak around 413 K, although its

relative intensity is reduced because of the continuous increase in signal intensity from the main desorption feature. Analogous spectra are observed for each of the different exposures for hydrocarbon desorption fragments such as m/z = 43 (Figure 3-3b) and m/z = 28 and 40. Sulfate fragments (for example m/z = 64 from SO_2) are, however, only detected concomitantly with the high temperature peak for the 49 hPa, 15 minute, exposure and only at temperatures above 473 K for the 520 hPa, 1 hour, exposure. Such fragments are seen from the non-exposed film only at temperatures above 723 K.

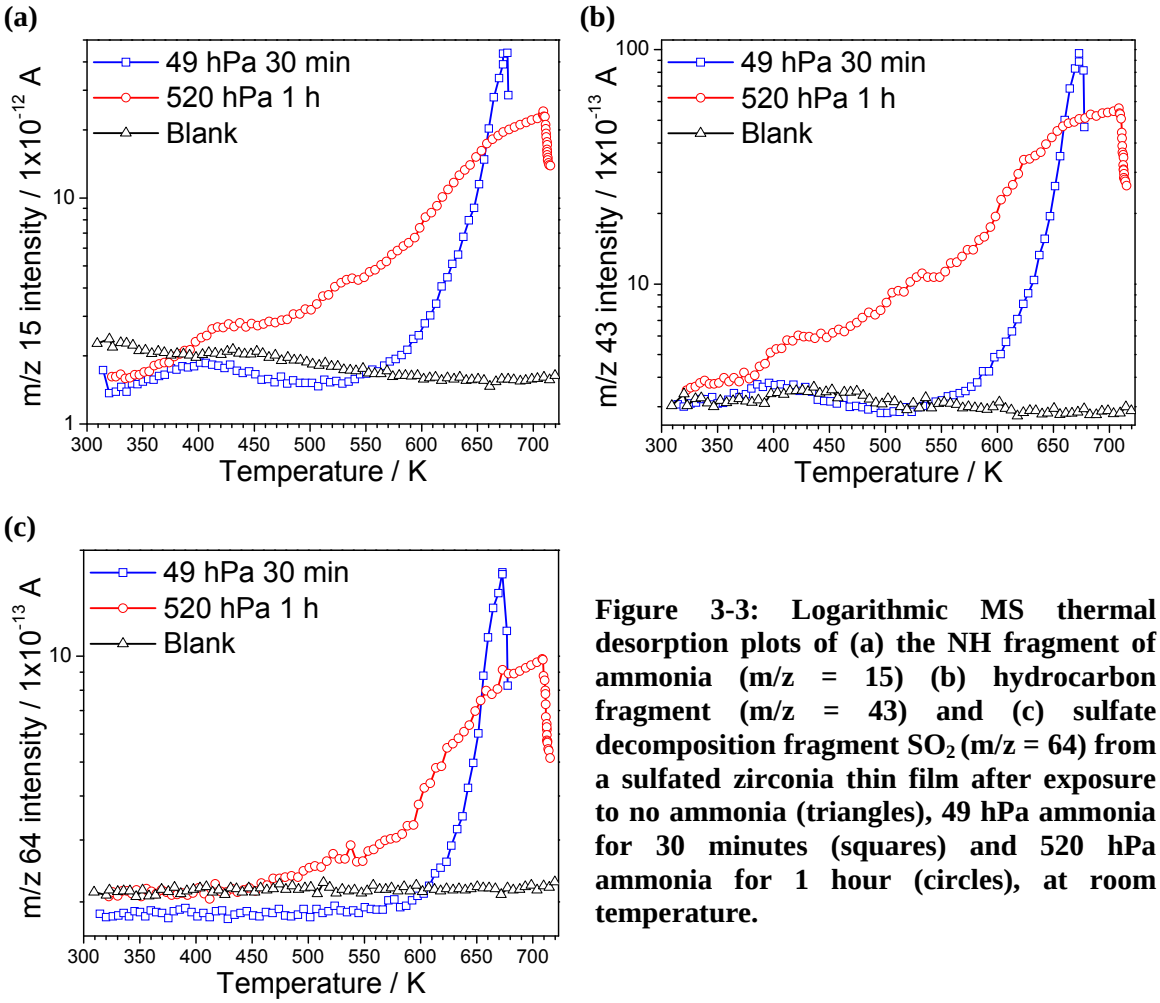

Figure 3-3: Logarithmic MS thermal desorption plots of (a) the NH fragment of ammonia (m/z = 15) (b) hydrocarbon fragment (m/z = 43) and (c) sulfate decomposition fragment SO_2 (m/z = 64) from a sulfated zirconia thin film after exposure to no ammonia (triangles), 49 hPa ammonia for 30 minutes (squares) and 520 hPa ammonia for 1 hour (circles), at room temperature.

3.4 Discussion

Adsorption of *n*-butane on both the sulfated zirconia thin films and oxidised silicon wafers is clearly seen by the MS detection of hydrocarbon fragments during the thermal desorption of the probe molecule. The apparent increase in the amount of adsorbed species on the sulfated zirconia thin film compared to the oxidised silicon wafer indicates

the presence of more adsorption sites; however, this may be due to an increase in surface roughness and hence also surface area. Desorption profiles from the sulfated zirconia thin film indicate the presence of at least two different adsorption sites. The temperature range over which desorption is seen from both the sulfated zirconia thin films and oxidised silicon wafers is similar, thus indicating an equivalent strength of interaction with the adsorbate.

From the increased m/z 41:43 ratio seen after the initial dosing of the sulfated zirconia thin film, as compared with measurements from the oxidised silicon wafers, it can be inferred that the sulfated zirconia thin films possess sites capable of dehydrogenation. This ratio may be lower than previously reported for temperature programmed desorption from active sulfated zirconia powders[27,63] due to the low fraction of tetragonal phase within the very thin (24 hour deposited) sulfated zirconia films used. Lower ratios seen for all subsequent measurements suggest these sites have been deactivated. Higher m/z 43:41 ratios are seen for all measurements as compared with the NIST *n*-butane ratio. This is possibly caused by the adsorption of trace impurities or the relative sensitivity of the MS used.

The shift to lower desorption temperatures and hence weaker adsorption sites with decreasing exposure pressure of *n*-butane is counter to the idea that the stronger adsorption sites are populated first – thus at higher exposure pressures desorption may be limited by diffusion (either thermal or gaseous) or incorrect due to a high background desorption. Increasing the heating rate leads to a broader desorption peak width, which also insinuates diffusion to be a limitation. Thus thermal desorption spectroscopy may not be the best technique to investigate the adsorption of *n*-butane on the sulfated zirconia thin films. Although, the detected desorption of hydrocarbons at relatively low temperatures from the sulfated zirconia thin films, after *n*-butane exposure, indicates a weak adsorption and thus is in good agreement with the small heats of adsorption (~45–60 kJ/mol) obtained for butanes on powder sulfated zirconia in calorimetric and temporal analysis of products (TAP) experiments.[27]

Ammonia desorption profiles obtained from the nanocrystalline sulfated zirconia films are in agreement with the findings of previous thermal desorption XPS studies[123] and are similar to those previously reported for active sulfated zirconia powder catalysts.[174] The

source of hydrocarbon fragmentation signals during thermal desorption is unclear. It could be that they are from ammonia reacting with adsorbates on the chamber walls, or the sample itself (i.e. adsorbed surface carbon or carbon remaining from the decomposition of the SAM), or a co-adsorbing impurity (although this is unlikely given the quality and increased adsorption strength of the ammonia). The reduction in sulfate stability is consistent with earlier reports of sulfated oxides (including sulfated zirconia) more readily undergoing decomposition upon exposure to basic probe molecules at elevated temperatures.[37]

3.5 Conclusions

The ammonia and *n*-butane adsorption experiments conducted on the nanocrystalline films detect two distinctly different types of sites. The stronger binding site has been shown to react with ammonia at high temperatures rather than release the basic probe, which is consistent with the literature.[37] Desorption of *n*-butane resulted in a broad peak at relatively low temperatures, which is also typical for powder sulfated zirconia samples. Fragmentation ratios indicating the formation of alkenes over the sulfate zirconia thin film were detected for the initial measurement. Thus the thin films have active sites capable of dehydrogenation, as has recently been shown for powdered sulfated zirconia. The application of thermal desorption spectroscopy to the sulfated zirconia thin films was, however, unable to yield any additional information above currently published reports. This is possibly due to the system limitations, resulting in relatively high background signals as compared with the amount desorbing from the small surface area of the sample. The adsorption properties of the nanocrystalline thin films could be shown to be equivalent to those of active powder sulfated zirconia catalysts.

4. Isobaric Measurements on Sulfated Zirconia Thin Films

4.1 Introduction

4.1.1 Determination of heats of adsorption

The quantitative determination of thermodynamic and kinetic parameters from adsorption and desorption studies, including heats of adsorption, are necessary for the understanding of adsorbate-adsorbent interactions. Such parameters are required for the development of adsorption models and therefore, also, the modelling of surface processes in heterogeneous catalysis.[214]

Heats of adsorption can be determined directly from calorimetric experiments {for example microcalorimetry or differential scanning calorimetry (DSC)}; however, measurements on flat surfaces are limited to very few systems because of the specific sample preparation prerequisites.[215] Irreversible adsorption processes and adsorbate-adsorbent reactions can be studied via calorimetry. Transient experiments on powders, such as temporal analysis of products, can also give data on both kinetic parameters and heats of adsorption. Modelling of diffusion parameters is however required.

Thermal desorption spectroscopy (TDS) [as discussed in Chapter 3] is widely used to determine thermodynamic and kinetic parameters of the adsorption of gases on flat surfaces. From TDS measurements the different types and number of adsorption sites can be evaluated. TDS, also, allows the activation energy for desorption (E_d) to be calculated. Only when adsorption is not an activated process does E_d equal the heat of adsorption. The determination of the reaction order and frequency factor for desorption are in principle possible as well, but very good TDS data is required. A further disadvantage of TDS is that adsorption must be performed at relatively low temperatures so that desorption does not occur. Adsorbate diffusion may therefore be kinetically limited, hence different states may not be sequentially occupied and thus equilibrium not achieved. Heating can therefore result not only in desorption but also the equilibration of states.

In order to overcome the problems associated with TDS measurements, adsorption-desorption (A-D) equilibrium methods, such as isotherms (constant temperature) or isobars (constant pressure), can be used.[216] Coverage-dependant isosteric (constant coverage) heats of adsorption can be deduced from the relative position of sets of

isotherms at different temperatures or isobars at different pressures using the Clausius-Clapeyron equation.[217]

As the Clausius-Clapeyron equation is deduced from thermodynamics, it is independent of the kinetics of adsorption and desorption. An equivalent equation can be derived from kinetic descriptions of adsorption and desorption using the Arrhenius law. The kinetic derivation is independent of the strength of interaction and is even valid for different gas and sample temperatures.[218]

In principle it is also possible to determine kinetic data from the shape of the isotherms or isobars, such as the reaction order for desorption and adsorption, the Kisliuk factor (which relates the dependence of the relative sticking probability on coverage) and the frequency factor for desorption.[216]

There are a number of prerequisites for the application of A-D equilibrium measurements, these include:

- Kinetics must be fast enough to establish equilibrium (i.e. the activation energy for adsorption must not be too high).
- The adsorbate must not decompose irreversibly on the surface.
- Adsorption must be reversible (the heat of adsorption must not be so high that equilibrium is strongly on the side of adsorption for the range of pressures and temperatures studied).

The equilibrium position is generally not a severe restriction when studying catalytic systems, as the relevant adsorbates are often not very strongly bound otherwise they would block the active sites.

4.1.2 Isobaric photoelectron spectroscopy measurements

Surface sensitive spectroscopic methods, such as photoelectron spectroscopy, can be used to measure adsorbate coverage under A-D equilibrium conditions. Evaluation of the spectroscopic data can therefore lead to information relating to how the adsorbate binds to the adsorbent, as well allowing the generation of isobars or isotherms.

UPS measurements under A-D equilibrium have been used to investigate a variety of systems. The Henzler group determined heats of adsorption of water on NaCl(100)[219] and KCl(100)[220]. Ranke and co-workers identified differing adsorption sites and heats of adsorption for ammonia on Ge(001), (113) and (111) surfaces;[216,221] and for water,

ethylbenzene and styrene on FeO(111), Fe_3O_4(111) and Pt(111) surfaces.[216,222-224] In the case of water, ethylbenzene or styrene adsorbed on FeO(111), Fe_3O_4(111) and Pt(111), isobar fittings have yielded reaction orders for desorption and adsorption, Kisliuk factors and frequency factors for desorption. XP spectra, measured also under adsorption-desorption equilibrium, have been used to support the assignments of the various adsorbate states and coverage determinations for water on FeO(111) and Fe_3O_4(111) surfaces. Isosteric heats of adsorption determined for water on FeO(111) and Fe_3O_4(111) are similar in value to heats of desorption deduced from TDS measurements on the same system.

4.1.3 Heats of adsorption of *n*-butane on sulfated zirconia

González *et al.*[225] measured *n*-butane heats of adsorption on two sulfated zirconia powder catalysts, which differed in catalytic activity by an order of magnitude, via microcalorimetry. They found that for both catalysts investigated initial *n*-butane doses (of 2-4 μmol/g) released heats of ~57 kJ/mol. The heats of adsorption on both catalysts linearly decrease with sequential *n*-butane doses, reaching a value of ~38 kJ/mol after an adsorption of 35 μmol/g. These heats of adsorption clearly differ from the heat of condensation of *n*-butane (22 kJ/mol).[226] The authors concluded that the difference in catalytic activity of the samples studied does not arise from an unusually strong affinity for the reactant molecule.

Li *et al.*[27] also investigated two sulfated zirconia powder catalysts; one active for *n*-butane isomerisation at 373 K, the other was inactive at this temperature and only reached a similar performance at 473 K. Differential *n*-butane heats of adsorption of approximately 50 kJ/mol were measured on both catalysts, for *n*-butane coverages of ca. 5 μmol/g. The heats of adsorption decreased to about 45 kJ/mol at a coverage of 30 μmol/g. At coverages < 5 μmol/g considerable variations in the differential heats of adsorption were observed, possibly indicating reaction on a minority of sites. The authors therefore concluded that the number of sites capable of dehydrogenation (their proposed reaction initiation pathway) must be less than 5 μmol/g.

TAP studies[227] on the sulfated zirconia samples described by Li *et al.*[27] indicate the adsorption of *n*-butane to be reversible on both samples. Heats of adsorption calculated from van't Hoff plots yielded values of 53 and 52 kJ/mol for the relatively active and

inactive materials, respectively. These values are in good agreement with calorimetric data on the same samples.

In a separate study, Li *et al.*[228] investigated by DSC sulfated zirconia prepared under different conditions from the aforementioned samples. Similar *n*-butane heats of adsorption, starting at approximately 60 kJ/mol (at low coverage) declining to 40 kJ/mol at 60 μmol/g, were obtained.

4.1.4 Aims

Given the difficulties in the application of TDS to the sulfated zirconia thin films (presented in Chapter 3), the interaction of *n*-butane with the films under A-D equilibrium was investigated using photoelectron spectroscopy. The application of low pressures and temperatures is ideally suited to study the adsorption of *n*-butane as sulfated zirconia is known to be catalytically active even at room temperature.[12]

The aims of performing isobaric studies on the sulfated zirconia thin films are to identify the various adsorption sites on the films and quantitatively describe how the isosteric adsorption heats of *n*-butane (the reactant) vary with coverage.

4.2 Experimental

4.2.1 Set-up

Samples were mounted for experiments on a sapphire sample holder using a stainless steel clip. The sample temperature was measured via a K-type thermocouple inserted into the side of the sample, as shown in Figure 4-1a. Validation of the thermocouple reading was performed using a silicon wafer and a pyrometer (silicon emissivity = 0.7);[229] differences in temperature readings from the thermocouple and pyrometer during heating of the silicon wafer were considered negligible (see Figure 4-1b and c). For the XPS isobaric measurements the samples were grounded through the clip, but for the UPS isobaric measurements they were grounded via the thermocouple to ensure good sample-thermocouple contact. The sample temperature was controlled by liquid N_2 cooling and resistive heating (for isobaric measurements) or electron bombardment (for *in situ* activation), in a similar setup to the one described in reference 212. The base pressure in the chamber was 2×10^{-10} hPa or lower. Atmospheric pressure activations were performed in an adjacent chamber with a flow directed across the sample and heating via a lamp

positioned in front of the sample.

4.2.2 XPS isobaric measurements

Interaction of both a calcined sulfated zirconia thin film and an oxidised silicon wafer with *n*-butane were studied using Al Kα excitation (hν = 1486.7 eV) XPS, with a pass energy of 50 eV. Scans of the Zr 3d, O 1s and C 1s regions were performed for experiments conducted on the sulfated thin films and the Si 2p, O 1s and C 1s regions for experiments on the oxidised silicon wafers. For each of the regions a step size of 0.05 eV and a dwell time of 0.1 second were used. Single scans were performed on all regions except the C 1s region. Initial measurements were performed with 2 scans for the C 1s region. Detailed measurements were performed with 4 or 5 scans of the C 1s region for the oxidised silicon wafer or sulfated zirconia thin film experiments, respectively.

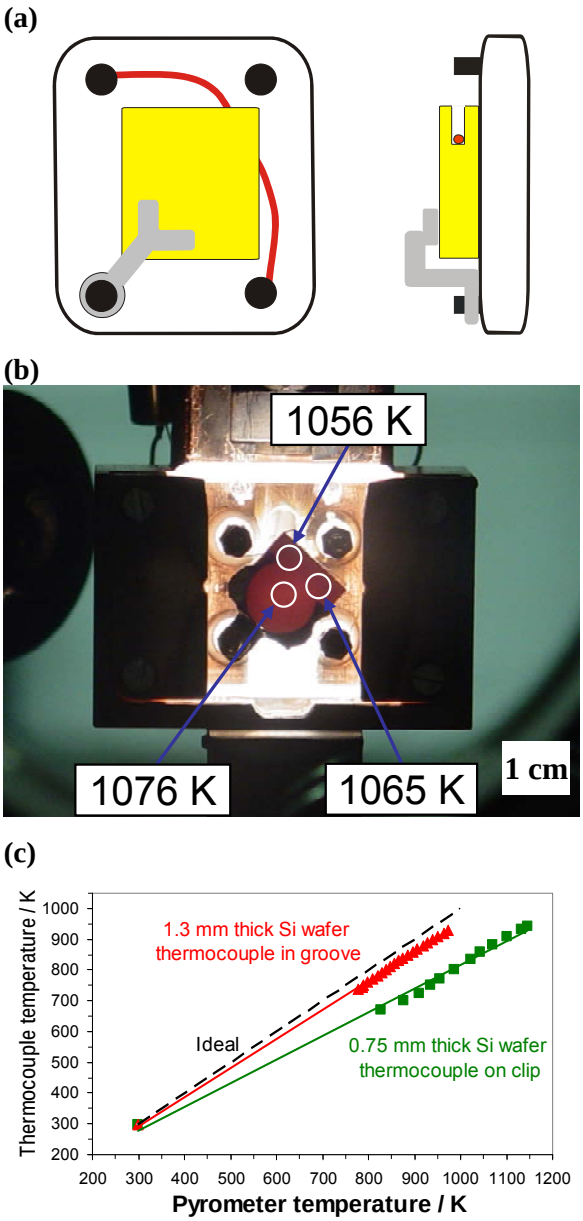

Figure 4-1: (a) Diagram of sample mounting, (b) pyrometer measurement of temperature gradient across sample at high temperature and (c) validation of thermocouple reading using a pyrometer.

Binding energies of the sulfated zirconia thin films were corrected to Zr $3d_{5/2}$ = 182.2 eV of ZrO_2,[154] and the binding energies of the oxidised silicon wafers were corrected using the elemental silicon component Si 2p = 99.7 eV of Si (100),[154] to account for temperature induced shifts. Shirley backgrounds were subtracted from all peaks apart from the C 1s, for which a linear background was used.

4.2.2.1 Initial XPS isobaric measurements

Initial measurements were performed on a sulfated zirconia film and an oxidised silicon wafer, both activated at 623 K in UHV with a temperature ramp of 20 K/min. Spectra of the UHV activated samples were recorded in A-D equilibrium, from room temperature to 100 K and back to room temperature, at *n*-butane pressures of 2.2×10^{-8} hPa and 2.2×10^{-7} hPa sequentially. Due to condensation of butane on the colder parts of the sample holder during the long exposure times at low temperatures, pressures of up to 10^{-5} hPa were observed while initially increasing the sample temperature. The electron analyser was switched off during these periods, typically between 100 and 140 K.

In order to determine the signal intensity of an "infinitely" thick carbon layer the sulfated zirconia thin film was also exposed to 1×10^{-6} hPa *n*-butane at 100 K until the signals originating from the sulfated zirconia film (Zr 3d, O 1s and S 2p) were no longer detectable.

A blind isobar experiment without X-ray irradiation was also performed on the oxidised silicon wafer, to investigate the effects of irradiation. The wafer was exposed to 2.2×10^{-7} hPa *n*-butane from room temperature to 100 K. XPS of the O 1s, C 1s and Si 2p regions were recorded prior to and immediately after the adsorption experiment at room temperature.

4.2.2.2 Detailed XPS isobaric measurements

Detailed isobaric measurements were performed on a reactivated oxidised silicon wafer and a new sulfated zirconia thin film, while decreasing the temperature. Activation of the sulfated zirconia thin film was performed at atmospheric pressure in a flow of 40 ml/min synthetic air at 573 K for 30 minutes (temperature ramp ~20 K/min). The air-activated sample was exposed to 2.2×10^{-8} hPa *n*-butane at temperatures from 200 K to 100 K. At 120 K the temperature was held constant for 40 minutes. The oxidised silicon wafer was reactivated at 623 K in 1×10^{-7} hPa O_2 for 1 hour, using a temperature ramp of ~20 K/min. The oxidised Si wafer was then exposed to 2.2×10^{-8} hPa *n*-butane while cooling from 200 K to 120 K.

4.2.2.3 Coverage determination from XPS isobaric measurements

C 1s Difference spectra, corresponding to the adsorbate signal, were obtained by subtracting the "clean" surface spectrum under UHV prior to *n*-butane exposure from the

spectra taken in A-D equilibrium. The area of the difference signal could be converted into a coverage dependant value using the Lambert-Beer absorption law {when coverage (θ) is defined as the number of adsorbed molecules divided by the total number of adsorption sites on the adsorbent}, as indicated in the below equation:

$$\theta \propto \frac{d}{l_e} = -\ln\left(1 - \frac{I_{ads}}{I_{0,ads}}\right)$$

Where d is the adsorbate thickness (averaged over the whole surface), l_e is the electron escape depth, I_{ads} is the adsorbate intensity and $I_{0,ads}$ is the intensity of an infinitely thick adsorbate layer. Hence, d/l_e is proportional to the adsorbate coverage. The escape depth is given by $l_e = \lambda_e \cos \alpha$, where λ_e is the electron mean free path and α the mean escape angle normal to the surface (for the system used the analyser is at 0°, therefore $l_e = \lambda_e$). λ_e depends strongly on the kinetic energy of the electrons and, albeit to a lesser degree, on the material the electrons are passing through. Reported values of λ_e (for various kinetic energies and materials) [154] can be used to estimate the adsorbate thickness, although wide error margins are to be expected due to the uncertainty in λ_e and the calculated values only have real meaning for full layer coverages. Calculated values are therefore quoted as equivalent adsorbate thicknesses.

4.2.3 UPS isobaric measurements

He II ($h\nu$ = 40.8 eV) ultraviolet photoelectron spectroscopy (UPS) was also used to study the interaction of *n*-butane with air-treated sulfated zirconia thin films and oxidised silicon wafers. Measurements were performed with a pass energy of 15 eV and a -5 V sample bias.

Secondary electron curves and He II satellite-induced emissions have not been subtracted from the UP spectra presented. Both binding energy and vacuum level (E_{vac}) aligned x-axis scales are given for all UP spectra (which differ by the work function of the spectrometer, 4.6 eV). Sample charging has not been evaluated.

4.2.3.1 Initial UPS isobaric measurements

Initial measurements were performed on an oxidised silicon wafer. Spectra were measured in A-D equilibrium at 1×10^{-6} hPa while decreasing the temperature from room temperature to 105 K, followed by holding the temperature constant at 105 K for 1 hour. In a subsequent experiment, the oxidised silicon wafer was cooled to 108 K and XP

spectra of the surface were taken. The sample was then exposed to $1x10^{-6}$ hPa *n*-butane and the change in signal followed by UPS. After 20 minutes XP spectra of the surface were taken. The XPS measurements were performed with a low resolution to minimise beam damage.

4.2.3.2 Detailed UPS isobaric measurements

Detailed measurements were performed on new samples activated at 573 K under atmospheric pressure in a flow of 40 ml/min synthetic air for 30 minutes, using temperature ramps of ~20 K/min. Spectra were measured in A-D equilibrium under constant *n*-butane pressures of $1x10^{-8}$, $1x10^{-7}$ and $1x10^{-6}$ hPa at temperatures from room temperature to ~110 K, sequentially. After each isobar the sample was moved out of the UV beam, the *n*-butane leak valve was closed and the sample was heated resistively up to room temperature. Before and after the sets of UPS isobars, XPS measurements of samples were performed in UHV.

After the set of UPS isobars the sulfated zirconia thin film was reactivated under the same conditions as for the original activation. The film was then exposed to $1x10^{-6}$ hPa at temperatures down to 100 K while turned out of the irradiating beam (a non-irradiated isobar). UP and XP spectra were recorded in UHV at room temperature prior to and after performing the non-irradiated isobar. The sulfated zirconia thin film was then reactivated again and exposed to $1x10^{-6}$ hPa *n*-butane for 3 hours at room temperature with He II UV irradiation. UP spectra were recorded after each hour and XP spectra of the sample were measured in UHV before and after the 3 hours *n*-butane exposure.

4.2.3.3 Coverage determination from UPS isobaric measurements

Difference spectra of the oxidised silicon wafer and sulfated zirconia thin film in A-D equilibrium have been analysed as outlined in reference 216. The clean spectrum obtained prior to performing the isobar was subtracted from the spectra taken under *n*-butane A-D equilibrium conditions, after applying an attenuation factor to the clean spectrum and shifting the energy scale of the spectra acquired under *n*-butane A-D equilibrium. The alignment shift and attenuation factor are applied such that there is not an increase in the difference spectra between binding energies of ~2.5-4 eV (where no spectral contributions from the adsorbate are expected). Misalignment of the spectra can result in the introduction of artificial structures, such artefacts are minimised by repetition

using differing alignment shifts and attenuation factors.

The attenuation of the clean spectrum can be converted into a coverage related value using the Lambert-Beer absorption law, using the following equation:

$$\theta \propto \frac{d}{l_e} = -\ln\left(\frac{I_{sub}}{I_{0,sub}}\right)$$

Where I_{sub} is the substrate (adsorbent) intensity and $I_{0,sub}$ is the substrate intensity prior to adsorption. Thus, ($I_{sub}/I_{0,sub}$) is the attenuation factor used to form the difference spectra.

The carbon layer thickness was estimated in a similar way for the XPS measurements of the silicon wafer after exposure to $1x10^{-6}$ hPa *n*-butane for 20 minutes at 108 K, using the attenuation of the Si 2p peak.

4.3 Results

4.3.1 Initial XPS isobaric measurements

C 1s XP difference spectra of the sulfated zirconia thin film under 10^{-7} hPa *n*-butane are shown in Figure 4-2a. An increase in the C 1s signal intensity is seen upon decreasing the temperature below ~140 K, concomitantly the substrate peaks (O 1s and Zr 3d) decrease in intensity, due to the adsorption of *n*-butane. Increasing the sample temperature from 100 K back to room temperature and evacuation results in a decrease of the C 1s signal; however, a significant fraction of the signal remains (approximately 35% of the signal at 100 K). The C 1s binding energy of the adsorbed species changes with increasing coverage from an initial value of ~284.3 eV at 136 K to ~284.8 eV at 100 K. Increasing the sample temperature shifts the C 1s signal to lower binding energies, after evacuation a peak at ~284.0 eV remains. No significant changes are observed in the Zr 3d and O 1s peaks beside a decrease in intensity with the increasing C 1s signal.

Repeating this experiment with an oxidised silicon wafer also results in the adsorption of *n*-butane at low temperatures and the formation of a carbonaceous species that remains after evacuation. A similar trend in shifts of the adsorbed species' C 1s signal is observed upon increasing coverage, increasing temperature and evacuation.

The initial isobars on both the sulfated zirconia thin film and oxidised silicon wafer performed under 10^{-8} hPa *n*-butane also show the formation of carbonaceous deposits which remain after evacuation. The total adsorbate coverage on the samples during the

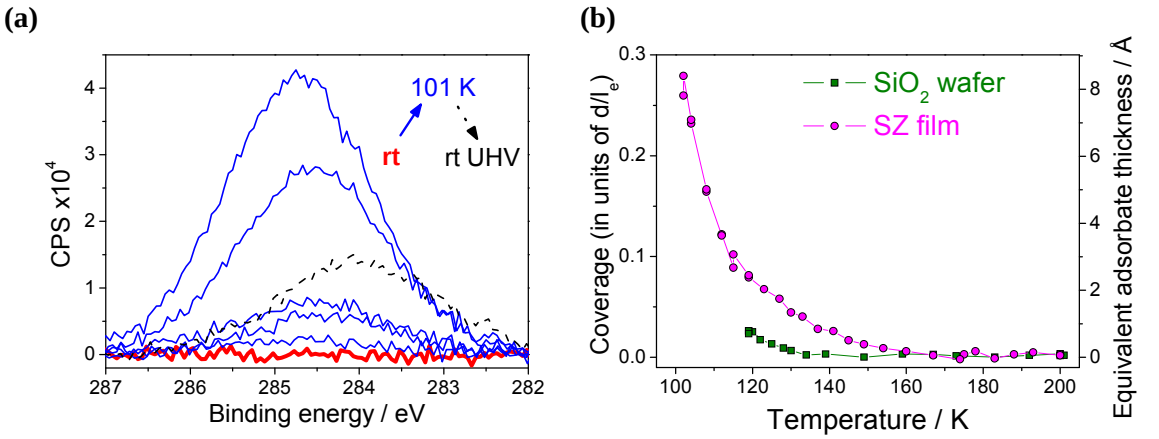

Figure 4-2: (a) "Clean" (as introduced) subtracted C 1s XP spectra of a sulfated zirconia thin film under A-D equilibrium of 2.2×10^{-7} hPa *n*-butane measured while decreasing temperature from room temperature to 100 K (solid lines) and after increasing temperature to room temperature and evacuation (dashed line). (b) 2.2×10^{-8} hPa *n*-Butane isobars on a sulfated zirconia thin film and oxidised silicon wafer.

10^{-8} hPa isobars is much lower than for the 10^{-7} hPa isobars (by roughly a factor of 2), as is the fraction that is irreversibly adsorbed (~10%).

No differences (given the large experimental errors of the initial measurements) were observed between the sulfated zirconia film and the oxidised silicon wafer regarding the adsorption of *n*-butane or the formation of carbonaceous residues.

Performing a "blank" isobaric experiment on the oxidised silicon wafer, without irradiating during *n*-butane exposure, results in no significant changes in the carbon signal. The carbon deposits that are not removed after evacuation are thus attributed to decomposition of the adsorbate by irradiation and are hereafter referred to as beam damage residues. The amount of beam damage residue formed is found to be proportional to the adsorbate coverage.

4.3.2 Detailed XPS isobaric measurements

Isobars derived from detailed XPS measurements are shown in Figure 4-2b. Measurements of the air-activated sulfated zirconia film at a constant temperature during adsorption do not show a significant increase in adsorbate coverage with time (in comparison to changes with temperature), thus the fraction of adsorbate coverage that is beam damaged during the measurement is considered negligible. Adsorption on the sulfated zirconia thin film under 10^{-7} hPa *n*-butane is initially detected at ~150 K and significantly increases below 120 K. The adsorbate coverage on a sulfated zirconia thin film is clearly higher than for the oxidised silicon wafer under the same conditions

between 150-120 K.

4.3.3 Initial UPS isobaric measurements

UP spectra of an oxidised silicon wafer under UHV (clean) and in $1x10^{-6}$ hPa *n*-butane are shown in Figure 4-3a. As the temperature is decreased all signals shift to higher binding energies, which may be caused by band bending[230] at the silicon-oxide interface, photovoltaic effects[231,232] and possibly also changes in charging from the oxide overlayer. In the presence of an adsorbate, shifts are also possible as a result of changes in the work function.[216] Upon cooling, the shape of the spectra changed indicating adsorption of *n*-butane. A decrease in overall signal intensity during adsorption is observed, clearly from the adsorbate having a lower photoelectron cross section than the adsorbent. At low temperatures (below 110 K) the overall signal significantly reduces in intensity with time. XPS measurements (taken with low resolution in order to minimise beam damage) of the oxidised silicon wafer at 108 K in UHV and after exposure to $1x10^{-6}$ hPa for 20 minutes show the deposition of carbon species with binding energies up to 10 eV higher than the initial carbon signal (Figure 4-3b). C 1s binding energies of above 292 eV are only possible from carbon bonded to fluorine,[154] which is not present (as shown by XPS); therefore, the thick adsorbate is obviously strongly charging due to the insulating nature of its adsorption state. It is shifted so far towards higher binding energies in the UP

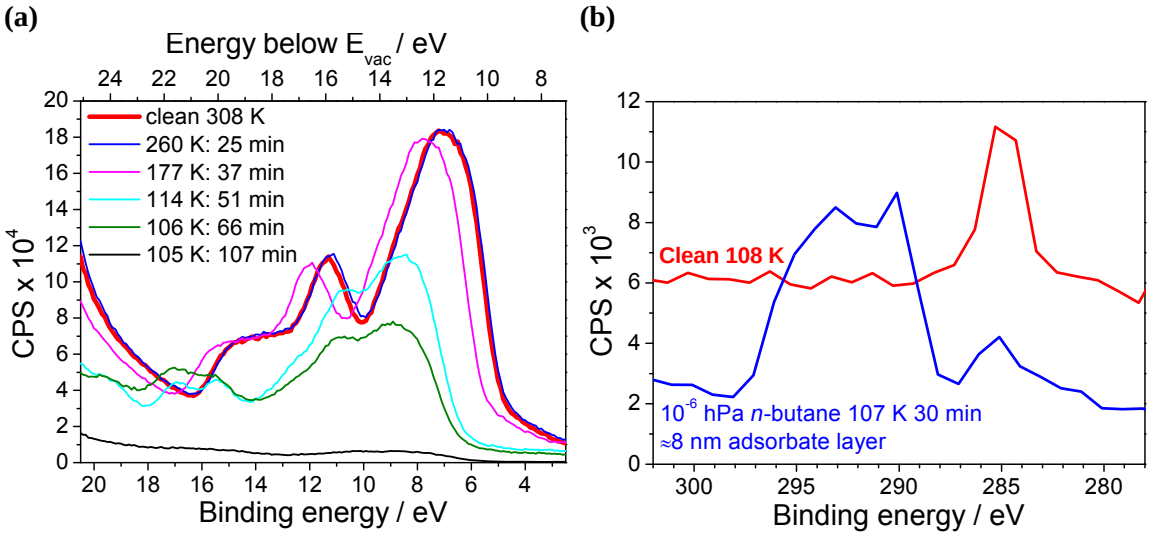

Figure 4-3:(a) UP Spectra of an oxidised silicon wafer as introduced (clean) at room temperature under UHV and under $1x10^{-6}$ hPa *n*-butane A-D equilibrium conditions from room temperature to 105 K, time exposed to *n*-butane given in minutes. (b) C 1s XP Spectra of "clean" oxidised silicon wafer at 108 K under UHV and after 30 minutes exposure to $1x10^{-6}$ hPa *n*-butane.

spectra that it disappears from the measured range. Only a minority contribution of uncharged adsorbate is still observed.

4.3.4 Detailed UPS isobaric measurements

UP spectra of the samples taken before and after each of the isobars in UHV show the build up of deposits that are not removed by evacuation (Figure 4-4), which increase with increasing pressure of the isobaric measurement (up to $d/l_e \approx 0.05$). Such deposits are present for both experiments performed on the oxidised silicon wafer and the sulfated zirconia thin film. These deposits detected by UPS are, however, below the XPS limits of detection.

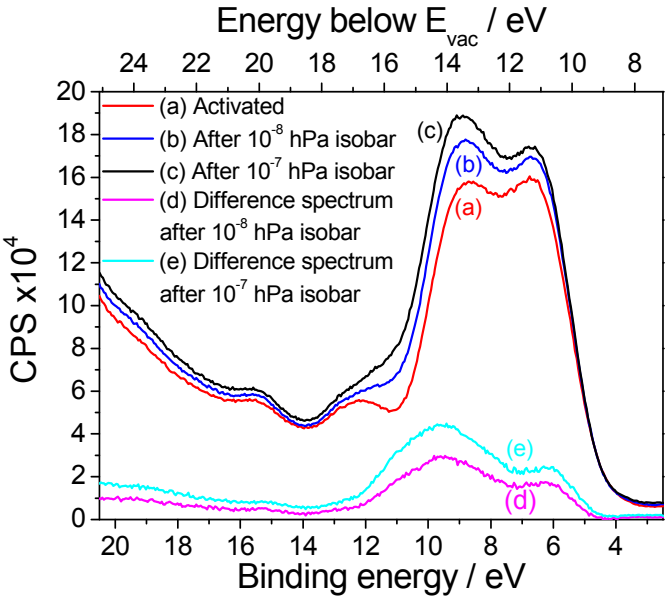

Figure 4-4: UP spectra of sulfated zirconia thin film after activation, 10^{-8} and 10^{-7} hPa *n*-butane isobars (prior to 10^{-7} and 10^{-6} isobars) and regeneration. Difference spectra indicating the "irreversible" adsorption formed after the 10^{-8} and 10^{-7} hPa *n*-butane isobars (prior to 10^{-7} and 10^{-6} isobars) also shown.

Regeneration of the sulfated zirconia thin film after the set of three isobars results in the removal of the majority of species remaining after evacuation. Exposing the regenerated sulfated zirconia to 1×10^{-6} hPa *n*-butane at 100 K without irradiation or for 3 hours at room temperature irradiating with He II radiation does not result in the valence band changing in shape. Therefore, the deposited species remaining after the isobaric measurements are beam damage residues and UV irradiation of the sample does not induce adsorption.

To limit the effect of the beam damage residues, the spectrum obtained (in UHV) immediately prior to each isobar is subtracted from the spectra obtained in A-D equilibrium to produce the difference spectra. Difference spectra (from both systems studied) generated for measurements performed under *n*-butane A-D equilibrium show the development of spectral features that resemble those of gaseous *n*-butane[233] but are significantly broadened. Adsorption is observed at relatively higher temperatures than

during the XPS measurements, probably because of to the increased surface sensitivity of UPS.

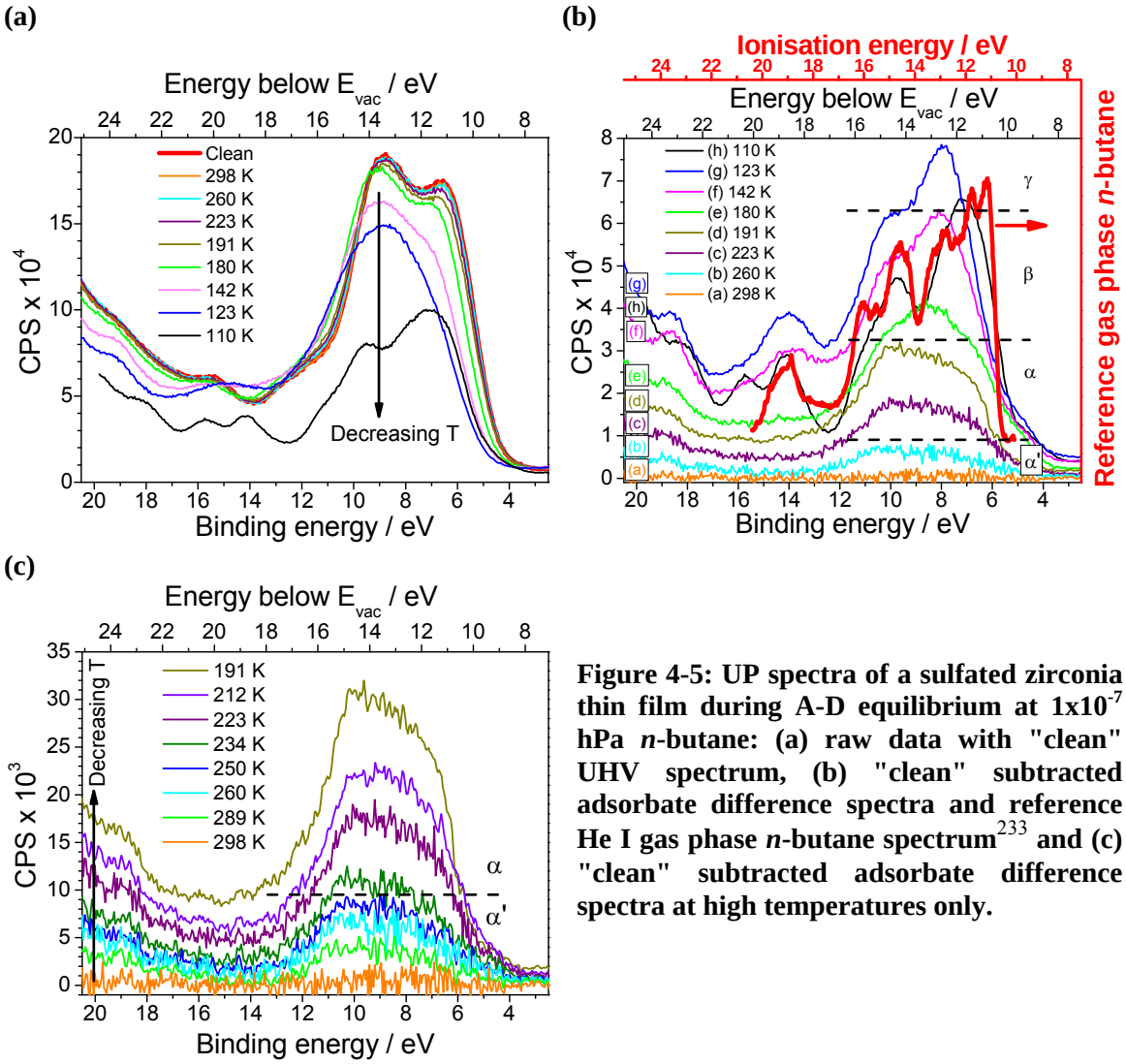

Figure 4-5: UP spectra of a sulfated zirconia thin film during A-D equilibrium at 1x10^{-7} hPa *n*-butane: (a) raw data with "clean" UHV spectrum, (b) "clean" subtracted adsorbate difference spectra and reference He I gas phase *n*-butane spectrum[233] and (c) "clean" subtracted adsorbate difference spectra at high temperatures only.

The sulfated zirconia difference spectra from the 10^{-6} hPa *n*-butane isobar are shown in Figure 4-5b and c, similar spectral changes are observed for the difference spectra obtained from the 10^{-8} and 10^{-7} hPa *n*-butane isobars. At low coverages ($d/l_e < 0.3$, labelled region α) the difference spectra are significantly perturbed (compared with the gas phase spectrum), indicating a strong interaction. Above a certain coverage ($0.3 < d/l_e < \sim1$, labelled region β) the development of features that resemble the gaseous spectrum of *n*-butane[233] becomes apparent, suggesting a low level of perturbation and hence a weak interaction. At high coverages ($d/l_e > \sim1$, labelled region γ) the overall intensity of the spectra decreases, due to charging as indicated by XPS measurements. Isobars generated

from the attenuation of the adsorbent indicate the α region can be further split into two different states, labelled α' for low coverages ($d/l_e < 0.05$) and α for higher coverages ($0.05 < d/l_e < 0.3$) in Figures 4-5c and 4-6b.

(a)

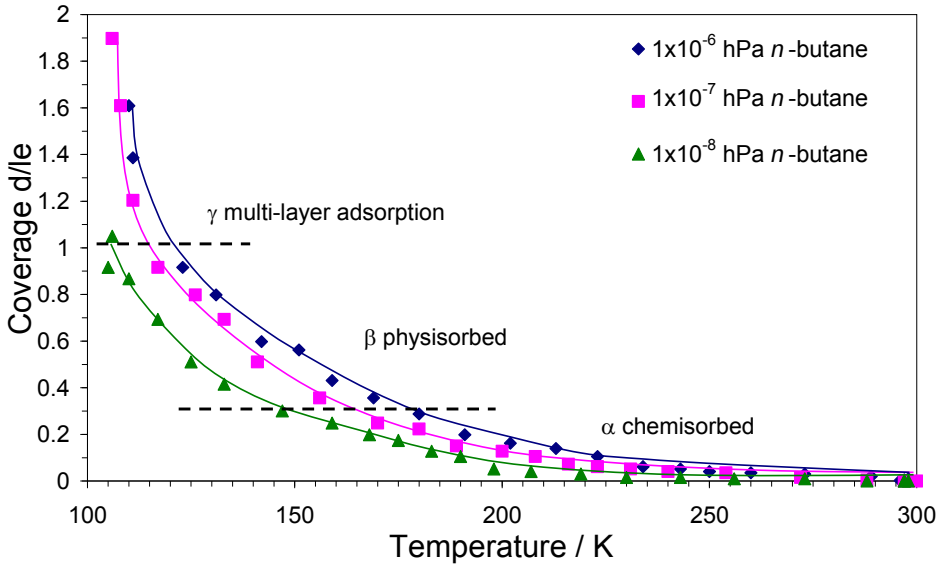

(b)

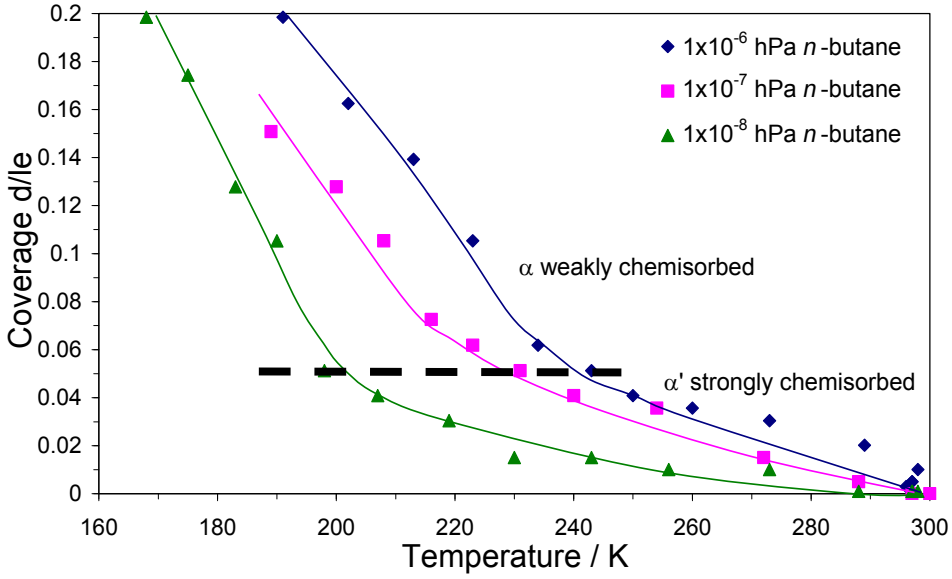

Figure 4-6: Isobars derived form A-D equilibrium UPS measurements on a sulfated zirconia thin film, (a) complete isobars and (b) initial coverages only.

Heats of adsorption (Figure 4-7) calculated from the isobars decrease initially from 69-41 kJ/mol with increasing coverage during the α' region; they then increase to ~47 kJ/mol and decrease again to 34 kJ/mol with increasing coverage in the α region; values of ~28 kJ/mol independent of coverage are obtained in the β region.

4.3.5 *n*-Butane adsorption and sulfate surface site densities

XPS measurements show the Zr:S atomic ratio (based on the Zr 3d and S 2p peak areas and reported relative sensitivity factors[155]) of the activated sulfated zirconia thin film to be 5.4. Thus assuming a homogeneous distribution of S and Zr within the thin film over the XPS measurement depth, a sulfate surface area of 31 Å²[178] and a zirconia surface 2 x 2 unit cell of 6.425 x 7.284 Å,[62] the sulfate groups are shown to cover ~33% of the surface, which is equivalent to a surface site density of ~1.1x10^{18} S atoms/m².

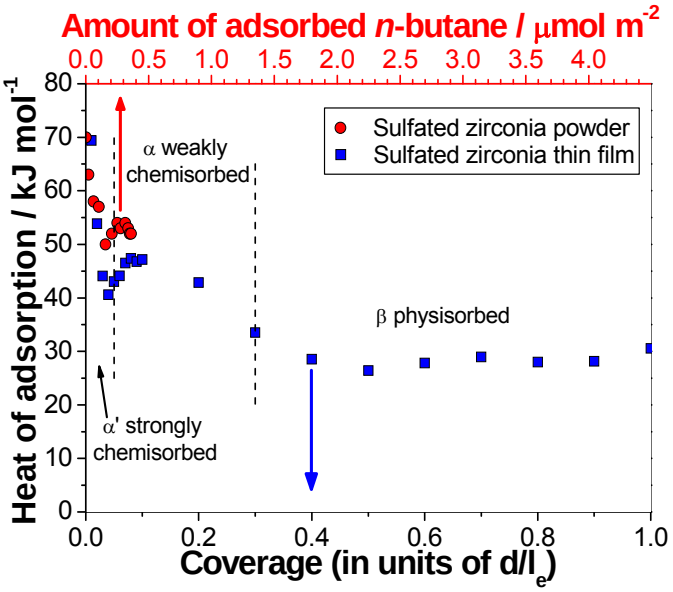

Figure 4-7: *n*-Butane heats of adsorption on a sulfated zirconia thin film (from isobaric measurements) and on a sulfated zirconia powder[242] (from microcalorimetric measurements). Amount of *n*-butane adsorbed on the sulfated zirconia powder is aligned to the *n*-butane coverage of the sulfated zirconia thin film assuming a cross sectional area of 33.2 Å² per butane molecule.[234]

Based on an *n*-butane cross sectional area of 33.2 Å², as determined for a monolayer coverage of *n*-butane on MgO,[234] a monolayer of *n*-butane thus corresponds to a total of 3.0x10^{18} molecules/m². Therefore, the 5 and 25% monolayer coverage adsorption regions α' and α equate to *n*-butane surface densities of approximately 1.5x10^{17} and 7.5 x10^{17} molecules/m² respectively, or a total of 0.9x10^{18} molecules/m².

4.4 Discussion

Organic materials are known to be sensitive to beam damage due to their insulating nature and relatively weak bonds.[235] Beam damage of organic materials is believed to be caused by low energy (secondary) electrons,[236] which are formed by the inelastic scattering of photoelectrons in a cascading effect.

From isobaric XPS measurements it was found that a small fraction of the total adsorbate coverage undergoes beam damage, resulting in the formation of residues that remain after evacuation. However, experiments performed on fresh samples during decreasing

temperature show the effect of beam damage during the measurement to be negligible. The adsorption of *n*-butane could thus be shown to be promoted on the sulfated zirconia thin film compared to an oxidised silicon wafer.

To deduce isosteric heats of adsorption, multiple isobars at different pressures would need to be performed on the same surface; this could be done in principle by only studying the initial stages of adsorption or reactivating the sample after each isobar. If just the very low coverages were to be studied (which can be considered the catalytically relevant chemisorption states), the amount of beam damage could be considered insignificant. However, in practice, differentiating between the interesting adsorbate coverages and levels at which beam damage becomes significant during an experiment is very difficult. Reactivating of the samples after each isobar to remove the beam damage residues may also result in changing surface chemistry (for example the OH coverage). In order to perform multiple isobars on the same surfaces UPS was used instead of XPS to avoid beam damage. As the excitation energy of He II UV radiation is much lower than for Al Kα X-ray radiation (48.8 eV vs. 1486.7 eV), significantly less low energy secondary electrons are expected from the cascading of inelastically scattered photoelectrons.

Measuring the adsorbate coverage during *n*-butane A-D equilibrium using UPS drastically reduces the amount of beam damage residue compared to XPS (to below the XPS detection limit). However, beam damage residues are still seen by UPS. In order to reduce adsorbate irradiation (and hence limit beam damage effects) UPS isobars were performed only while decreasing the sample temperature, the sample was turned out of the beam while the temperature was increased and subsequent isobars were performed at higher pressures.

The UP spectra of the beam damage residues (Figure 4-4) are similar to graphitic species.[223] The high signal intensity of such species and low attenuation factor of the clean spectrum indicate that the residues probably form 3-dimensional islands. As the reported heats of adsorption of *n*-butane on graphitic materials (32.6-33.9 kJ/mol)[237-239] are much lower than for sulfated zirconia and the shape of the difference spectra generated do not change with increasing pressure of the isobaric measurements (and hence also amount of beam damage residues), it is therefore assumed that at low coverages (during chemisorption) adsorption occurs on the sulfated zirconia film and not

on the beam damage residues. Saturation coverages of the different adsorption sites, as indicated by changes in the UP spectra and isobar gradients, are not influenced by the increase of the beam damage residues for subsequent measurements. The reduction in surface area of the sulfated zirconia film by beam damage residues is thus considered negligible.

The development of an adsorbate state that charges at higher coverages is believed to be due to either the formation of multilayers or a change in adsorption geometry (Figure 4-8). XPS measurements of the *n*-butane exposed oxidised silicon wafer, after the UPS signal is significantly reduced, reveal the adsorbate coverage to be in excess of a typical monolayer (when a monolayer is defined as the complete occupancy by the adsorbate of all adsorbent adsorption sites). Thus a multi-layered adsorbate structure must exist. However, the change in the shape of the spectra as well as their reduction in intensity at very low temperatures indicates that the adsorption geometry of the initial adsorption states may change as well. The charging adsorbate state was not seen during XPS isobaric measurements, thus it may have been decomposed by X-ray irradiation. As the charging state is only observed at high coverages (i.e. during multilayer adsorption) it is not considered relevant to catalytically active sites and hence has not been further investigated. The detailed UPS A-D equilibrium measurements were therefore discontinued when a significant decrease in signal intensity was observed.

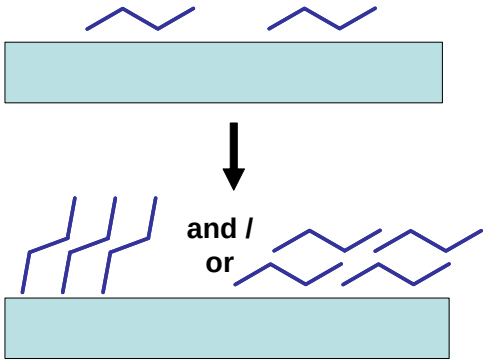

Figure 4-8: Proposed adsorbate charging model.

Difference spectra generated from UPS measurements on the sulfated zirconia thin film indicate that at lower coverages the adsorbate interacts more strongly with the adsorbent, this is clear from the shape of the valence band relative to the *n*-butane gaseous spectrum and the higher valence band binding energies. Three of the four adsorbed *n*-butane C 2s orbitals are observed (between binding energies of 13-20 eV), the fourth orbital is assumed to be hidden by the secondary electron curve; only one C 2s orbital (ionization energy = 19 eV) of the gas phase *n*-butane is visible due to the lower excitation energy used (He I = 21.2 eV as opposed to He II = 40.8 eV). The gas phase *n*-butane spectrum is

shifted by -0.4 eV, with respect to the vacuum level aligned scale of the adsorbate spectra, due to the relaxation effect (although, as the sulfated zirconia thin film and hence also the adsorbate may be charging, the absolute relaxation shift could be larger than the value given here).

The mean free path of the photoelectrons during the UPS measurements is approximately 0.5 nm,[158] which is similar to the thickness of a complete *n*-butane monolayer coverage reported on various surfaces {0.41 nm on MgO (100)[234] and Ag (111)[240]}. The saturation of the β state, which occurs at $d/l_e \approx 1$, is therefore attributed to the completion of a monolayer coverage. The surface of the sulfated zirconia thin film can therefore be described as approximately 5% region α', 25% region α and 70% region β. Considering the heats of adsorption and spectral features the adsorption states α', α and β are attributed to strong chemisorption, weak chemisorption and physisorption, respectively. The region γ is attributed to multilayer adsorption, it is not necessarily condensation as such a state has been reported to occur only after 2.5 monolayers on multiwalled carbon nanotubes (which have lower heats of adsorption than sulfated zirconia).[241]

Initial *n*-butane heats of adsorption obtained on the sulfated zirconia thin film of ~59 kJ/mol are in good agreement with previously reported results on sulfated zirconia powders (50-60 kJ/mol),[27,225,227,228] as is the general trend of the heats to decrease with increasing coverage. An increase in the heats of adsorption with increasing *n*-butane coverage, as seen in the α region on the sulfated zirconia thin films, has also been observed on some powder sulfated zirconia materials[242] (as shown in Figure 4-7). Such an increase may be due to adsorbate-adsorbate interactions. The presence of adsorbate-adsorbate interactions would indicate the alkane molecules are situated next to one another. The skeletal isomerisation process proceeding via a bimolecular mechanism is thus plausible under such surface coverages.

Aligning the amount of *n*-butane dosed onto the sulfated zirconia powder with the coverage of the sulfated zirconia film in Figure 4-7, assuming a cross sectional area of 33.2 Å² per butane molecule {as measured on MgO(100)},[234] reveals the onset of increase in adsorption heats to occur at approximately the same loadings on both materials. The heats of adsorption during the α region for the sulfated zirconia thin film are slightly lower than for the presented powder material (~47 kJ/mol versus 52-54

kJ/mol), however they are within the range of reported values on powders at higher coverages (45 kJ/mol[27] for 0.20 μmol/m², 38 kJ/mol[225] for 0.36 μmol/m² and 40 kJ/mol[228] for 0.55 μmol/m²).

The calculated sulfur surface site density assumes a homogeneous distribution of sulfur and zirconium throughout the XPS measurement depth of the sulfated zirconia thin film. It is, however, often assumed that the sulfate groups are situated on the surface of zirconia crystals. The sulfate surface density was also estimated assuming a sulfate layer on top of a zirconia film, taking into account the attenuation of the zirconium signal.[243] Such a model results in the calculated thickness of the sulfate layer being in excess of a monolayer coverage, which is not considered viable given the preparation route of the zirconia thin films and the fact that polymeric sulfates (higher than disulfates) were not observed by theoretical studies.[62]

Previously reported IR studies indicate the adsorption of *n*-butane to occur on hydroxyl groups on sulfated zirconia.[244] Furthermore, XPS investigations on the interaction of sulfated zirconia thin films with *n*-butane under reactive conditions (see Chapter 5) show the attenuation of the zirconium signal to be greater than sulfur upon carbon deposition. However, given the similar coverages and densities of the chemisorbed *n*-butane (α' and α) and sulfate surface sites, chemisorption of *n*-butane is therefore proposed to occur not on the surface sulfate species but in close proximity to them. As the surface areas (and hence structures) of both sulfate and *n*-butane molecules are assumed (based on literature values) the correlations between the activated sulfate and total chemisorbed butane surface coverages or densities are surprisingly good.

4.5 Conclusions

The adsorption of *n*-butane on sulfated zirconia thin films and oxidised silicon wafers under A-D equilibrium conditions has been detected by XPS and UPS. The conducting nature of the thin films used is essential in order to investigate the interaction with *n*-butane under A-D equilibrium conditions by UPS.

Irradiation of adsorbed *n*-butane during XPS and UPS measurements results in the formation of beam damage residues (although to a much lesser degree using UPS). The application of specific experimental conditions showed that beam damage could be

considered negligible for single XPS isobars or multiple UPS isobar measurements. XPS isobaric measurements have thus shown the sulfated zirconia thin films to promote the adsorption of *n*-butane as compared to an oxidised silicon wafer.

UPS isobaric measurements showed the chemisorption of *n*-butane on the sulfated zirconia thin films occurs via the sequential filling of two different sites; with coverages of 0-0.05 and 0.05-0.3; and heats of adsorption from 59-40 and 47-34 kJ/mol, respectively. The chemisorption of *n*-butane is proposed to occur in the close proximity of surface sulfate groups on sulfated zirconia. Physisorption on the films results in heats of ~28 kJ/mol for coverages between 0.3 up to a monolayer saturation. Multilayer adsorption results in the formation of an insulating adsorbate structure. *n*-Butane adsorbs reversibly on the sulfated zirconia thin film under the conditions studied.

The detection of adsorbate-adsorbate interactions during the weak chemisorption region indicates the alkane molecules are adsorbed in close proximity to one another. Alkane isomerisation proceeding via a bimolecular mechanism is thus considered viable under such coverages.

5. Interaction of *n*-Butane with Sulfated Zirconia Thin Films under Reaction Conditions

5.1 Introduction

5.1.1 XPS of sulfated zirconia

The application of photoelectron spectroscopy to study sulfated zirconia powders is hindered due to the insulating nature of the oxide. Electrostatic charging results in the binding energy scale needing to be corrected by typically 3.5 to 7 eV.[83] The necessity to calibrate the energy scale can cause some uncertainty in the exact binding energies and thus has lead in some cases to the discussion of relative shifts.[245] Various binding energies have been reported for the Zr $3d_{5/2}$ peak of ZrO_2, from 182.0 to 182.8 eV.[154,246-249]

5.1.2 XPS of deactivated sulfated zirconia

Studies on deactivated sulfated zirconia samples by XPS have shown the appearance of a very minor amount of S^{4+} (at ~166-167 eV).[83] These findings are consistent with an earlier report from the same group of the presence of S^{4+} in deactivated platinum containing sulfated zirconia.[250] In both reports no S^{2-} was detected, this has been confirmed by the sulfidation of Pt containing sulfated zirconia, which results in the appearance of an additional peak at ~162.5 eV.[251]

5.1.3 XPS on zirconia thin films

In a recent study Chang and Doong[252] reported the effects of different temperatures and atmospheres (air or nitrogen) during thermal treatment of zirconia films on their chemical composition and crystalline properties, determined by XPS and XRD respectively. Fitting of the O 1s spectra revealed two components, one at 529.9 eV and the other at 531.5 eV that are ascribed to Zr-O and Zr-OH respectively. The Zr 3d is fitted using a separation of 1.08 eV between the different zirconium oxidation states taken from reference 248, into Zr^{4+}, Zr^{3+}, Zr^{2+} and even Zr^{+}. From comparing the phase transformation temperatures deduced from the XRD data with the XPS results it was concluded that the reduction of Zr^{4+} to lower oxidation states and the generation of oxygen vacancies play crucial roles in stabilizing the formation of the meta-stable tetragonal phase. It must be noted however that reduced fractions of Zr^{4+} were only detected in the "bulk" measurements of the films, after the original surface had been removed by argon bombardment. The application of argon bombardment is, however, known to potentially chemically alter samples.[243]

5.1.4 XPS on sulfated zirconia thin films

Jentoft *et al.*[123] presented XP spectra for a sulfated zirconia thin film as deposited, after calcination (in an adjacent preparation chamber) and after He sputtering. Charging corrections (using Zr $3d_{5/2}$ = 182.2 eV)[154] of only 2.0 eV (as deposited) and 1.7 eV (calcined) were applied, which are significantly less than for sulfated zirconia powders. Calcination was shown to remove almost all of the carbon (the main C 1s component at 284.5 eV). The O 1s peak is shown to consist of at least two components, one at 530 eV assigned to O^{2-} of ZrO_2 and one at 531.5 eV, the latter of which is significantly reduced relative to the other and shifts slightly to higher binding energies after calcination and almost disappears after sputtering. The S 2p maximum is shown to shift after calcination from 168.4 eV to 169.0 eV, which is consistent with the presence of S^{6+}. After sputtering the S 2p signal shifts to 161.2 eV, which is consistent with S^{2-}. The disappearance of the oxygen species and the high binding energy oxygen species strongly suggest that the O 1s peak at 531.8 eV belongs to the sulfate species.

5.1.5 Motivation

In order to increase the resolution of the XP spectra, and in particular of the sulfur species, high resolution XPS has been applied to a sulfated zirconia thin film using a synchrotron light source. The use of a specialised, differentially pumped, set up allowing *in situ* XPS studies at relatively high pressures (up to ~0.5 hPa) has also been employed.[253] *In situ* investigations on sulfated zirconia are essential, given the reacted catalysts are known to undergo chemical changes upon exposure to air.[254] The effects of activating the sample in oxygen and exposing the sample to *n*-butane under reactive conditions have thus been studied by *in situ* XPS to evaluate any changes that may be due to the formation and removal of catalytically active sites. Carbon K edge near edge X-ray absorption fine structure spectroscopy (NEXAFS) was also performed in order to determine the nature of any carbonaceous deposits formed on the film's surface.

5.2 Experimental

The experiment was performed using the undulator beam line U49-2/PGM2 at the Berlin synchrotron facility (BESSY, Berliner Elektronenspeicherring-Gesellschaft für Synchrotronstrahlung), details of the setup are described in reference 253. The sample, a

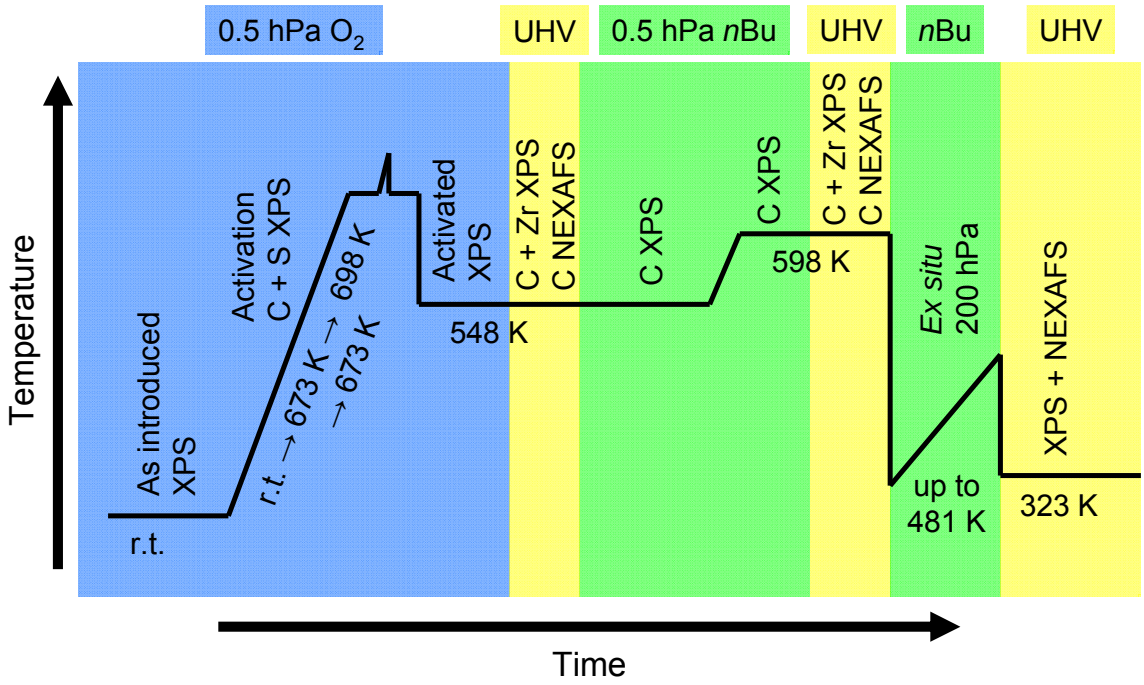

Figure 5-1: Schematic of the experiment performed at the BESSY synchrotron facility. *n*Bu = *n*-butane.

calcined sulfated zirconia thin film deposited over 48 hours on a 1.3 mm n-type silicon wafer with a groove drilled into the side for the thermocouple placement, was mounted on a sapphire holder. A schematic of the conducted experiment is shown in Figure 5-1.

Activation was performed in 0.5 hPa oxygen, the sample was heated at 10 K/min to 673 K for 25 minutes and flashed at 698 K. The sample temperature was then lowered to 548 K and held for approximately 165 minutes, following which the chamber was evacuated to 10^{-7} hPa for approximately 20 minutes in order to remove all gaseous oxygen and then filled with 0.5 hPa *n*-butane. The sample was exposed to 0.5 hPa *n*-butane at 548 K for 70 minutes, during which the irradiated spot position on the sample was changed, then the temperature was ramped at 10 K/min to 598 K and held for 30 minutes. After *n*-butane exposure the chamber was evacuated to 10^{-7} hPa for 45 minutes and the irradiated spot position was changed again. To increase the level of carbon deposition the sample was then cooled and removed from the main chamber to an *ex situ* reactor and exposed to 100 hPa *n*-butane during heating from 323 K to 481 K at 10 K/min. After evacuation and transfer back into the main chamber, post exposure measurements were performed at 323 K under 10^{-7} hPa.

XP spectra of the Zr 3d, O 1s, S 2p, S 2s, C 1s, Si 2p, Si 2s regions and overview survey

scans were performed on the sulfated zirconia film (i) as introduced, measured in 0.5 hPa oxygen at room temperature, (ii) after activation, measured in 0.5 hPa oxygen at 548 K and (iii) after being exposed to 100 hPa *n*-butane, measured under vacuum at 323 K. The S 2p and C 1s regions were also scanned during activation in 0.5 hPa oxygen from room temperature to 698 K. Spectra of the C 1s and Zr 3d regions were recorded prior to and after exposure to 0.5 hPa *n*-butane, under vacuum at 548 and 598 K respectively and the C 1s region was recorded during exposure to 0.5 hPa *n*-butane at 548 and 598 K. NEXAFS of the C K edge was performed prior to *n*-butane exposure on the activated surface and after exposure to 0.5 hPa and 100 hPa *n*-butane under vacuum.

The survey scan, O 1s, C 1s, Zr 3d, S 2p, Si 2s, and Si 2p XP spectra were recorded using photon energies of 720, 720, 470, 380, 350, 350 and 300 eV respectively; apart from during activation when the S 2p region was collected using a photon energy of 470 eV. The photon energies were selected to increase the surface sensitivity of the emitted photoelectrons being measured.[258] All XP spectra were collected with a pass energy of 10 eV. For each of the different photon energies used the Zr 3d peak was also recorded in order to correct the binding energy scale.

Casa XPS was used to analyse the XPS data. Shirley backgrounds were used for the analysis of the Zr 3d and O 1s peaks and linear backgrounds for all other peaks, due to the shape of the secondary electron curve. Binding energies were corrected using Zr $3d_{5/2}$ = 182.2 eV of ZrO_2.[154] In all displayed figures the ring current (RI) has been normalized to 250 mA. Relative elemental signal intensities (given as percentages) were calculated for the film and carbonaceous overlayer components after ring current, photon flux and photon energy specific cross section[255] normalization using the Zr 3d, S 2p, O 1s and C 1s peaks. The thickness of the deposited carbonaceous layer was estimated from the attenuation of the sulfated zirconia film signal intensities assuming a two layer model, as outlined in reference 243, and a photoelectron escape depth of 1.2 nm, as calculated for through an organic overlayer from reference 158. In order to estimate the thickness the signal intensities were normalised using the ring current and the background signal on the high binding energy side of the peak, to correct for differences in the mean free paths of the emitted photoelectrons through the different gas phases.

All reported fits were performed with a Gauss to Lorentz ratio of 0.1 and software

determined full widths at half maximums (FWHMs). Attempts to fit the C 1s spectra with two asymmetric peaks (using fixed degrees of asymmetry) were unsuccessful; therefore, three symmetric components were used. The S 2p spectra were fitted using the theoretical area ratio of $2p_{3/2}$ to $2p_{1/2}$ of 2:1, the spectra after subsequent exposures were fitted using fixed values for the difference in binding energies (1.2 eV) and the FWHMs ratio (1:1) of the two sub levels as calculated from the as introduced spectrum.

Carbon K edge NEXAFS were collected at 190 eV with a pass energy of 50 eV and the photon energy scale was calibrated by aligning the C 1s π* (C=C) transition of graphite to 285.4 eV.[256] Analysis of the spectra was performed as outlined in reference 257. Normalisation was performed using a clean silver surface (recorded at 453 K in 0.5 hPa helium after pretreatment at 773 K in 0.5 hPa helium) and the spectrum of the activated surface was subtracted from the spectra measured after exposure to *n*-butane.

Throughout the experiment the gas phase was analysed by mass spectrometry (MS) via leak valves (from both chambers) which were set to give a maximum operational pressure of $1x10^{-6}$ hPa for the MS. m/z Ratios recorded by the MS are given in Chapter 3 in Table 3-1. In order to correct for a blank MS signal *n*-butane was introduced into the main chamber at 0.5 hPa without the sample being present.

5.3 Results

5.3.1 As introduced

Spectra in Figures 5-2 and 5-3 show the sulfated zirconia thin film on introduction ("as introduced") to contain zirconium, sulfur, and oxygen, as expected, as well as silicon from the substrate and carbon from either atmospheric contamination or residual decomposition products from the SAM. Relative elemental signal intensities for

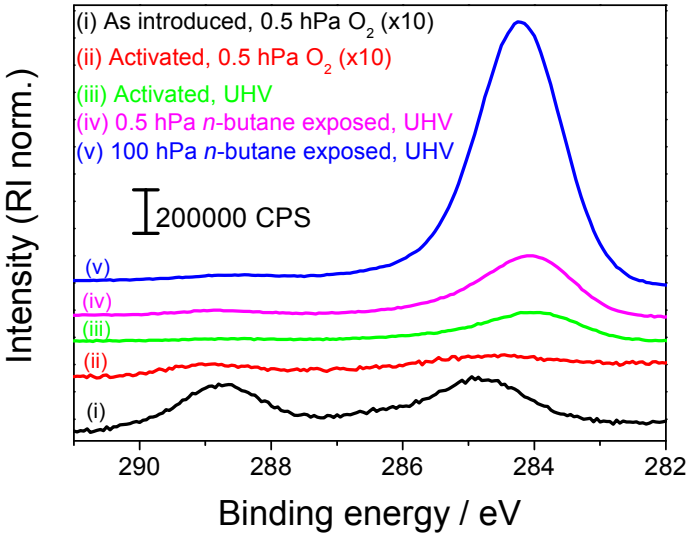

Figure 5-2: C 1s spectra (i) after introduction, at room temperature in 0.5 hPa O_2; after activation up to 698 K in O_2, (ii) measured at 548 K in 0.5 hPa O_2 and (iii) under UHV; (iv) after exposure to 0.5 hPa *n*-butane up to 598 K, measured under UHV at 598 K; followed by (v) exposure to 100 hPa *n*-butane up to 481 K, measured under UHV at 323 K.

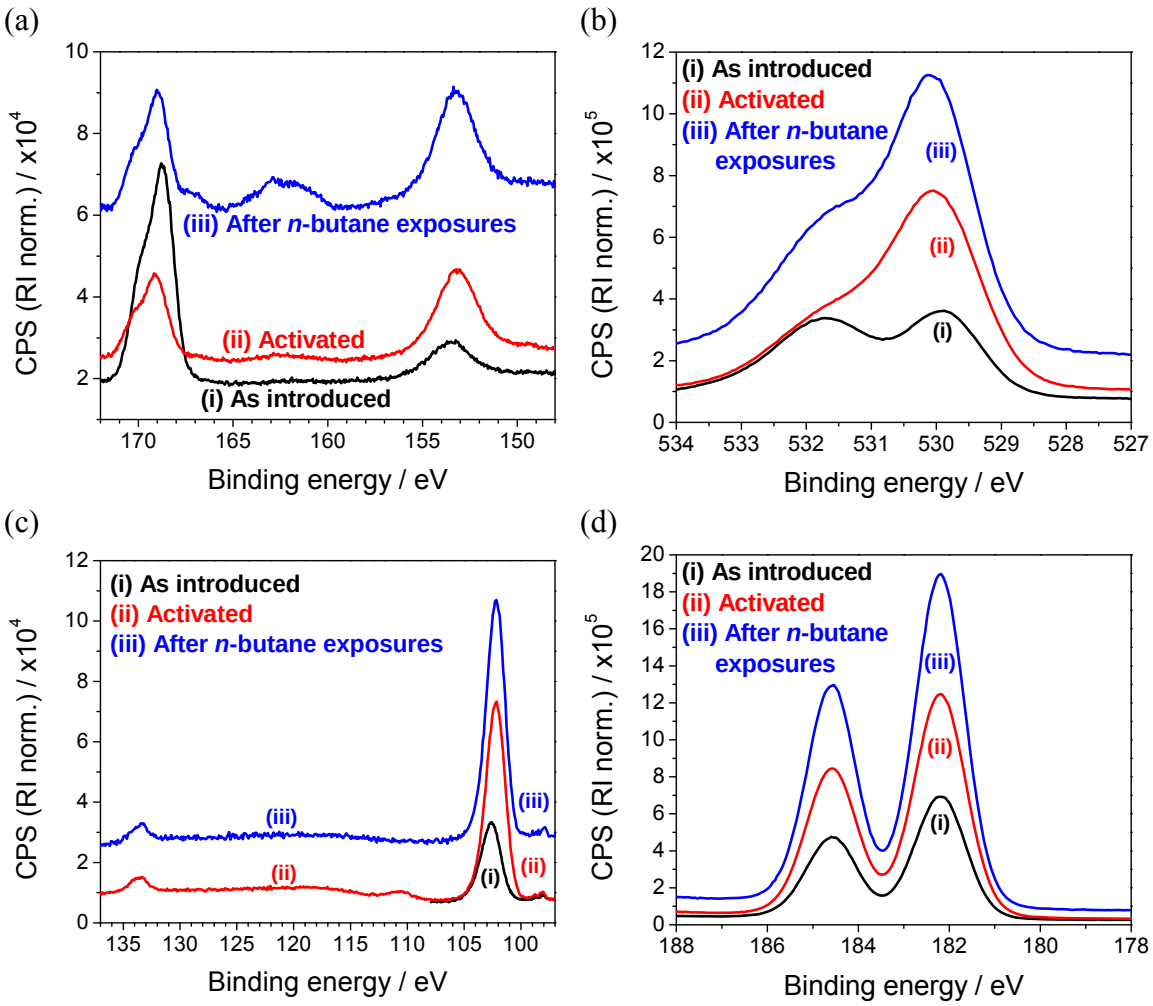

Figure 5-3: (a) S 2p and Si 2s, (b) O 1s, (c) P 2p and Si 2p and (d) Zr 3d XP spectra of the sulfated zirconia thin film (i) as introduced measured in 0.5 hPa O_2 at room temperature, (ii) after activation measured in 0.5 hPa O_2 at 548 K and (iii) after *n*-butane exposure to 0.5 hPa up to 598 K followed by 100 hPa up to 481 K, measured under vacuum at 323 K.

Table 5-1: Relative elemental signal intensities from the sulfated zirconia thin film and carbonaceous deposits (i) as introduced at 299 K, (ii) after activation at 548 K both measured in 0.5 hPa O_2 and (iii) after subsequent exposure to *n*-butane at 0.5 hPa up to 548 K and 100 hPa up to 498 K, measured under UHV. Zr3d, O1s, S2p and C1s peaks used to perform calculations. Silicon and phosphorus contributions are excluded.

Conditions	Zr %	O %	S %	C %
(i) As introduced	18.0	66.3	4.4	11.2
(ii) Activated	22.3	74.8	1.2	1.7
(iii) After exposures	9.2	30.4	0.6	59.8

the main components of the sulfated zirconia thin film and carbon are given in Table 5-1. Zirconium and sulfur were detected in oxidation states +4 and +6 respectively. The O 1s peak consists of two major species, one at higher binding energy (~532 eV), which is attributed to sulfate species and hydroxyl groups, and a lower binding energy species

(~530 eV) from oxide anions. Silicon is detected predominantly in the +4 oxidation state from the silica layer, however a very low amount of elemental silicon is visible. Plasmons[258] from the Si 2s peak were detected from 161-163 eV and ca. 166 eV. The higher binding energy Si 2s plasmon overlaps with the S 2p peak; however, its effect on the quantification and fitting of the sulfur peak is considered to be negligible. The C 1s peak shown consists of two peaks. The lower binding energies peak can be fitted (not shown) using a minimum of two components, the main species is at 284.8 eV and the higher binding energy shoulder at 286.5 eV, these are ascribed to aliphatic polymers and singly bound oxygenated carbon species. The higher binding energy peak at 288.8 eV is ascribed to more highly oxidised carbon (possibly acetal or carbonyl species).

5.3.2 Activation

During activation the C 1s peak area increased with increasing temperature from room temperature to 572 K, concurrently the S 2p peak area decreased. Above 572 K the C 1s peak area decreased with increasing temperature and the S 2p peak increased. At 673 K the C 1s peak area is seen to decrease gradually and the S 2p peak area to remain roughly constant. Increasing the temperature to 698 K to remove the remaining carbon species results in the decrease of both C 1s and S 2p peak areas, hence the temperature was reduced to 673 K again.

Spectra recorded before and after activation, see Figures 5-2 and 5-3, show the decrease of the C 1s and S 2p peaks after activation. After activation the substrate silicon peaks (Si 2s and Si 2p as well as their plasmons) are more prominent as a result of the loss of both carbon and sulfur. The relative intensity of the high binding energy oxygen species decreases after activation which is consistent with concomitant decrease of the sulfur content and possibly also partly due to a loss of hydroxyl groups. In addition phosphorus contamination (P 2p = 133.3 eV) is seen.

Evacuation of the chamber results in an increase in C 1s signal; this is clearly not just because of the improvement in electron transmission from the removal of the gas phase as the signal increases by a number of orders of magnitudes and the peak shape changes to include a lower binding energy species. The observed deposits are probably due to the adsorption of residual carbonaceous species from the chamber.

5.3.3 *In situ* XPS

During exposure of the sample to 0.5 hPa *n*-butane at 548 K, formation of a surface carbon species was observed, which increased with exposure time. It could be shown that the adsorbed carbon signal in non-irradiated areas was lower by changing the spot position (Figure 5-4), indicating that the carbon deposition was partly beam induced. Increasing the temperature to 598 K caused an increase in the amount of carbon deposited on the film; however, by changing the irradiated area again it could be shown that a significant proportion of the deposition seen was still due to beam influence.

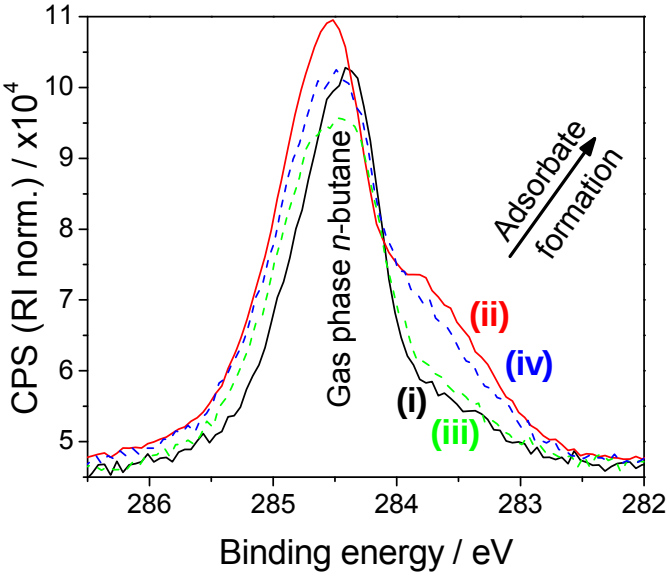

Figure 5-4: *In situ* C 1s XPS in 0.5 hPa *n*-butane at 548 K, irradiated spot changed from position A (solid lines) to position B (dashed lines). Spectra shown for position A after (i) 8 and (ii) 47 minutes irradiation and for position B after (iii) 1 and (iv) 25 minutes irradiation.

5.3.4 *Ex situ* XPS

In order to avoid beam influenced deposition, C 1s XPS was performed under 10^{-7} hPa vacuum on areas that were not irradiated during *n*-butane exposure. After subsequent treatments of 0.5 hPa *n*-butane at 548 K and 100 hPa *n*-butane at maximally 481 K, stable carbon deposits (which do not change with time) were observed (see Figure 5-2). These carbon deposits, as well as those formed in UHV after activation, can be fitted using at least three components (Figure 5-5). The main peak consists of at least two components; a lower binding energy species at ca. 283.9-284.2 eV corresponding to chain-like carbon with a shoulder at higher binding energies assigned to aliphatic polymers (ca. 285.0-285.2 eV) and the minor peak at ca. 288.3-288.7 eV relates to oxygenated species (Table 5-2). From the broad FWHMs and relative shifts of these three components it can be inferred that they are not individual species but rather comprise of a variety of species in slightly differing environments. The relative intensity ratio of the three components is similar after both activation, as measured in UHV, and exposure to 0.5 hPa *n*-butane;

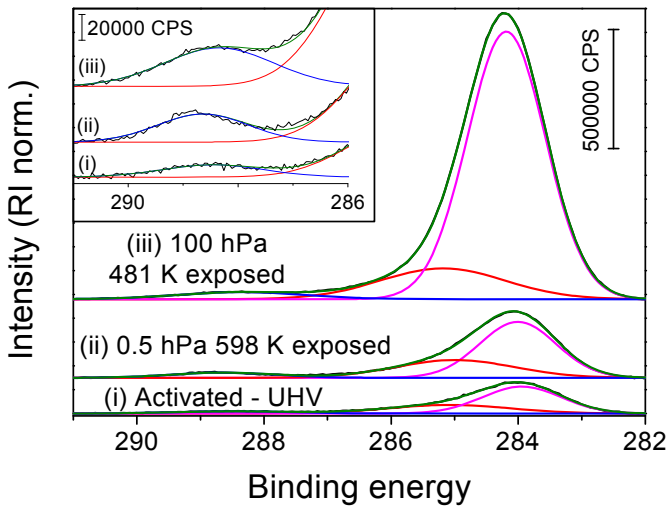

Figure 5-5: Fits of C 1s spectra (i) after activation, measured at 458 K; after subsequent exposure to (ii) 0.5 hPa *n*-butane up to 598 K, measured at 598 K, then (iii) 100 hPa *n*-butane up to 481 K, measured at 323 K, all measurements performed under UHV.

however, the chain-like species increases significantly after exposure to 100 hPa *n*-butane.

From the comparison of all of the spectra taken in oxygen after activation with those measured under UHV after exposure to *n*-butane (Figure 5-3) the improvement in electron transmission through vacuum can be seen; as in spite of the increase in carbon coverage after exposure, which should cause all other peaks to decrease, all signals increase in intensity. The relative elemental signal intensities given in Table 5-1, however, show the increase in the carbon coverage and decrease in film components. From the attenuation of Zr 3d, O 1s or S 2p signals from the sulfate zirconia thin film the thickness of the deposited carbonaceous overlayer is estimated to be either 0.6, 0.5 or 0.4 nm, respectively.

Table 5-2: Fits of C1s spectra after (i) activation, measured at 458 K and after subsequent exposure to (ii) 0.5 hPa *n*-butane up to 598 K, measured at 598 K and (iii) 100 hPa *n*-butane up to 481 K, measured at 323 K. All measurements performed under UHV.

Conditions	Chain-like			Aliphatic polymers			Oxygenated		
	BE / eV	%	FWHM / eV	BE / eV	%	FWHM / eV	BE / eV	%	FWHM / eV
(i) Activated	283.9	61.8	1.5	285.1	30.5	2.2	288.5	7.7	2.2
(ii) 0.5 hPa exposed	284.0	61.8	1.4	285.0	30.4	2.2	288.7	8.8	2.0
(iii) 100 hPa exposed	284.2	81.5	1.4	285.2	15.0	2.3	288.3	3.5	2.4

After the consecutive *n*-butane exposures, reduction of sulfate can be seen by the appearance of a shoulder at lower binding energies of the S 2p peak, which is ascribed to S^{4+}, and an additional broad peak situated between 160-165 eV, from sulfur in lower oxidation states (Figure 5-3a). Fitting the S 2p region shows the presence of at least four different species, the maxima of the 3/2 sub level for which are situated at 169.0 eV for

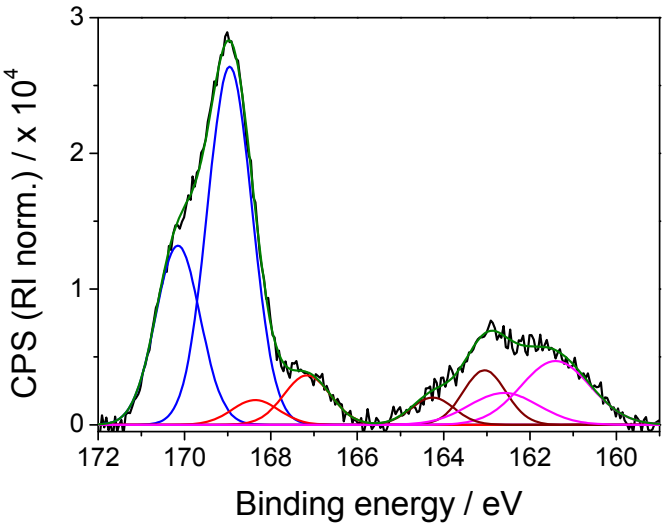

Figure 5-6: Fit of S 2p spectra, taken after subsequent 0.5 hPa *n*-butane up to 598 K and 100 hPa *n*-butane up to 481 K exposures, measured at 323 K under UHV.

S^{6+}, 167.2 eV for S^{4+} and two additional reduced states at 163.1 and 161.4 eV (Figure 5-6 and Table 5-3). The zirconium to sulfur ratio (based on the relative elemental intensities of the Zr 3d and S 2p peaks) therefore decreases from 18.5 as measured after activation to 15.0 after the consecutive *n*-butane exposures.

In the Si 2s and Si 2p regions (Figure 5-3a and c) there are no major changes to the Si^{4+} or elemental silicon peaks after exposure to *n*-butane, apart from their further attenuation by the carbonaceous deposits, thus their plasmons are no longer visible in the 2p region and therefore considered to be negligible in the 2s region. The ratio of the O 1s higher binding energy component (~532 eV) to the lower binding energy component (~530 eV) increases slightly after the *n*-butane exposure (Figure 5-3b). The Zr 3d and P 2p peaks all do not alter significantly after exposure. Closer inspection of the low binding energy tailing of the Zr 3d peak reveals no differences that may prove the presence of a Zr^{3+} species.

Table 5-3: Fitting of S 2p spectra after subsequent *n*-butane exposures at 0.5 hPa up to 598 K and 100 hPa up to 481 K, measurement performed under UHV at 323 K. Binding energies of S $2p_{3/2}$ peak given.

Species	BE / eV	%	FWHM / eV
S^{6+}	169.0	63.8	1.2
S^{4+}	167.1	9.2	1.3
S^{0} or S^{2-}	163.1	9.3	1.2
S^{2-}	161.4	17.7	1.9
Total reduced fraction	-	36.2	-

5.3.5 NEXAFS

Auger electron yield NEXAFS analysis of the C K edge, performed also under 10^{-7} hPa vacuum after the aforementioned subsequent *n*-butane exposures (Figure 5-7), show the development of a feature at ~285.0 eV. The transition only becomes clearly visible after the higher pressure *n*-butane exposure. This transition is not consistent with absorbance

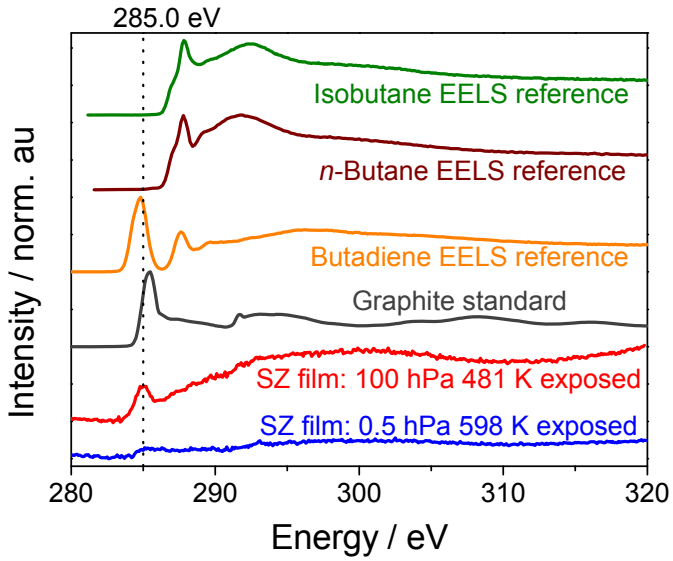

Figure 5-7: C K edge NEXAFS spectra for the sulfated zirconia thin film after subsequent treatments of 0.5 hPa *n*-butane up to 578 K and 100 hPa *n*-butane up to 481 K, measured in vacuum at 578 K and 323 K respectively, the graphite standard used for correction of the energy scale and EELS reference spectra taken from reference 262.

Table 5-4: Main absorption bands for the 100 hPa *n*-butane exposed SZ film, graphite standard and literature electron energy loss spectroscopy (EELS) references from 262.

Material	Main transition	Technique
Exposed SZ film	285.0 eV	NEXAFS
Graphite	285.4 eV	NEXAFS
Propane	287.0 eV	EELS
n-Butane	287.1 eV	EELS
n-Pentane	287.0 eV	EELS
Isobutane	287.0 eV	EELS
1-Butene	284.9 eV	EELS
2-Butene	285.0 eV	EELS

features arising form either the reactant, *n*-butane, or the isomerisation product, isobutane (Table 5-4).[259] The observed transition is however characteristic of π* resonances from unsaturated sp or sp^2 carbon bonds and is consistent with unsaturated hydrocarbon species such as butenes[260] and also amorphous carbon.[261]

5.3.6 Mass Spectrometry

No increase in MS signals indicating the evaporation of sulfur containing compounds were observed during activation. The detection of isobutane during *n*-butane exposure, via the relative MS fragmentation intensities, did not produce values above a blind experiment (in which *n*-butane was introduced into the empty chamber).

5.4 Discussion

The XPS peak positions and elements present are properties of the as introduced films which are similar to those previously reported for sulfated zirconia thin films.[123] Minor differences such as peak shapes can be explained by the increased surface sensitivity from the selected photon energies used.

During activation the initial decrease in sulfur is consistent with an increase in the carbon coverage. However, at higher temperatures the loss of sulfur is not understood. The film was previously calcined in synthetic air at 823 K and TDS experiments (see Chapter 3) have shown that under vacuum the films are stable up to 723 K, thus within the temperature and pressure ranges of this experiment.

The occurrence of beam influenced deposition during *in situ n*-butane XPS was not unexpected given that beam damage has previously been observed for isobaric studies using a conventional XPS source (see Chapter 4) and reports in the literature of organic molecules decomposing under irradiation.[263]

Formation of stable carbon deposits on the surface after *n*-butane exposures proves that the film contains reactive centres. Evaluation of the carbonaceous species via fitting the C 1s spectra results in at least three major components, as fitting using two asymmetrical peaks of fixed asymmetry was not possible for all of the carbon spectra. The use of three symmetric peaks is however an oversimplification of the system as the C 1s peak is generally known to be asymmetric towards higher binding energies.[235] Furthermore, the broad FWHMs of the three components and their shifting positions with coverage imply the presence of additional minor components. The assignment of such minor components based from the data presented here is however ambiguous. In comparison with literature,[157] the three main different environments identified have been ascribed to chain-like carbon (~240.0 eV), aliphatic polymers (~285.3 eV) and oxygenates (~288.5 eV). The chain-like carbon has been described as short hydrocarbon molecules possibly hydrogen deficient, such as butane and butene. Aliphatic polymers are proposed to be formed via the oligomerisation of alkenes on the surface. Separating of the hydrocarbons into saturated and unsaturated species from the presented XPS data is not possible as such components are reported to differ by only 0.3 eV.[235] The dehydrogenation of the hydrocarbon species, as indicated by the development of an unsaturated species by NEXAFS, is not responsible for the binding energy shifts to higher values with increasing coverage as alkenes are reported to have lower binding energies than alkanes.[235] Formation of oxygenated species have been reported to stabilise the catalytically active carbenium ions.[85,228] Various carbon-oxygen functional groups may be present as predicted from the oxidation pathway of butane on oxide surfaces,[264] including alkoxide

(285.5-286.6 eV),[265-272] acetal and carbonyl (288.0-289.2 eV)[246] species. Additionally, graphitic-like "coke" precursors (284.4-284.6 eV)[157,246] may also exist on the surface. The presence of minor amounts of graphitic-like and alkoxide species could be responsible for the shift of the assigned chain-like and aliphatic polymer species to higher binding energies after exposure to 100 hPa *n*-butane. Alternatively, the shift of these hydrocarbon species to higher binding energies may be caused by the formation of multilayers, as the estimated thickness of the deposited carbon layer is of the order of an *n*-butane monolayer as determined by isobaric UPS measurements in Chapter 4 and literature values.[234,240] Multilayer adsorption of butadiene has been reported to result in a shift of the C 1s binding energy from 284.0 to ~285.0 eV, which is attributed to the weaker interaction with the surface.[273]

From the greater attenuation of zirconium as compared with sulfur after the accumulation of stable reaction deposits, as indicated by the lower calculated carbonaceous layer thickness using the S 2p versus Zr 3d signals and the decrease in zirconium to sulfur ratio after exposures, it can be inferred that the carbonaceous layer is not homogeneous and the deposits are situated preferentially on top of the zirconia rather than the sulfur species. The decreased relative intensity of the O 1s lower binding energy component from oxide anions, in comparison the higher binding energy component from sulfate and hydroxyl species, is consistent with this hypothesis. Such findings are also in agreement with the reported interaction of *n*-butane with single crystalline films of sulfated zirconia.[162]

The appearance of plasmons from the Si 2s region may affect the quantification and position of the S 2p for the activated sample, however such effects are considered negligible for the as introduced sample because of the low level of silicon seen. Fitting of the as introduced S 2p sub levels results in a binding energy separation (1.2 eV) which is similar to reported literature values of 1.19,[274] 1.2[275] and 1.3[276] eV. After the consecutive *n*-butane exposures reduction of the sulfate is observed. These reduced sulfur species are observed in the same region as the silicon 2s plasmons were, however the plasmons are judged not to interfere with the evaluation of the sulfur species due to the relative reduction in the silicon signals with increasing carbon coverage and also the absence of plasmons from the Si 2p region.

The detection of S^{4+} on sulfated zirconia after *n*-butane exposure is consistent with previous XPS studies on powder sulfated zirconia.[83] Components at lower binding energies than S^{4+} can be ascribed to sulfur in lower oxidation states. The peak at 163.1 may be from S^0 (elemental sulfur) or S^{2-}, whereas the peak at 161.4 eV may be ascribed unambiguously to S^{2-}.[154,277] The position of the sulfide peak at 161.4 eV is consistent with the sulfide formed after argon sputtering of sulfated zirconia thin films,[123] however the broad HWFM of this peak in comparison to the other components indicates this may be a combination of different species. To the author's knowledge the formation of sulfides on the surface of sulfated zirconia after *n*-butane exposure has not previously been detected in XPS studies, but hydrogen disulfide has been reported to evolve from sulfated zirconia during *n*-butane isomerisation at 523 K as determined by gas chromatography mass spectrometry[72] and to be present on the surface of sulfated zirconia after exposure to *n*-butane at 573 K as indicated by DRIFTS.[244,278]

It is known from the literature that various sulfur complexes are liable to beam damage.[279-283] No evidence of beam effects (changes with irradiation time) were observed for the sulfate species during these measurements. The influence of the beam on additional sulfur species (with oxidation states < +6) formed after butane exposure was however not investigated. Reduction of the sulfate after exposure to *n*-butane can therefore be assumed to not be effected by irradiation, whereas subsequent beam induced reactions of the reduced products cannot be excluded. It is thus possible to quantify the overall reduced fraction of sulfate, but further time-dependent studies would be required in order to verify that none of the sulfur species produced after *n*-butane exposure are artefacts formed by the measurement technique.

Oxidation of the carbonaceous deposits as indicated by the development of a peak at ~288.5 eV is consistent with the reduction of the sulfate species. In the literature, sulfate reduction is facilitated by the formation of water, as detected by IR spectroscopy.[63,284] The formation of water on the sulfated zirconia thin films was not detected by XPS, as indicated by the absence of an O 1s peak at ~533.1 eV.[285] However, under the measurement conditions used any water formed would be expected to desorb from the surface. Water was not detected by MS during the measurements, although this may be because of a lack of sensitivity.

Formation of an unsaturated species after *n*-butane exposures, as detected by NEXAFS, proves the films have sites capable of dehydrogenation. The absence of any discrete C-H* and σ* resonances, thus rendering them indistinguishable from the edge jump, is believed to be caused by the presence of multiple species differing only slightly in nature. However, the distinct π* resonance seen is believed to be either the butene intermediate from the oxidative dehydrogenation initiation pathway or possibly a side product from this initiation step.[63,90] This unsaturated species may also be the allylic species reported to be formed on sulfated zirconia powders, as determined by UV-vis spectroscopy.[15,74,286]

5.5 Conclusions

The development of carbonaceous surface deposits proves the films contain reactive centres. The ability of the catalyst to dehydrogenate *n*-butane proves that an oxidative dehydrogenation pathway is possible and thus is in good agreement with the formation of an alkene being the initiation step of the isomerisation mechanism.[63,90] This is further confirmed by the concurrent reduction of sulfate. The detection of oxygenated carbon species is consistent with a stabilised carbocation being the catalytically active site.

6. Design and Construction of a Thin Film Reactor

6.1 Introduction

6.1.1 Reactors for the catalytic testing of model thin films and supported particles on flat substrates and single crystals

Catalytic model thin films and supported particles on flat substrates and single crystals have surface areas in the order of square centimetres only, thus making the detection and analysis of reaction products over them at high pressures (>10^{-2} hPa) and temperatures very difficult. For model catalysts with high turnover frequencies (~1 s^{-1}), catalytic activities can be measured in batch reactors (volume ~ 500 cm^3) and analysed via gas chromatography. In the case of low turnovers, reactors with volumes of a few millilitres can be used; however, "a robust design of a reactor with very low volume is still to be accomplished".[287]

Campbell[288] has reviewed the reactors available for the catalytic testing of well defined surfaces and Gunter *et al.*[287] have described some possible reactors for the testing of model catalytic films and supported particles on flat substrates. Important parameters discussed in the aforementioned reviews regarding the design features of such reactors are summarised below.

When determining surface structure-reactivity relationships on well defined surfaces, minimal exposure of the catalysts to undesired vapours during and between high pressure kinetic testing and surface analysis is essential. Proven designs for such studies generally consist of a high pressure cell attached to a vacuum chamber through a transfer arm or a retractable reactor that encloses the sample.[289] To minimise potential surface contamination it is important that the sample is transferred to vacuum in as rapid and clean way as is possible. The reactor (and transfer device) should therefore be constructed from low-surface-area, non porous and bakeable materials. If, however, the sample can be exposed to air prior to and after reaction then much simpler designs are possible; for example, Kuipers *et al.*[290] used a glass reactor suspended in an oven.

Normally only the sample is heated during reaction in order to prevent side reactions or degassing of contaminants from the walls of the reactor. Metallic samples are generally heated via resistive heating. For oxide catalysts resistive heating is not possible, unless the oxide is deposited on a metal. If the oxide completely covers the metal resistive

heating with a low background can be achieved, such as in reference 291. For oxides deposited on one side of a metal support the catalytic activity of the metal must be negligible, as in reference 292. Oxide samples may also be heated directly via, for example, an infrared spotlight.[293] Alternatively, the entire reactor can be heated provided all background reactions are insignificant.

A very important design consideration is the volume of the reactor. In order to determine accurate kinetics the reactant(s) and product(s) must be well mixed and at observable concentrations. Typical gas diffusivity at atmospheric pressure and room temperature is in the order of 0.1 cm^2/s, thus the average diffusion length during 100 s is only approximately 3 cm. Due to convection currents the actual mixing in a batch reactor will be considerably faster than this but it should not be expected that remote parts (further than ~5 cm) from the sample are efficiently mixed during time periods of less than 100 s. Therefore the reactor should be of a compact design, such as in reference 294, or include a recirculation device, as in reference 295. To avoid potential contamination and wall reactions the compact reactor design is favoured by several groups.[288,294,296]

As previously stated, model thin films and supported particles on flat substrates and single crystals have very low surface areas (~1 cm^2). Assuming a typical reaction rate of 10^{-2} molecules/site/s and that the whole surface is active (a gross overestimation for model oxide catalysts), the overall amount of product formed in 100 s is very small:

$$\text{Product} = (10^{-2}\ \text{molecules/site/s})(10^{15}\ \text{sites/cm}^2)(1\ \text{cm}^2)(100\ \text{s}) = 10^{15}\ \text{molecules}$$

If the reactor is at 100 kPa and has a volume of 1 litre this corresponds to only ~40 ppb product. Given that GC detection limits are of the order of 0.1-1 ppm, constructing a reactor with a small volume is thus very advantageous (if not necessary). However, a compromise must be made between reducing the reactor volume and maintaining enough volume to take aliquots for analysis. In some cases the reactor is operated in a continuous flow mode[297] but this suffers from the same disadvantages as a large-volume reactor. Another factor that favours having a small volume reactor is possible impurity contamination from reactant gases, at 100 kPa 0.1 ppm trace impurities are a potential source of approximately one full monolayer coverage for every ⅓ litre reactor volume. Aliquots of the reaction gas for analysis can be taken from the reactor manually by using a syringe and septum port or automatically by a built-in valve system. More complex

methods, such as rapidly compressing the reactor aliquot into the GC sampling loop prior to injection using a reservoir of carrier gas[298] or using cold fingers to trap condensable products, can be used to increase product detection sensitivity.

6.1.2 Aims

To validate the sulfated zirconia thin films as model catalysts their catalytic activity must be measured and related to powder sulfated zirconia catalysts. To measure the catalytic activity of the sulfated zirconia thin films, a custom reactor needs to the constructed, which meets the following prerequisites:

- Low volume.
- Flow mode operational for activation, up to 573 K.[64,65]
- Batch mode operational for reaction, up to 505 kPa and 373 K.
- Testing of a single sulfated zirconia thin film.
- Sampling of reaction gases must be possible during reaction.
- GC analysis.

To produce a measurable conversion over the sulfated zirconia thin films in as short a time as possible the reactor should have a small volume. Given the low conversion expected, a batch reactor should be constructed to increase reactant-catalyst contact times. Testing a single sulfated zirconia thin film will allow *ex situ* characterisation of the measured film and hence activity-structure relationships to be investigated. Over pressurising of the reactor will increase the reaction rate (as the reaction order is known to be between 1.3-1.4 with respect to *n*-butane concentration)[94] and allow multiple samples of the reaction gas to be taken.

Estimations based on a sulfated zirconia thin film with a 1 cm² surface area, in a 10 ml reactor filled to 25 kPa *n*-butane at 373 K, show the limit of detection (LOD) and limit of quantification (LOQ) to be reached only after 2 and 6 hours batch operation, respectively. Where the LOD is equivalent to three times, and the LOQ to ten times, the standard deviation of the inherent (blank) isobutane impurity to *n*-butane ratio of the reactant gas, as measured by automated GC injections. Calculations were performed assuming a sulfated zirconia reactivity of 0.57 μmol/m²/h at 5 kPa *n*-butane[286] and an *n*-butane reaction order of 1.4.[94]

6.2 Experimental

6.2.1 Reactor design

The constructed reactor consists of two flanges, a sampling port and inlet and outlet lines (as shown in Figure 6-1). The sample is placed between two 69.85 mm stainless steel flanges in an indented bed directly under the sampling port. A silver plated copper gasket (inner diameter 36.855 mm) is used to seal the flanges. In the flange under the wafer two 315 W heating cartridges are inserted in holes drilled into the flange. The temperature of the cartridges is controlled by a K-type thermocouple which is inserted into a hole drilled into the flange (~1 mm directly under the sample).

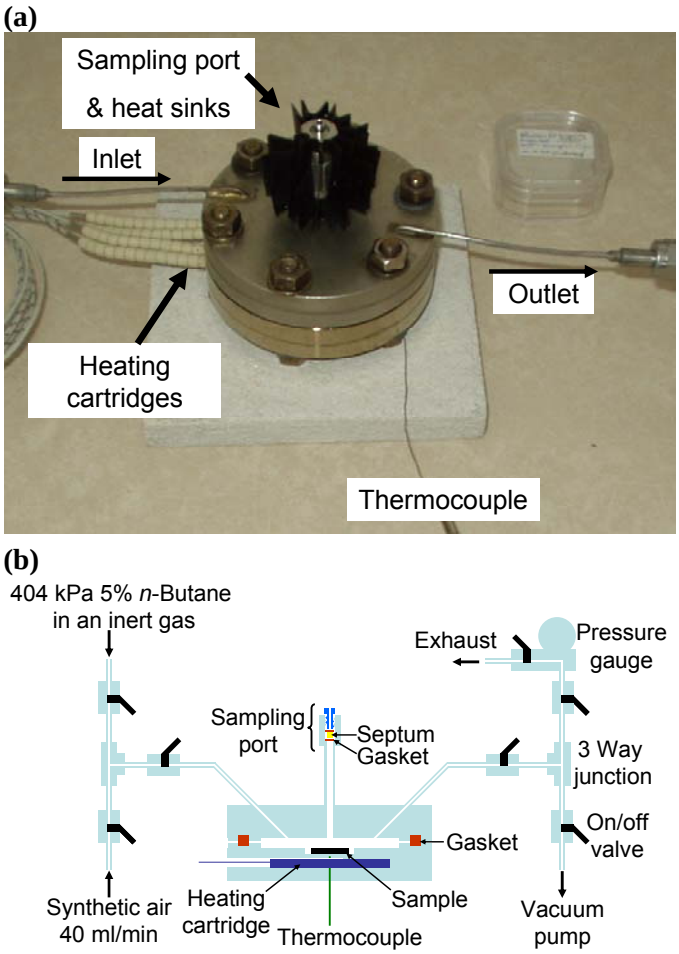

Figure 6-1: (a) Photograph and (b) cross section diagram of the constructed thin film reactor.

Sampling of the gas phase is possible by syringe using the sampling port welded into the centre of the flange directly above the sample. Inside the sampling port, a 5 mm bleed/temperature optimised GC inlet septum is secured between two 6.35 mm silver plated stainless steel gaskets in a VCR® connection. The sampling port is separated from the reactor by a short tube and heat sinks are attached to it to keep the septum cool during activation.

Inlet and outlet lines are welded into the flange above the sample on either side of the sampling port. Initial experiments were performed using VCR® connected ball valves to seal the inlet and outlet lines during batch mode operation, giving the reactor a volume of 5.1 ml. Changing to high-purity high-pressure diaphragm-sealed VCR® connected valves increased the reactor volume to 7.5 ml.

6.2.2 Test measurements

Test measurements were performed on 2.0 mg of calcined MelCat sulfated zirconia powder (to validate the reactor), oxidised silicon wafers (to act as "blind" measurements) and calcined sulfated zirconia films deposited over various time periods. Preparation details for the sulfated zirconia powder sample used are given in Chapter 7 section 7.2.2.

Samples were activated at 573 K in a flow of 40 ml/min synthetic air for 30 minutes using a ramp of 10 K/min. Following the activation, the reactor was flushed at 373 K with 40 ml/min helium or nitrogen for 20 minutes to remove oxygen. The reactor was then filled with the reactant gas (5% *n*-butane in helium or nitrogen) by either flushing the reactor for 2-5 minutes at 40 ml/min with the reactant gas or evacuating the chamber to 10^{-3} hPa, followed by pressurising the reactor to 505 kPa with the reactant gas (*n*-butane partial pressure = 25 kPa) and then closing the inlet and outlet valves.

Multiple samples (2 or 3) of 0.1 ml reaction gas were taken by syringe after a given time period and analysed by GC. Repeated sampling from the same reaction after a different number of days are indicated as subsequent measurements. However, all results presented for reactions of the thin films are from measurements taken on the day on which the septum was initially punctured.

After each test reaction the flange and sampling port gaskets, as well as the septum, were replaced in order to prevent leaks.

6.3 Results

Calculations using the results of manually injected blanks taken immediately after filling the actual reactor, without a sample, to 505 kPa with 5% *n*-butane in an inert gas, show the LOD and LOQ to be achievable after 4 and 13 hours, respectively. These estimations still assume a reaction rate and order taken from the literature.[94,286] This corresponds to conversions of 0.003 and 0.009% to reach the LOD and LOQ.

The conversions in Figure 6-2 of isobutane to *n*-butane were calculated using the relative change in isobutane to *n*-butane signals for individual injections, to avoid errors from differences in injected volumes, using the following equation:

$$\text{Conversion} = \frac{[\text{iBu}_{\text{sample}}] - \left(\frac{[\text{iBu}_{\text{blank}}]}{[n\text{Bu}_{\text{blank}}]} \times [n\text{Bu}_{\text{sample}}]\right)}{[\text{iBu}_{\text{sample}}] - \left(\frac{[\text{iBu}_{\text{blank}}]}{[n\text{Bu}_{\text{blank}}]} \times [n\text{Bu}_{\text{sample}}]\right) + [n\text{Bu}_{\text{sample}}]} \times 100$$

Where $[\text{iBu}_{\text{sample}}]$ and $[n\text{Bu}_{\text{sample}}]$ are the concentrations of isobutane and *n*-butane detected after a set reaction time, respectively. $[\text{iBu}_{\text{blank}}]$ and $[n\text{Bu}_{\text{blank}}]$ correspond to the original isobutane impurity and *n*-butane concentrations.

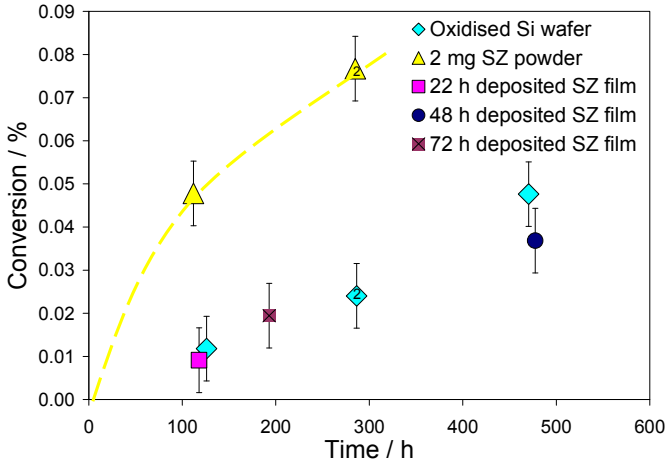

Figure 6-2: Percentage conversion of *n*-butane to isobutane in a batch reactor at 373 K, filled to 400 kPa with 5% *n*-butane in an inert atmosphere. Points with a 2 inset are subsequent measurements.

Figure 6-2 shows that the conversion of *n*-butane to isobutane increases with reaction time over the oxidised silicon wafers, the powder sulfated zirconia and the sulfated zirconia thin films. The sulfated zirconia powder produces a significantly higher conversion than the oxidised silicon wafers or sulfated zirconia thin films. Differences between the oxidised silicon wafers and the sulfated zirconia thin films are within the errors of the measurements and there does not appear to be a trend. Converting the conversions of the sulfated zirconia powder into rates results in values of 1.16 µmol/g/m² after 112 hours and 0.73 µmol/g/m² after 285 hours. The calculation of such rates assumes that the total concentration of butane (isobutane and *n*-butane) after the measurement time is equal to the concentration at the start of the reaction as no side products (with carbon chain lengths of 2-6) were detected in significant amounts.

In Table 6-1 the change in *n*-butane concentration, calculated from the GC signal area relative to the initial blank measurement, is given for the reactions performed. There is a clear decrease of *n*-butane concentration with reaction time, which is greater than the possible error arising from performing manual injections and the loss from conversion to isobutane or side reactions. Helium leak testing of the reactor septum port, inlet and outlet lines was unable to detect any leaks above 10^{-9} hPa/l/s. Measuring the reactor

pressure via an attached pressure gauge (reactor and pressure gauge combined volume = 29.5 ml) showed, after activation and pressurising the reactor to 430 kPa at 373 K for 10 days, the pressure to decrease by approximately 100 kPa. If the decrease in *n*-butane signal is taken into account, the conversions detected over the powder sulfated zirconia correspond to rates of only 0.42 μmol/g/m² after 112 hours (at 9 kPa *n*-butane) and 0.10 μmol/g/m² after 285 hours (at 3.5 kPa *n*-butane).

Table 6-1: Percentage decrease in *n*-butane concentration over the testing period. (2) Indicates subsequent measurements.

% Decrease in *n*-butane concentration	After: 5 days	12 days	20 days
Oxidised Si wafers	48	80[(2)]	92
SZ powder	64	86[(2)]	-
SZ thin films	64	-	86

6.4 Discussion

A prototype reactor (not shown here) was constructed by adapting an in-house flow reactor designed to measure the conversion of ethylbenzene to styrene over well defined epitaxial iron-oxide layers.[212] This reactor consisted of a resistively heated stainless steel cup placed above the sample and was sealed using a gold gasket and a single central screw. The septum was housed in a simple screw cap port with a hole drilled in the middle. A number of flaws were found with such a design. The septa used were found to disintegrate at temperatures above 473 K and leak. These problems were solved by elongating the sampling port and adding heat sinks (to keep the septa below 373 K during activation) and changing the sampling port to a VCR® connection inside which the septum is placed between two stainless steel gaskets. The gold seal was also found to leak over extended time periods (hours). Therefore, the gasket, reactor housing and heating source were changed to those described in the experimental section of this chapter. The redesigned reactor (presented in this chapter) was initially found to be stable to pressurisation over several weeks.

The rate of isomerisation over the sulfated zirconia powder appears to decrease with reaction time. Calculated isomerisation rates of the sulfated zirconia powder are lower than expected, as compared with steady state rates from flow reactor measurements presented in Chapter 7 section 7.3.2 and published results,[286] taking into account the *n*-

butane reaction order.[94] At the low conversions measured, the reaction profile would be expected to increase linearly with time. The low activity of the powder and decrease in reaction rate with time are probably due to both the decrease in partial pressure of *n*-butane from the leak and deactivation of the catalyst (which may be enhanced by back diffusion of oxygen through the leak).

The cause of the "blind" oxidised silicon wafer tests showing a conversion is unclear. It is apparent from the decrease in the *n*-butane concentration and pressure measurements of the reactor (after undergoing the activation program) that the reactor has developed a leak. Attempts to locate and prevent the leak by replacing the inlet and outlet valves, tightening the flange gasket while flushing the reactor with an inert gas (between activation and reaction) and inserting aluminium foil between the septum and inside gasket in the sampling port were all unsuccessful. The source of the leak is probably the flange gasket, as it will undergo thermal expansion during activation then contraction when the temperature is lower for reaction. In addition, it is not designed to be over pressurised. However, as both product and reactant should leak from the reactor, a leak should not lead to a positive conversion for a "blind" experiment. If the blind conversion is from contamination (for example from the powder experiment) then its activity should also decrease with increasing reaction time, however the conversion appears to increase linearly with reaction time. Thus the "blind" conversion is believed to be due to either an inherent reactor flaw or the oxidised silicon wafer being active. If the "blind" activity is caused by an inherent reactor flaw then it would have to be deducted from the sulfated zirconia powder conversion, thus the rate detected over the powder would be even lower.

Given that the sulfated zirconia thin films have a total surface area ~300 times smaller than the powdered material measured and hence their conversions would be expected to differ by the same order of magnitude, such conversions would be impossible to detect with the constructed setup. The lower than expected powder activity, "blind" silicon oxide activity, detected leak and high deviation of the manual injections together mean that the constructed reactor was not able to measure the catalytic activity of the sulfated zirconia thin films.

In order to measure the catalytic activity of the films a completely new reactor would have to be designed and constructed. Such a reactor would need to have no leaks and

improved detection and quantification limits. To ensure the reactor does not leak the seal would have to be isolated from the heating source. This could possibly be achieved by using a localised heating source directly under the sample, for example by inserting a button heater inside the reactor although the reactor volume would probably have to be increased. Alternatively, the reactor could be welded shut and the sample cut out after each reaction, the reactor volume would therefore change slightly for each measurement. The septa could also be isolated from the reactor via a valve which would only be opened when a sample is being taken. However, the large error bars from taking manual injections would need to be reduced in order to detect the very low conversion expected from the sulfated zirconia thin films. Replacing the sampling port with a GC sampling valve would enable direct automated injections of the reactant gas onto the GC and allow the sampled gas to be replaced with reactant gas thus keeping the overall pressure of the system constant. The implementation of such changes is not a simple task and therefore was not possible during the time restrictions of this thesis.

Sulfated zirconia has been reported to have a turnover frequency of 10^{-4} s^{-1} and site density of $5x10^{-6}$ mol/g ($\approx 3x10^{12}$ sites/cm²),[228,299] as compared to typical well defined model catalysts which have turnovers of the order of 10^{-2} s^{-1} and site densities of up to 10^{15} sites/cm².[288] Thus the difficulties encountered in measuring the activity of the sulfated zirconia thin films are attributed not only to trying to measure a conversion over such a small amount of material but also the extremely low intrinsic activity of sulfated zirconia. Despite the orders of magnitude difference in yields expected over the sulfated thin films, as compared to previously measured model systems, further opportunities to improve the reactor design were highlighted within this chapter, which may prove successful in the future.

6.5 Conclusions

A batch reactor to measure the conversion of *n*-butane to isobutane over the sulfated zirconia thin films was designed and constructed. Measurements with a small amount of sulfated zirconia powder showed the conversion of *n*-butane to isobutane albeit with rates lower than expected. Catalytic measurements of the sulfated zirconia thin films, however, failed because of technical problems with the constructed reactor and the low intrinsic

activity of the material. The reactor was shown to leak and have a "blind" reactivity as measured over an oxidised silicon wafer; in addition high error bars were observed. Therefore, in order to realise the measuring of the catalytic activity of the films, it would be necessary to design and construct a new reactor. Proposed suggestions for a new reactor include isolating the sealing from the heating source or welding the reactor to avoid leaks and building a GC sampling valve into the reactor, to improve detection and quantification limits.

7. Rational Design of Powder Sulfated Zirconia Catalysts

7.1 Introduction

7.1.1 Disulfated zirconia

The presence of a disulfate (pyrosulfate, $S_2O_7^{2-}$)[56] species on zirconia was initially proposed by Bensitel *et al.*[47] after they observed an IR band at 1403 cm^{-1}at high sulfate coverages, which disappeared on exposure to water. Morterra *et al.*,[48,300,301] also, assigned the formation of an IR band at ~1406 cm^{-1}, seen at sulfate coverages over half a monolayer, to polynuclear sulfates, probably disulfates. Experiments indicated these disulfates to be located on the regular patches of low index crystal planes (top terminations of the scale-like particles) of zirconia. Increasing the sulfate loading (thus favouring the presence of disulfate species) was shown to increase the number of Brønsted acid sites, while lowering the number of Lewis acid sites but enhancing their strength. These acidic sites were found to be liable to hydrolysis.

Escalona Platero *et al.*[302] also ascribed an IR band at 1398 cm^{-1}, from sulfated zirconia produced by the thermolysis of zirconium sulfate, to disulfate species. They found the disulfate groups disappeared at coverages below about 10% of a monolayer. High temperature treatment was shown to remove the disulfate groups, trace amounts of molecular water and strong Brønsted acid sites.

Xia *et al.*[303] compared sulfated zirconia materials prepared using either ammonium peroxydisulfate (persulfate, $S_2O_8^{2-}$)[56] or sulfuric acid. The peroxydisulfated material was shown to be more active for the isomerisation of *n*-butane at 308 K, which the authors claim is due to it having more "superacid" sites rather than having stronger sites. However, IR bands for the sulfuric acid prepared material are reported to show a strong absorption band in the 1380-1390 cm^{-1} region, whereas the peroxydisulfated material showed a band at 1398 cm^{-1}, which the authors postulated are due to disulfate species, in agreement with references 47 and 48.

Marus *et al.*[304] also prepared sulfated zirconia catalysts using either ammonium peroxydisulfate or sulfuric acid. In contrast to the study by Xia *et al.*,[303] the maximum *n*-butane isomerisation activity of the peroxydisulfated catalysts was found to be lower than that of the sulfuric acid prepared catalysts. However, the authors showed for catalysts prepared from both sulfating agents the amount of carbon required to completely

deactivate them was equivalent to one carbon atom per two active sulfate atoms, using a TGA/FTIR technique. Thus despite the lower activity of the peroxydisulfated catalysts the authors still suggest the active sites to be composed of two sulfate atoms, such as disulfate. They propose the active sites may be formed from either two vicinal sulfate groups or two pregrouped sulfur atoms on certain zirconia sites.

Density-functional theory (DFT) and statistical thermodynamics calculations were used by Hofmann and Sauer[62] to investigate the adsorption of H_2O and H_2SO_4 (or SO_3) on tetragonal zirconia (101). The authors showed that monosulfates and disulfates may occur on the surface of zirconia, but no higher condensated sulfates were observed. Simulated surface phase diagrams depend strongly on temperature and H_2O and H_2SO_4 (or SO_3) partial pressures. The calculations indicated that vibrational bands in the region of 1420-1400 cm^{-1} are from disulfate species and those at 1400 cm^{-1} are from adsorbed SO_3 species. They thus predicted, in agreement with experimental IR literature,[302,57] the transformation of water rich sulfate structures into disulfates during calcination (at 873 K), which at higher temperatures (1073 K) undergo transformation to adsorbed SO_3.

Li *et al.*[63] proposed the disulfate (or SO_3) species, seen by IR at 1404 cm^{-1}, to be liable in the presence of *n*-butane to an initiation reaction that creates the catalytic active centres on sulfated zirconia. This is said to occur via the stoichiometric oxidative dehydrogenation of butane by disulfate or SO_3 groups to produce butene (present mostly as alkoxide groups), water and SO_2. They report the detection of all three oxidative dehydrogenation reaction products by thermal desorption and *in situ* IR spectroscopy. The butene surface concentration is stated to determine both the catalytic activity and deactivation (via formation of oligomers) of sulfated zirconia. They also showed the IR band at 1404 cm^{-1} shifted to lower wavenumbers (1398 cm^{-1}, with a shoulder at 1378 cm^{-1}) with time on stream (consistent with the reduction of disulfate or SO_3) and, by DFT, favourable reaction energies for the oxidation of butane to butene particularly over sulfate loadings of two S atoms per (1 x 2) surface cell.

Further work by Li *et al.*[26] showed that washing sulfated zirconia samples with water decreased their catalytic activity and shifted the maximum of the band seen at 1404 cm^{-1} to lower wavenumbers (~1391 cm^{-1}). It is thus proposed that the catalytic activity of the materials is proportional to their concentration of labile chemisorbed SO_3, most likely in

the form of disulfate. Klose *et al.*[284] assigned all IR bands seen between 4000-1000 cm^{-1} on sulfated zirconia, based on reference 62, concluding that disulfate groups are the main sulfur species. Several other groups have reported the possible presence of disulfate species[194,305,306] on sulfated zirconia.

7.1.2 Preparation of sulfated zirconia from precursors containing two sulfur atoms

Afanasiev *et al.*[307] synthesised sulfated zirconia from zirconium oxychloride, potassium disulfate and a KNO_3-$NaNO_3$ eutectic in a molten nitrate bath. The reaction mixture was pretreated in nitrogen at 423 K followed by heating to 773 K for 2 hours. However, no disulfate IR bands, near 1400 cm^{-1}, were detected in the synthesised material.

Xia *et al.*[303] prepared peroxydisulfated and sulfated zirconias using ammonium peroxydisulfate and sulfuric acid sulfating agents. Zirconium hydroxide was immersed in 0.5 mol/l of the sulfate precursors for 30 minutes; followed by filtration, drying overnight at 383 K and calcination at 923 K. The peroxydisulfated material was found to have a lower surface area (58.2 versus 113.0 m^2/g) and sulfur content (1.99 versus 3.3 wt.% SO_3) compared to the sulfated material. The lower surface area is reported to be probably caused by immersing the amorphous zirconia in an aqueous ammonium salt solution. For the isomerisation of *n*-butane at 308 K, higher conversions were detected over the peroxydisulfated material (45.4 versus 37.1% after 20 hours). The reaction was, also, performed at 523 K, resulting in the peroxydisulfated material initially having the lower activity of the two materials (25.6 versus 27.3%, after 2 minutes) but to be more stable with respect to time on stream (20.4 versus 17.5%, after 360 minutes). After 6 hours the coke content of the peroxydisulfated material was found to be lower (1.14 versus 1.25 wt.%), thus explaining the deactivation of the sulfuric acid prepared material.

Marcus *et al.*,[304] also, prepared peroxydisulfated and sulfated zirconia catalysts from ammonium peroxydisulfate and sulfuric acid. Zirconia was immersed in various normalities of either ammonium peroxydisulfate (0.3-0.6 N) or sulfuric acid (0.2-0.6 N) for 15 minutes. The resulting product was decanted, dried overnight at 383 K, then calcined at 873 K in oxygen for 1 hour. The materials were tested for the isomerisation of *n*-butane at 473 K and their activities are given as a conversion after 15 minutes on stream, as it is reported they all have equivalent deactivation constants. Of the peroxydisulfate materials the 0.4 N prepared was shown to have the maximum

conversion (13.6%), whereas for the sulfated materials the 0.5 N prepared was shown to have the maximum conversion (18.77%). The sulfur contents and surface areas of the most active samples from the different precursors were found to be very similar (3.32 versus 3.43% and 160 versus 149 m^2/g, for the peroxydisulfated and sulfated materials, respectively).

Dias *et al.*[308] prepared peroxydisulfated and sulfated zirconia catalysts with and without an MCM-41 support using ammonium peroxydisulfate and ammonium sulfate. The "conventional" materials were prepared by immersing the zirconia precursor in 0.5 M solutions of the sulfating agents for 30 minutes, followed by filtration, drying at 383 K for 24 hours, then calcination at 923 K for 3 hours in air. Whereas, the supported materials were prepared by first impregnating MCM-41 with aqueous $ZrOCl_2.8H_2O$, via incipient wetness. Sulfation was also performed via incipient wetness, followed by drying (at 393 K for 1 hour or 383 K for 24 hours) then calcination at 823 K for 3 hours in air. The conventional peroxydisulfated and sulfated materials had similar surface areas (85 versus 90 m^2/g) and sulfur contents (0.33 versus 0.37 mmol/g). Whereas, the supported peroxydisulfated material had a lower surface area (382 versus 426 m^2/g) but higher sulfur content (1.2 versus 0.9 mmol/g) than the supported sulfated material. Catalytic testing of the materials for the conversion of xylose to furfural showed the conventional materials to have similar activities (rates of 7.4 versus 7.7 mmol/g/h after 30 minutes and conversions of 80 versus 86% after 4 hours, for the peroxydisulfated and sulfated materials were measured, respectively). The supported peroxydisulfated material was shown to be initially more active (14.1 versus 8.9 mmol/g/h after 30 minutes), but similar high conversions (95 and 94%) were detected after 4 hours.

Lavrenov *et al.*[309] reported that the type of sulfating agent is believed to be of no importance. They state that similar results were obtained using sulfuric acid, ammonium sulfate, ammonium peroxydisulfate or gaseous mixtures of either sulfur dioxide or hydrogen disulfide and oxygen. Results are only given for materials prepared from ammonium sulfate though, as it is "the least reactive and neutral reagent" and hence allows greater control over the sulfation procedure and improves reproducibility.

Mishra *et al.*[68,179,310] sulfated dried zirconium hydroxide with ammonium peroxydisulfate via the wetness impregnation technique. Calcination of the material was performed at 873

K for 3 h. The resulting material was found to be active for the isomerisation of *n*-butane at temperatures as low as 308 K under atmospheric pressure.

7.1.3 Motivation

It has been proposed that disulfate groups form the catalytically active sites on sulfated zirconia.[63] Thus it is envisioned the sulfation of zirconia using sulfating agents containing two sulfur atoms would enhance the formation of these disulfate groups and, thus, also the activity of the material produced. Various groups have prepared sulfated zirconia from sulfating agents containing one and two sulfur atoms with varying results, with regards to whether or not using two pregrouped sulfur atoms enhances activity.[303,304,308] A comprehensive study is thus proposed to investigate the effect of using sulfating agents with two pregrouped sulfur atoms. The aim of this study is thus to prepare sulfated zirconia from both sulfating agents with two pregrouped sulfur atoms {ammonium peroxydisulfate and ammonium thiosulfate ($S_2O_3^{2-}$)} and an equivalent mono-sulfur reagent (ammonium sulfate), over a range of sulfate loadings (2, 4.5 and 9 wt.% SO_3), using different sulfate impregnation techniques (incipient wetness and immersion followed by either filtration or evaporation). The effect of the aforementioned sulfation parameters on both the activity of the produced materials for the isomerisation of *n*-butane to isobutane and the formation of an IR band at ~1400 cm^{-1} will be investigated.

7.2 Experimental

7.2.1 Synthesis of powder sulfated zirconias

Zirconium hydroxide (MEL chemicals, XZO 632/03, batch 95/256/01) was dried at 383 K for 21 hours prior to sulfation. Dried 13 g zirconium hydroxide batches were sulfated using ammonium peroxydisulfate, ammonium thiosulfate or ammonium sulfate, via three different impregnation techniques (numbered below). Sulfate loadings, given as weight (wt.) % SO_3, were calculated based on the weight of the dried zirconium hydroxide. Doubly distilled water has been used for all syntheses. All sulfate solutions were prepared immediately prior to their use.

(1) Impregnation via incipient wetness was performed to produce 2, 4.5 and 9 wt.% SO_3 sulfated zirconia. The dried zirconium hydroxide batches were ground while drop wise adding the relevant sulfating agent dissolved in 5.2 ml of water over 20 minutes. The

samples were then dried in a desiccator for at least 24 hours prior to calcination. Samples produced in this way are referred to as incipient wetness prepared.

(2) Zirconium hydroxide batches were immersed in 150 ml aqueous solutions containing 0.1 and 0.22 M of ammonium peroxydisulfate for 15 minutes to produce 2 and 4.5 wt.% SO_3 loadings respectively (molarities were derived by linearly extrapolating results from reference 304). Batches were also immersed in ammonium sulfate and ammonium thiosulfate aqueous solutions with equivalent sulfur concentrations to those used for ammonium peroxydisulfate. The solid material was then vacuum filtered, dried at 383 K for 21 h and stored in a desiccator prior to calcination. The resulting samples are referred to as immersion prepared.

(3) Samples loaded with 2 and 4.5 wt.% SO_3 were prepared by immersing zirconium hydroxide batches in the various sulfating agents dissolved in 50 ml of water followed by rotary evaporation of excess water. The samples were then dried at 383 K for 21 h and stored in a desiccator prior to calcination. Samples produced in this way are referred to as evaporation prepared.

The samples produced from the ammonium peroxydisulfate, ammonium thiosulfate or ammonium sulfate are hereafter denoted $xPSZ_y$, $xTSZ_y$ or xSZ_y, respectively; where x corresponds to the SO_3 wt.% loading and y indicates the impregnation technique (iw = incipient wetness, im = immersion and ev = evaporation prepared).

7.2.2 Calcination of sulfated zirconia powders

Calcination of the synthesised materials was performed in a 8.4 ml quartz boat, as described in reference 311. The boat is designed so that a thermocouple is located in the middle of the bed. The samples were heated to 823 K for 3 hours, using a temperature ramp and maximum cooling rate of 3 K/min. The oven temperature was recorded by a thermocouple placed between the calcination tube and oven wall. In all experiments a flow of 200 ml/min synthetic air was used, except for sample $4.5PSZ_{im}$ which was performed in static air. For comparison, the zirconium hydroxide used and a commercial sulfated zirconia precursor material (MEL Chemicals, XZO 682/01, batch 92/184/01, 5-6 wt.% SO_3) were, also, calcined, after being dried at 383 K for 21 hours. Hereafter, the commercial sulfated zirconia and zirconium hydroxide materials are denoted SZ_{com} and Z_{com}, respectively.

7.2.3 Catalytic testing

Most of the calcined materials were tested for the isomerisation of *n*-butane to isobutane in a plug flow reactor. Reactions were performed using 1 g of material, apart from SZ_{com} for which 500 mg was used. The catalysts were activated at 573 K for 30 minutes in 48 ml/min of synthetic air, followed by flushing at 373 K for 20 minutes in 48 ml/min of helium. The temperature was ramped at 15 K/min. Isomerisation was performed at 383 K with a feed of 80 ml/min 5 vol.% (or 1 vol.% for SZ_{com}) *n*-butane in helium. Online analysis was performed using a Micro-GC (Varian, 4900) with a CP-Sil 5 CB column and thermal conductivity detector.

7.2.4 TG-DSC-MS

Thermogravimetry (TG) and differential scanning calorimetry (DSC) simultaneous analyses were performed on selected samples using a STA 499 C instrument (Netzsch) with online MS (Pfeiffer, QMS 200). Samples $4.5PS_{iw}$ and $9PS_{iw}$ (both not calcined) were heated to 1373 K at 3 K/min in 21% oxygen in helium. Selected calcined materials (see Table 7-2) were heated in argon to 1373 K, held at this temperature for 30 minutes then cooled to 473 K, using heating and cooling rates of 10 K/min.

7.2.5 BET surface area

Surface areas of selected calcined samples (see Table 7-2) were measured by nitrogen adsorption according to the method of Brunauer, Emmett and Teller (BET). The samples were outgassed, prior to measurements, *in vacuo* at 523 K for 3 hours. The BET surface areas were calculated from multipoint analyses, additionally the pore size distributions were determined according to the Barrett, Joyner and Halenda (BJH) method.

7.2.6 XRD

X-ray diffractograms of calcined samples $2PSZ_{iw}$, $4.5PSZ_{iw}$ and $9SZ_{iw}$ were recorded using a Bruker AXS D8 advance diffractometer in reflection (Bragg-Brentano) geometry with Cu Kα radiation, a secondary graphite monochromator and scintillation detector.

Fittings of the diffractograms were performed using the Topas v.3.0 program. Monoclinic and tetragonal zirconia fractions were derived directly from Rietveld fits of ICSD 156entries 89426 and 97004, respectively. The fraction of XRD amorphous phase was estimated by fitting a model consisting of 7 broad Gaussian peaks. The model was derived from the XRD pattern of a commercial sulfate doped zirconium hydroxide

sample (MEL Chemicals, XZO 1249/01, produced 15.5.06, ~7 wt.% SO_3), after being dried for 21 hours at 383 K. Relative intensities and peak positions of the model were fixed but peak widths and total intensity were varied for the fitting of mixed precursor and crystalline samples.

7.2.7 XPS

X-ray photoelectron spectra of calcined samples $4.5TSZ_{im}$ and $4.5SZ_{im}$ were taken with a Leybold LHS 12 MCD instrument[248] using Mg Kα excitation. Detailed scans of the Zr 3d, O 1s, S 2p and N 1s regions were recorded for each sample, the C 1s region was also recorded for $4.5TSZ_{iw}$. Binding energies were corrected to Zr $3d_{5/2}$ = 182.2 eV of ZrO_2,[154] to account for electrostatic charging. Shirley backgrounds were subtracted from the Zr 3d and O 1s peaks and linear backgrounds were used for the S 2p and C 1s peaks.

7.2.8 DRIFTS

Diffuse reflectance infra-red Fourier transform spectroscopy (DRIFTS) was performed using a Bruker IFS 66 FTIR spectrometer (1-2 cm^{-1} resolution) equipped with an *in situ* cell (Graseby Specac, Environmental Chamber) with a chemically resistant ZnSe window, a diffuse-reflectance attachment (Graseby Specac, "The Selector") and a D315M MCT detector. The samples were placed in a gold cup, which is situated on a heatable platform. Selected calcined materials were activated *in situ* at 573 K for 30 minutes in 48 ml/min of 20.5% oxygen in nitrogen, followed by cooling to 373 K, the temperature was ramped up and down at 15 K/min. The cell was then flushed at 373 K with 48 ml/min nitrogen for at least 20 minutes prior to measuring under the same conditions. Spectra were background corrected using a KBr reference measured in nitrogen.

Positions of overlapping bands, appearing as shoulders, have been determined using the second derivative.[312] For quantitative relevant band intensities the spectra were converted using the Kubelka-Munk (KM) function, after normalising the reflectance spectra at 4800 cm^{-1} to 0.9 (to account for any differences in bed height).

7.3 Results

7.3.1 Calcination of catalysts

Comparative measurements of bed and oven temperatures during calcinations of materials loaded with 4.5 wt.% SO_3 are presented in Figure 7-1. For all samples the bed temperature was shown to lag behind the oven temperature between 423 and 573 K (oven temperature), indicating an endothermic process is occurring. This is due to the removal of water. At higher temperatures, between ca. 703 to 798 K, for the 2 and 4.5 wt.% SO_3 samples an exothermic process occurs causing the bed temperature to increase by up to 100 K above the oven temperature. This rapid overheating of the sample is seen at higher temperatures for the 4.5 wt.% SO_3 loaded materials (as compared to 2 wt.% SO_3 loaded materials prepared using the same technique and sulfating agent), but is not observed for the 9 wt.% SO_3 loaded materials. For each of the different sulfation techniques used trends are observed for the 2 and 4.5 wt.% SO_3 loaded materials with regards to the oven temperature at which the maximum bed overshoot temperature is reached. However, the trends differ for the different sulfation techniques, for incipient wetness: $PSZ_{iw} > SZ_{iw} > TSZ_{iw}$, for immersion: $TSZ_{im} > SZ_{im} > PSZ_{im}$ and for evaporation $TSZ_{ev} > PSZ_{ev} > SZ_{ev}$. There do not appear to be any trends in the maximum bed overshoot temperature.

7.3.2 Catalytic testing

Maximum *n*-butane isomerisation activities and after 12 hours are given for tested materials in Table 7-1 and selected reaction profiles are shown in Figure 7-2. None of the 2 wt.% SO_3 loaded materials were found to be catalytically active. For each of the sulfating techniques used the 4.5SZ loaded materials were found to be the most active. The 4.5PSZ materials, prepared by a given sulfation technique, were generally found to be more active than the 4.5TSZ materials, apart from the inactive $4.5PSZ_{im}$ sample which was calcined in static air. For the 4.5SZ materials the immersion technique produced the most active material and the evaporation technique the least active. The immersion technique, also, produced the most active 4.5TSZ material; however, the incipient wetness technique produced the least active. For the 4.5PSZ materials the incipient wetness prepared sample was found to be more active then the material prepared by evaporation.

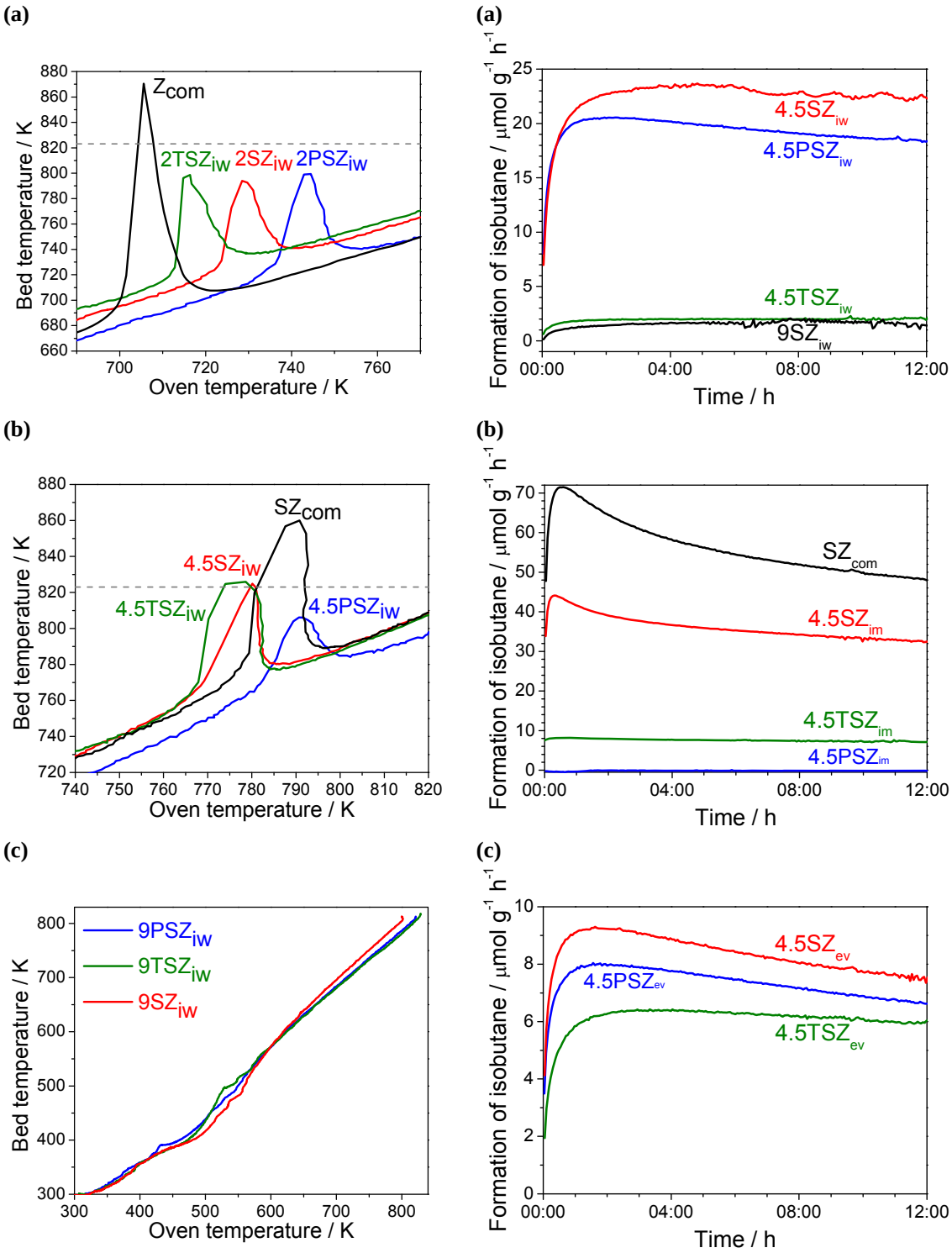

Figure 7-1: Calcination glow curves for (a) 2 wt.% (b) 4.5 wt.% and (c) 9 wt.% SO_3 loadings of various sulfating agents on zirconia, including Z_{com} (a) and SZ_{com} (b). Dashed lines indicate maximum oven temperature.

Figure 7-2: Isomerisation of *n*-butane to isobutane over sulfated zirconia catalysts synthesized via (a) incipient wetness, (b) immersion (including commercially prepared material, SZ_{com}) and (c) evaporation techniques.

Table 7-1: Calcination oven temperatures at "glow" maximum and catalytic activities for the isomerisation of 5 kPa *n*-butane at 383 K, except (i) which was measured in 1 kPa *n*-butane. (ii) Calcined in static air, n.d. = not detected and - = not measured.

Catalyst	Glow maximum oven temperature K	Catalysis Maximum rate μmol/g/h	Time / h	Rate after 12 h μmol/g/h
SZ_{com}	791	71.8[(i)]	0:49	48.5[(i)]
Z_{com}	697	n.d.	-	n.d.
$2PSZ_{iw}$	745	-	-	-
$2SZ_{iw}$	729	n.d.	-	n.d.
$2TS_{iw}$	716	n.d.	-	n.d.
$4.5PSZ_{iw}$	791	20.5	2:03	18.4
$4.5SZ_{iw}$	780	23.7	4:50	22.3
$4.5TSZ_{iw}$	779	2.2	2:00	2.2
$9SZ_{iw}$	n.d.	1.4	2:45	1.4
$2PSZ_{im}$	714	n.d.	-	n.d.
$2SZ_{im}$	750	n.d.	-	n.d.
$2TSZ_{im}$	754	n.d.	-	n.d.
$4.5PSZ_{im}$[(ii)]	724	n.d.	-	n.d.
$4.5SZ_{im}$	780	44.1	0:18	32.5
$4.5TSZ_{im}$	786	8.2	0:35	7.1
$2PSZ_{ev}$	742	-	-	-
$2SZ_{ev}$	719	-	-	-
$2TSZ_{ev}$	747	-	-	-
$4.5PSZ_{ev}$	777	8.0	1:35	6.6
$4.5SZ_{ev}$	758	9.3	1:37	7.5
$4.5TSZ_{ev}$	787	6.4	3:20	6.0

SZ_{com} was shown to be more active than the synthesised samples, despite using a lower feed concentration. The pure zirconia material, Z_{com}, was found to be inactive.

7.3.3 TGA-DSC-MS

TG and DSC plots for samples $4.5PSZ_{iw}$ and $9PSZ_{iw}$, prior to calcination, are shown in Figure 7-3a. The measurements were performed under conditions (gas atmosphere and temperature ramp) selected to mimic the heating ramp of the calcination procedure. A mass loss of ~14% from both materials is seen upon heating to 823 K (the calcination temperature). Above ~873 K a second mass loss is observed, the degree of this mass loss differs for the samples. This second mass loss corresponds to a further loss of 3.4% for $4.5PSZ_{iw}$ and 7.8% for $9PSZ_{iw}$. The DSC signal indicates that the sample $4.5PSZ_{iw}$ undergoes an exothermic process from 600 K onwards with a peak at 798 K, this is in good agreement with the temperature overshoot seen during the calcination of this

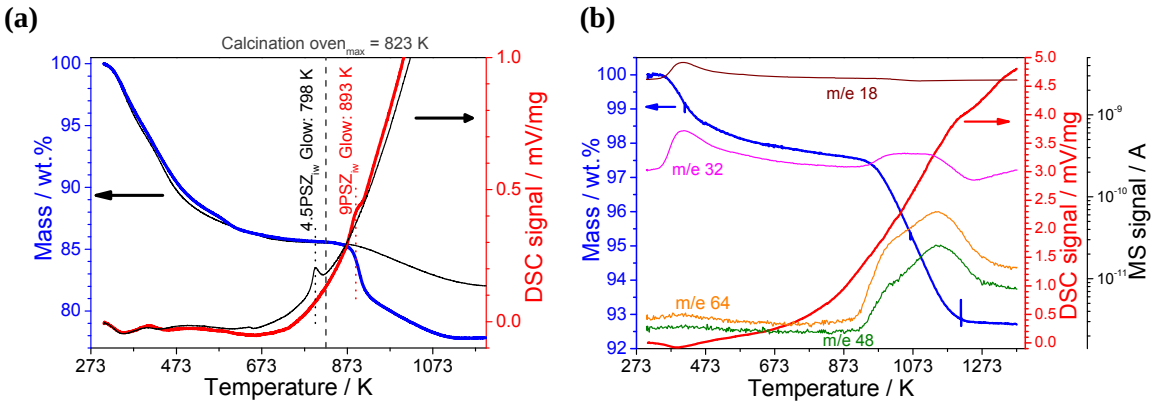

Figure 7-3: TG and DSC analysis of (a) 4.5PSZ$_{iw}$ (thin lines) and 9PSZ$_{iw}$ (thick lines) prior to calcination and (b) 4.5 PSZ$_{iw}$ after calcination, including selected MS m/z ratios.

material at 791 K (oven temperature). The exothermic process appears to be delayed for the 9PSZ$_{iw}$ sample; a broad peak is seen at 893 K concurrent with the second mass loss.

In Figure 7-3b TG, DSC and MS data are shown for the calcined sample 4.5PSZ$_{iw}$.The calcined sample, also, appears to lose mass in two different steps, one between room temperature and ~923 K and the second from ~923 K to ~1273 K. For both the samples before and after calcination the evolution of water is detected during the first mass loss (as indicated from m/e 18 and 17 MS signals, from H_2O^+ and OH^+). Concomitant detection of oxygen (MS signals m/z 32 and 16, from O_2^+ and O^+) during this mass loss is believed to be an artefact, from the decomposition of water in the MS.[244] During the second mass loss, for both the materials measured prior to and after calcination, sulfate fragments (MS signals m/z 64 and 48, from SO_2^+ and SO^+) and oxygen are detected. According to Srinivasan *et al.*[159] sulfate decomposes by the following pathway: $SO_3 \rightarrow SO_2 + ½O_2$. Based on the second mass loss being due to such a reaction SO_3 wt.% contents for measured calcined materials are presented in Table 7-2. The calculated SO_3 wt.% contents all agree well with the loadings of the materials.

7.3.4 BET surface area

Similar surface areas of ~160 m²/g were measured from the 4.5 wt.% SO_3 samples (see Table 7-2). The materials were also shown to have similar pore size distributions, with modal values of ~25 Å and maximum pores of ~40 Å.

7.3.5 XRD

X-ray diffractograms and calculated phase compositions for the selected 2, 4.5 and 9 wt.% SO_3 materials measured are presented in Figure 7-4. The 2 wt.% SO_3 material

Table 7-2: BET surface areas and sulfate contents, calculated from TG and XPS experiments, of samples measured.

Sample	Surface Area m^2/g	TG measurements: wt.% SO_3 hydrated	wt.% SO_3 dehydrated	XPS measurements: atomic% S	wt.% SO_3
$2PSZ_{iw}$	-	2.3	2.4	-	-
$4.5PSZ_{iw}$	160.2	4.9	5.0	-	-
$4.5SZ_{iw}$	165.6	-	-	-	-
$4.5TSZ_{iw}$	161.7	-	-	-	-
$4.5SZ_{im}$	161.0	5.2	5.3	3.6	7.6
$4.5TSZ_{im}$	155.1	4.5	4.6	4.1	8.9
$4.5PSZ_{ev}$	163.1	4.4	4.5	-	-

($2PSZ_{iw}$) is shown to consist of a mixture of monoclinic and tetragonal phases. Whereas the 4.5 wt.% SO_3 material ($4.5PSZ_{iw}$) is predominantly the tetragonal phase, with only a small fraction of the monoclinic phase. However, the 9 wt.% SO_3 material ($9SZ_{iw}$) has a large fraction of XRD amorphous material, the crystalline material present is consistent with the tetragonal phase.

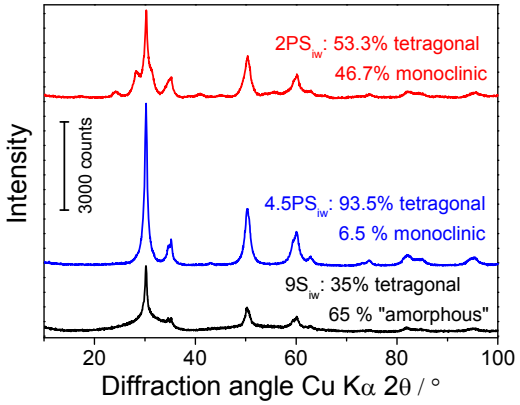

Figure 7-4: X-ray diffractograms of calcined $2PSZ_{iw}$, $4.5PSZ_{iw}$ and $9SZ_{iw}$.

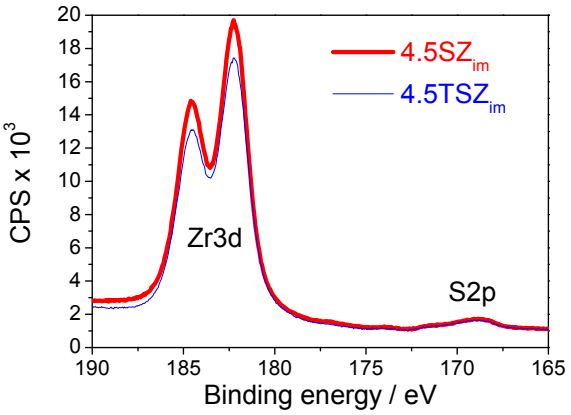

Figure 7-5: Zr3d and S2p XP spectra of calcined samples $4.5SZ_{im}$ (thick) and $4.5TSZ_{im}$ (thin lines).

7.3.6 XPS

XP Spectra of the Zr 3d and S 2p regions for calcined samples $4.5SZ_{im}$ and $4.5TSZ_{im}$ are shown in Figure 7-5. The peaks are skewed towards lower binding energies because of differential charging of the samples, as confirmed in the O 1s region. Charging corrections of ~5 eV have been applied to the spectra of both samples. The S 2p peaks of the two samples are similar; they are centred at ~169 eV, indicating the sulfur present has an oxidation state of +6. No nitrogen was detected in either sample. The $4.5TSZ_{im}$ sample was shown to have a low concentration of carbon, ~2.5 atomic %. The $4.5SZ_{im}$ sample

also has a low carbon concentration (below the detection limit of the survey scans). Sulfate concentrations for the two samples are comparable (as shown in Table 7-2).

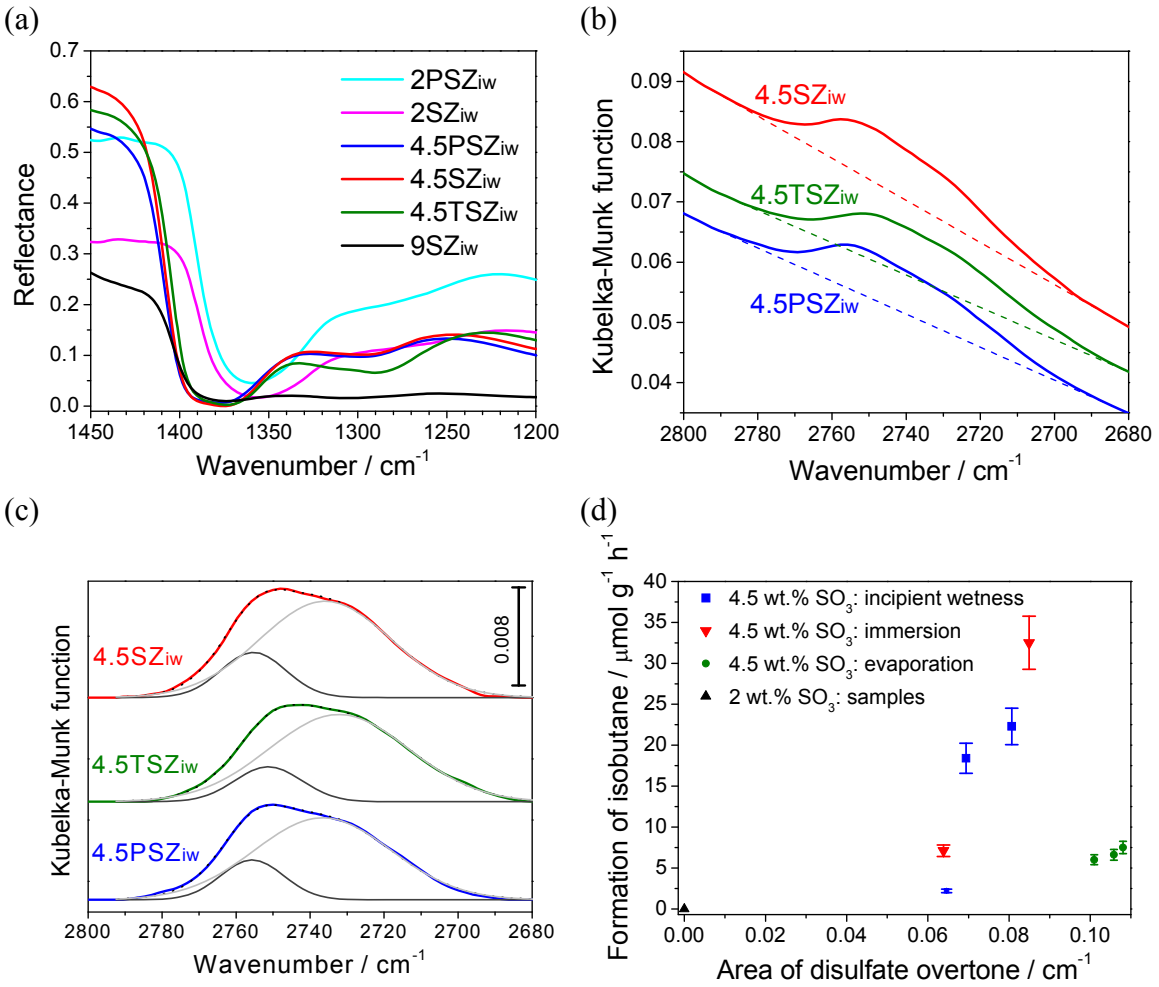

Figure 7-6: DRIFT Spectra of (a) ν(S=O) region of sulfated samples prepared via incipient wetness, (b) overtone of main ν(S=O) bands and (c) peak fitting of the overtone for 4.5 wt. % SO_3 sulfated zirconia samples prepared by incipient wetness. (d) Area of disulfate overtone band versus isomerisation activities for 4.5 and 2 wt.% SO_3 loaded samples measured.

7.3.7 DRIFTS

DRIFT spectra of measured activated samples show similar features to those previously reported for sulfated zirconia.[284] Spectra of the S=O stretching region of incipient wetness prepared samples and band positions for all measured samples are given in Figure 7-6a and Table 7-3. The S=O stretching region shows three main bands, the predominant band is centred at 1369-1387 cm^{-1} (or 1356-1360 cm^{-1} for the 2 wt.% SO_3 loaded samples). An overlapping band is seen as a shoulder at slightly higher

wavenumbers (1398-1400 cm^{-1} or 1383-1385 cm^{-1} for the 2 wt.% SO_3 loaded samples). A weaker band is seen at lower wavenumbers, at 1292-1300 cm^{-1} for all 4.5 wt.% SO_3 loaded samples. For the 9 wt.% SO_3 sample measured this band is weaker still and at slightly higher wavenumbers (1304 cm^{-1}). Samples loaded with 2 wt.% SO_3 show a very weak band at 1279 cm^{-1}.

Table 7-3: ν(S=O) DRIFTS band positions (in cm^{-1}) of measured sulfated zirconia samples and assignments based on references 62 and 313. Note: sh = shoulder, w = weak and vw = very weak bands.

Sample	$[S_2O_7^{2-},2H^+]$ or $[SO_3]$	$[HSO_4^-,SO_4^-, 3H^+,2H_2O]$ or $[SO_4^{2-},2H^+]$		$[SO_4^{2-}, 2H^+,3H_2O]$	$[HSO_4^-,SO_4^-, 3H^+,2H_2O]$
$2PSZ_{iw}$	-	1385 sh	1360	-	1279 vw
$2SZ_{iw}$	-	1383 sh	1356	-	1279 vw
$4.5PSZ_{iw}$	1400 sh	1377	-	1298	-
$4.5SZ_{iw}$	1400 sh	1375	-	1298	-
$4.5TSZ_{iw}$	1400 sh	1377	-	1296	-
$4.5SZ_{im}$	1400 sh	1375	-	1300	-
$4.5TSZ_{im}$	1400 sh	1377	-	1296	-
$4.5PSZ_{ev}$	1398 sh	1387	-	1300	-
$4.5SZ_{ev}$	1398 sh	1369	-	1292	-
$4.5TSZ_{ev}$	1400 sh	1373	-	1284	-
$9SZ_{iw}$	1398 sh	1373	-	1304 w	-

Table 7-4: Fits of the DRIFTS main ν(S=O) overtone, after Kulbelka-Munk function conversion, for all 4.5 wt.% SO_3 loaded samples measured, assignments based on references 62 and 284.

Sample	$[S_2O_7^{2-},2H^+]$ or $[SO_3]$		$[HSO_4^-,SO_4^-, 3H^+,2H_2O]$ or $[SO_4^{2-},2H^+]$			
	Position / cm^{-1}	Area / cm^{-1}	Position / cm^{-1}	Area / cm^{-1}	Position / cm^{-1}	Area / cm^{-1}
$4.5PSZ_{iw}$	2756	0.069	2737	0.308	-	-
$4.5SZ_{iw}$	2755	0.081	2736	0.349	-	-
$4.5TSZ_{iw}$	2751	0.065	2732	0.337	-	-
$4.5SZ_{im}$	2754	0.085	2733	0.352	-	-
$4.5TSZ_{im}$	2752	0.064	2732	0.307	-	-
$4.5PSZ_{ev}$	2753	0.106	2730	0.623	2693	0.022
$4.5SZ_{ev}$	2754	0.108	2735	0.464	-	-
$4.5TSZ_{ev}$	2755	0.101	2740	0.485	-	-

Quantification of the S=O stretching bands seen between 1279-1400 cm^{-1} is not possible, even after normalisation and conversion using the Kubelka-Munk function, because of the strong intensity of these bands and uncertainties arising from the background. However, overtones of the two stronger S=O stretching bands are seen between ~2680-

2780 cm^{-1} (see Figure 7-6b), the relative intensities of which can be compared. Fits of these overtone bands were performed (Figure 7-6c) using a linear background and constraining the full width half maximum (FWHM) of the higher wavenumber component to between 17-20 cm^{-1}. Two components were used to fit the spectra of all samples except $4.5PSZ_{ev}$ for which three components were used due to the increased width of the overtone (~20 cm^{-1} towards lower wavenumbers) indicating the presence of another overlapping band. The positions and areas of the fitted components for all 4.5 wt.% SO_3 loaded samples measured are given in Table 7-4. Bandwidths varied between 17.0-18.3 cm^{-1} for the band at ~2754 cm^{-1} and 35-39 cm^{-1} for the band at ~2735 cm^{-1}, the additional component of $4.5PSZ_{ev}$ has a bandwidth of 28 cm^{-1}. Materials prepared using the evaporation technique were found to have the largest areas of all components. Incipient wetness and immersion prepared materials were found to have similar areas (for materials loaded with the same sulfating agent). For all techniques the 4.5SZ materials had the largest higher wavenumber component and the 4.5TSZ materials the smallest.

7.4 Discussion

The presence of an exothermic "glow" process during the calcination of sulfated zirconia has previously been ascribed to a reduction in surface area and complete crystallisation of the material.[314-318] Increasing the sulfur content has been reported to shift the "glow" to higher temperatures,[319] as shown here by calcination curves for the 2-4.5 wt.% SO_3 materials. High loadings of sulfur (9 wt.% SO_3) increase the temperature required to completely crystallise the material to above the calcination temperature used, as shown by TGA-DSC, hence no "glow" is observed during calcination and XRD reveals the calcined material ($9SZ_{iw}$) to be predominantly XRD amorphous. In order to fully crystallise the materials with high sulfur loadings the calcination temperature should be increased. TGA/DSC/MS plots, however, show the "glow" to coincide with the loss of sulfate. The samples with high sulfur loadings are therefore considered not to be stable with respect to forming a fully crystalline material under the conditions used. Materials loaded with 9 wt.% SO_3 were therefore only prepared via incipient wetness and just one sample was catalytically tested. The material $9SZ_{iw}$ was found to have a low catalytic activity, which is attributed to its low fraction of tetragonal phase.

Low sulfur loadings (2 wt.% SO_3) result not only in the "glow" being at a lower oven temperature (compared to 4.5 wt.% SO_3 loaded materials) but, also, the fraction of tetragonal phase is significantly reduced (by the formation of the monoclinic phase), as shown by XRD. The metastable tetragonal phase of zirconia is known to be stabilised by the presence of sulfate, if, however, the sulfur loading is very low then the stable monoclinic phase is, also, formed.[18] The tetragonal phase has been shown to be a necessary but not sufficient requirement to form a highly active catalytic material.[27] Nevertheless, materials with low sulfur contents were still prepared, from the different sulfating agents, to test if the minimum sulfur content required to produce an active material is due to the absence of disulfates caused by the isolation of mono-sulfate species. All materials prepared with a loading of 2 wt.% SO_3 were, however, found to be inactive for the isomerisation of *n*-butane.

The oven temperature at which the "glow" occurs for samples loaded with the same sulfur content (either 2 or 4.5 wt.% SO_3) would be expected to depend on the sulfate precursor used, given that the sulfate structures have different thermal stabilities. However, the order in which the glow exotherms occur for the different sulfating agents varies depending on the sulfation technique used. A possible explanation is that the sulfur content or the degree of hydration of the materials (prior to calcination) may change slightly for the materials loaded with different sulfating agents depending on the sulfation technique used. The catalytic activities of the 4.5 wt.% SO_3 loaded materials do not seem to correlate with the "glow" trends observed.

Sample 4.5PSZ_{im} was found to be the only inactive 4.5 wt.% SO_3 loaded material, this is believed to be due the different calcination conditions used for this sample. Comparisons with this sample are therefore not considered meaningful, thus the sample was excluded from further characterisation and will not be discussed hereafter.

Sulfate contents (determined as wt.% SO_3) of selected calcined samples as derived from TGA/MS results show similar values to the loaded amounts. Slight differences in sulfate content do not show any consistent trend with catalytic activity. Higher sulfate contents from XPS results than from TGA/MS calculations indicate the sulfate surface concentration to be enhanced compared to the bulk. Given that only slight variations in sulfur contents and surface areas of the samples measured were observed, the differing

activities of the materials are not believed to result from different concentrations of sulfur at the surface.

XP spectra of the calcined ammonium thiosulfate loaded sample measured ($4.5TSZ_{im}$) show the sulfur on the material to be completely oxidised to S^{6+}. The generally lower activities of the ammonium thiosulfate loaded materials, as compared with the ammonium sulfate loaded, cannot therefore be due to the oxidation state of sulfur. This is to the author's knowledge the first report of active sulfated zirconia isomerisation catalysts being prepared from ammonium thiosulfate.

DRIFTS measurements show that only samples possessing at band at ~1400-1398cm^{-1} are catalytically active. The presence of such a band is ascribed to disulfate groups, given the results of reference 62 and the preparation conditions used. Integrating the overtone of this band[284] for active samples, after peak fitting to remove contributions from overlapping band(s), shows no direct correlation between band intensity and catalytic activity (Figure 7-6d). Materials prepared from precursors with two sulfur atoms, also, do not have a more intense disulfate overtone band. Given the relative high stability of both peroxydisulfate and thiosulfate salts in aqueous solutions[320,321] the pregrouped sulfur atoms are therefore assumed to dissociate either upon adsorption or during calcination.

The materials prepared via the evaporation technique have the most intense overtone bands, possibly due to them having higher surface sulfate concentrations. During the evaporation technique the sulfate is forced to precipitate on the surface of zirconium hydroxide, whereas using the incipient wetness or immersion techniques sulfate deposition within the pores of zirconium hydroxide is more likely to occur via capillary forces or diffusion, respectively. If materials prepared using the same sulfating technique are compared a correlation (although not linear) is observed between the disulfate overtone band area and the catalytic activity of the materials. The same trends in both disulfate band area and catalytic activity are seen for each of the sulfating techniques used.

The presence of disulfate groups on sulfated zirconia are therefore considered a prerequisite for forming an active isomerisation material; however, other factors such as the sulfation technique are considered more influential on the catalytic activity than the concentration of the disulfate groups. These more "influential" factors may be directly

linked to the formation of "defect" sites which dictate the activity of adjacent catalytic sites.

7.5 Conclusions

Powdered sulfated zirconia materials were successfully synthesised from three different sulfating agents (ammonium sulfate, peroxydisulfate and thiosulfate), each added via three different impregnation techniques (incipient wetness, immersion and evaporation). Preparing sulfated zirconia from sulfating agents containing two sulfur atoms did not increase the catalytic activity of the material. DRIFTS showed the formation of disulfate groups also not to be promoted by use of precursors containing two pregrouped sulfur atoms. The concentration of the disulfate band was shown not to correlate directly with the catalytic activity of the materials produced. However, only materials with a disulfate band were found to be active and for materials prepared in a similar way, higher disulfate concentrations result in more active materials. The formation of disulfate groups is therefore a prerequisite for catalytic activity. It is proposed that the catalytic sites are generated from these disulfate species but that their isomerisation activities depend on their environment rather than their total concentration.

8. Conclusions

The aim of this thesis was to investigate the surface chemistry of sulfated zirconia in order to reveal information about its active isomerisation sites. To study the surface chemistry of sulfated zirconia various model systems have been prepared to allow the application of surface science techniques and to test the theory that disulfate groups[62,63] are responsible for the generation of active sites on the catalyst.

8.1 Synthesis of Model Systems

Sulfated zirconia model systems were successfully produced via a range of different preparation techniques. Thin films of sulfated zirconia were prepared on oxidised silicon wafers, via the use of a self-assembled monolayer to promote heterogeneous deposition from an acid stabilised aqueous solution of zirconium sulfate. Developments were made to the thin film synthesis to reduce contamination and homogeneous deposition, characterisation (following the changes) showed any such abnormalities in the films to be negligible.

Thermal treatment of the films was optimised to chemically mimic the powder process using an oxygen-containing atmosphere. The film thickness and heterogeneous deposition mechanism were shown to be critical factors for formation of the tetragonal phase. Surface stabilisation of the amorphous phase is proposed to prevent very thin (<5 nm) films from undergoing crystallisation. Homogeneous precipitation of an analogous powder, from an equivalent deposition medium, was found to form a mixture of tetragonal and monoclinic phases after thermal treatment under the conditions studied. The development of a mixed phase oxide after the investigated thermal treatments is proposed to occur as a result of re-crystallisation of orthorhombic zirconium sulfate during homogeneous precipitation as opposed to the amorphous thin films which are formed during heterogeneous deposition. Thermally treated thin films were found to have the essential features (including equivalent sulfur content, crystalline phase and acidic properties) of active powder catalysts,[162] thus validating them as a model system. The use of sulfated zirconia thin films improved the application of various surface science techniques to the material, as compared with results from powder studies.

Sulfating agents containing one (ammonium sulfate) and two sulfur atoms (ammonium peroxydisulfate and thiosulfate) were used to produce sulfated zirconia powders via various impregnation techniques (incipient wetness, immersion and evaporation). Experimental determinations of the overall sulfur content of the materials after thermal treatment agreed well with the calculated loadings, however sulfur was found to be enriched at the surface. Sulfur was detected only in the +6 oxidation state after thermal treatment, thus indicating the complete oxidation of the thiosulfate loaded material. The level of sulfur loading was shown to dictate the crystalline phase of the material; too high (9 wt.% SO_3) and the materials did not fully crystallise, too low (2 wt.% SO_3) and the more stable monoclinic phase was also formed in significant amounts. The thermally treated 4.5 wt.% SO_3 loaded material was shown to consist of predominantly the tetragonal phase.

8.2 Sulfated Zirconia Surface Sites

Two distinctly different chemisorption sites were detected on sulfated zirconia by both ammonia and *n*-butane adsorption studies. Ammonia adsorption on the sulfated zirconia thin films followed by thermal desorption resulted in the evolution of ammonia in two stages. A broad peak at relatively low temperatures indicating weakly bound molecules and a second peak at higher temperatures with concurrent loss of sulfate were observed. The basic probe molecule therefore not only adsorbs but also reacts with certain sites on the sulfated zirconia thin films, these two types of interactions arise from different surface sites.

Low temperature XPS measurements showed *n*-butane adsorption to be promoted over the sulfated zirconia thin films, as compared with the oxidised silicon wafers used as substrates. However the adsorbed reactant molecule, *n*-butane, was found to be liable to beam damage during exposure to *n*-butane. In order to measure multiple adsorption-desorption equilibrium isobars, with a single sample, at different pressures the effects of beam damage were reduced to a negligible level by the use of a low energy excitation source (UV radiation) and conducting the experiments in a manner to minimise adsorbate irradiation. UPS isobars could thus be measured on the sulfated zirconia thin films. This technique has previously never been applied to such a complex system as sulfated

zirconia and is only possible due to the conducting nature of the model thin films. The application of this technique allowed not only the generation of information regarding the strength of interaction (heats of adsorption) but also provided spectroscopic data (UP spectra) showing how the interaction changes with coverage.

Adsorption of *n*-butane equivalent to 5 and 25% of a monolayer coverage on the sulfated zirconia thin films, releasing heats of between 59-40 and 47-34 kJ/mol, is ascribed to strong and weak chemisorption respectively. The deduced heats of adsorptions are in good agreement with values obtained from powder sulfated zirconias.[27,225,227] An increase in adsorption heat was observed between coverages of ~5-8% of a monolayer, this is believed to be due to adsorbate-adsorbate interactions. Physisorption on the films generates heats of ~28 kJ/mol, for coverages between 30% up to a complete monolayer. Multilayer adsorption results in the formation of an insulating adsorbate structure. *n*-Butane adsorption is reversible under the conditions studied.

Sulfated zirconia powders, loaded with 4.5 wt.% SO_3, have sulfate S=O stretching bands that can be ascribed to mono-sulfate and disulfate groups. Materials with low sulfate loadings (2 wt.% SO_3) only show the presence of mono-sulfate bands. The highly loaded sulfate (9 wt.% SO_3) material measured showed intense sulfate stretching bands, but the disulfate band was relatively weak. For the 4.5 wt.% SO_3 loaded materials, those prepared via the evaporation technique were shown to have the most intense disulfate bands. For each of the different preparation techniques used the materials prepared from ammonium sulfate were found to have the most intense disulfate bands and those prepared from ammonium thiosulfate the weakest. Thus the use of sulfating agents containing two sulfur atoms does not promote the formation of disulfate spices, possibly due to their dissociation on adsorption or during calcination. The disulfate band was found to be much weaker than the mono-sulfate ascribed band for all samples studied.

Given the adsorption studies on the sulfated zirconia thin films and the DRIFTS analysis of the selectively synthesised powders it is proposed that the more strongly chemisorbing sites, which reacted with ammonia and have 59-40 kJ/mol *n*-butane heats of adsorption, correspond to a minority, disulfate species. Hence the weaker, more dominant chemisorption sites are ascribed to mono-sulfate species. The formation of the disulfate groups depends on various preparation factors, such as the sulfate loading, the synthesis

method and the sulfate precursor. The range of *n*-butane heats of adsorption and width of ammonia thermal desorption peaks for both the disulfate and mono-sulfate species are attributed to there being a distribution of similar adsorption sites. It is thus envisioned the chemical environment of the disulfate and mono-sulfate species play a key role in their adsorption properties.

8.3 Reactivity of Sulfated Zirconia

Beam influenced deposition was observed during *n*-butane *in situ* studies on the surface of the sulfated zirconia thin films under reactive conditions. Carbon deposits were, however, found to be stable to irradiation after removal of the gas phase. The formation of carbonaceous surface deposits, after *ex situ* exposure to *n*-butane under reactive conditions, proves the films contain reactive centres. The application of a synchrotron light source enabled the high resolution analysis of the chemical states of the surface deposits and the sulfated zirconia thin films. Evaluation of these stable carbon deposits by XPS revealed the existence of at least three different chemical environments; which are ascribed to "chain" like carbon (such as small hydrocarbons), aliphatic polymers and oxygenated carbon. Further analysis by NEXAFS reveals the presence of unsaturated hydrocarbons, which are consistent with butenes. The dehydrogenating ability of the sulfated zirconia thin films was also confirmed by the increased detection of alkene fragments, as compared to oxidised silicon wafers, during TDS after exposure to *n*-butane at room temperature. During reactive exposure to *n*-butane sulfate groups were shown to be reduced.

The formation of unsaturated hydrocarbon surface species and sulfate reduction, under reaction conditions, are attributes that support oxidative dehydrogenation (Figure 8-1) being the isomerisation initiation mechanism.[63,90] The detection of oxygenated species is also consistent with a stabilised carbocation being the catalytically active site. Aliphatic polymers detected are proposed to be formed via the oligomerisation of alkenes on the surface.

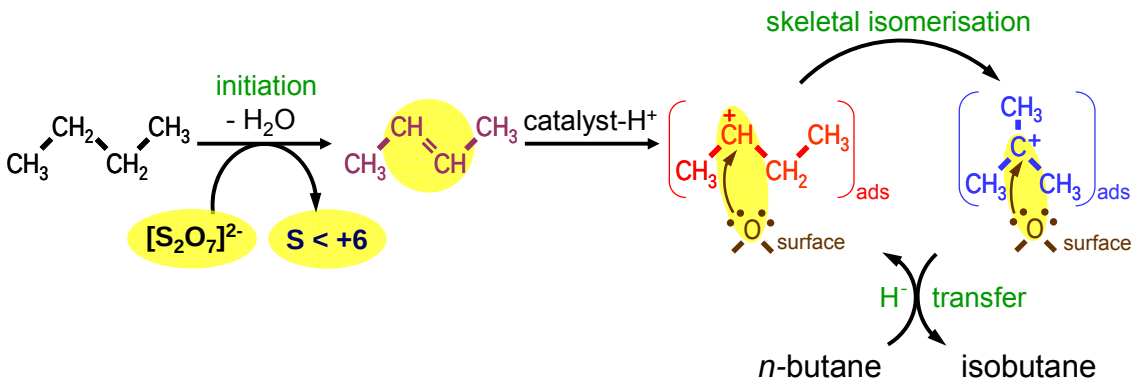

Figure 8-1: Proposed sulfated zirconia isomerisation mechanism, via oxidative dehydrogenation initiation. Evidence for highlighted chemical species detected.

Detection of adsorbate-adsorbate interactions at higher chemisorption coverages (above 5% of a monolayer) indicate the alkane molecules are positioned next to one another. The skeletal isomerisation proceeding via a bimolecular mechanism is thus plausible under such surface coverages.

Catalytic testing of the synthesised powder sulfated zirconias for the isomerisation of *n*-butane showed the use of precursors containing two sulfur atoms not to increase the catalytic activity of the material. Only materials that possess vibrational bands indicating the presence of disulfate groups were, however, found to be active. The relative disulfate concentrations, as determined from the fitted disulfate overtone band area, did not directly correlate with the catalytic activity of the samples. For materials prepared using the same sulfation technique the same trends in activity and disulfate band area were observed (ammonium sulfate > ammonium peroxydisulfate > ammonium thiosulfate prepared).

The presence of disulfate groups is therefore considered a prerequisite for catalytic activity. It is proposed that the reactivity of the active sites, generated by the oxidative dehydrogenation of the reactant alkane by these disulfate groups, is not just dependent on their concentration but also on more influential factors such as their chemical environment. The existence of adjacent defects is postulated as one factor that may affect the chemical reactivity of the active groups. From adsorption studies on the sulfated zirconia thin films it is believed the disulfate groups exist in a variety of slightly differing chemical environments. The formation of disulfate groups and the surface chemistry of zirconia are thus highly dependent on the synthesis conditions.

8.4 Contributions of Model Systems to the Scientific Understanding of Sulfated Zirconia Isomerisation Catalysts

The use of a model thin film system has allowed the materials gap which exists within catalysis research to be bridged. Thin films of sulfated zirconia have enabled surface science techniques to be applied while not compromising the chemical complexity of the catalyst.

Equilibrium adsorption-desorption investigations under isobaric conditions on the thin films, using UPS, which would not have been possible on powder materials, have yielded concurrent heats of adsorption and spectroscopic data. Such measurements, producing heats similar to those acquired from powder catalysts,[27,225,227,228] have enabled the different types of adsorption to be identified and quantified. This level of interpretation has not been possible from previously published data of adsorption heats on sulfated zirconia powders catalysts.

Studying the films under reactive conditions has shown the development of carbonaceous deposits on their surface, thus proving the films have reactive centres and validating them as model systems. Detailed analysis of the deposited species and film's surface has revealed the following chemical information:

(i) The deposited species is unsaturated, with a π^* resonance typical of butene, thus proving the dehydrogenation ability of sulfated zirconia.

(ii) Concurrent reduction of sulfate, indicating the unsaturated deposits are formed by oxidative dehydrogenation.

(iii) Formation of oxygenated carbonaceous groups, which are consistent with the stabilisation of the proposed carbocation intermediate.

The identification of such groups have been greatly aided by the use of the thin films to allow high resolution XPS to be performed and the utilisation of a specialised design setup enabling the films to be investigated under well-defined conditions. These findings prove oxidative dehydrogenation is responsible for the generation of alkenes on the surface of sulfated zirconia, thus they strongly concur with the initiation of the isomerisation pathway proceeding by this mechanism (Figure 8-1).[63,90] The presence of butene and sulfate reduction over sulfated zirconia are consistent with earlier reports from powder sulfated zirconia catalyst studies; including the detection of butene by

temperature programmed reaction spectroscopy;[63] allylic species by UV-vis spectroscopy,[15,74,286] olefinic species by DRIFTS,[278] sulfide by thermal desorption followed by ion chromatography[63] and XPS;[83] and hydrogen disulfate by online gas chromatography mass spectrometry[72] and DRIFTS.[278] This is however to the authors knowledge the first time both butene and sulfate reduction have been detected on the surface of sulfated zirconia after exposure at such relatively moderate conditions.

From the synthesis and investigation of powder sulfated zirconia catalysts it has been found, as previously proposed,[62,63] that disulfate groups are necessary for the formation of catalytically active sites on sulfated zirconia. However, no direct correlation between the concentration of such species and catalytic activity was observed, thus implying that further variable(s) need to be identified to fully understand the catalytic behaviour of sulfated zirconia. One such variable proposed is the presence of defect sites. The use of defect sensitive techniques, such as electron paramagnetic resonance spectroscopy, to study sulfated zirconia is currently ongoing within the department of Inorganic Chemistry at the Fritz Haber Institute and through external collaborations. It is believed that such studies, along with the identification of disulfate groups and their concentrations on sulfated zirconia as presented in this thesis, may yield information regarding parameters governing the skeletal alkane isomerisation activity of reactive sites on the catalyst generated by oxidative dehydrogenation.

The model systems investigated in this thesis have thus lead not only to an improved understanding of the surface sites on sulfated zirconia catalysts, but also of the initiation and reaction alkane isomerisation mechanisms.

9. References

[1] A. Huebner, M. Buchan and W. Martin, in Encyclopedia of Catalysis, ed. I. T. Horváth, E. Iglesia, M. T. Klein, J. A. Lercher, A. J. Russell and E. I. Stiefel, John Wiley & Sons, New York, 2003, Vol. 4, pp. 268-279.

[2] D'Ans Lax, *Taschenbuck für Chemiker und Physiker*, Band II Organische Verbindungen, 4. Auflage, Springer-Verlag, Berlin, 1983.

[3] G. A. Olah, G. K. Surya Prakash and J. Sommer, *Superacids*, John Wiley & Sons, New York, 1985, pp. 254-259

[4] C. N. Scatterfield, *Heterogeneous Catalysis in Practice*, McGraw-Hill, 1980.

[5] K. Tanabe and W. Hölderich, *Appl. Catal., A* ,1999, **181,** 399-434.

[6] R. A. Sheldon and R. S. Downing, *Appl. Catal,. A*, 1999, **189**, 163-183.

[7] C. Gosling, R. Rosin, P. Bullen, T. Shimizu and T. Imai, *Petroleum Technology Quarterly*, Winter 97/98, 55-59.

[8] P. J. Kuchar, R. D. Gillespie, C. D. Gosling, W. C. Martin, M. J. Cleveland and P. J. Bullen, *Hydrocarbon Eng.*, 1999, March, 50-57.

[9] G. C. Anderson, R. R. Rosin, M. A. Stine and M. J. Hunter, *2004 NPRA Annual Meeting*, San Antonio, TX, USA, March 21–23, 2004, paper AM-04-46.

[10] M. J. Hunter, *Proceedings of DGMK-Conference "Chances for Innovative Processes at the Interface between Refining and Petrochemistry"*, Berlin, October 9-11, 2002, p. 41-52.

[11] V. C. F. Holm and G. C. Bailey, *US Pat.*, 3 032 599, 1962.

[12] M. Hino, S. Kobayashi and K. Arata, *J. Am. Chem. Soc.*, 1979, **101,** 6439-6441.

[13] M. Hino and K. Arata, *J. Chem. Soc., Chem. Commun.*, 1980, 851-852.

[14] P. Nascimento, C. Akratapoulou, M. Oszagyan, G. Coudurier, C. Travers, J. F. Joly and J. C. Védrine, *Proceedings of the 10th International Congress on Catalysis*, July 19-24, 1992, Budapest, Hungary, *New Frontiers in Catalysis*, ed. L. Guczi, F. Solymosi, P. Tetényi, Elsevier, Amsterdam, 1993, pp. 1185.

[15] F. R. Chen, G. Coudurier, J. F. Joly and J. C. Védrine, *J. Catal.*, 1993, **143,** 616-626.

[16] M. G. Cutrufello, U. Diebold and R. D. Gonzalez, *Catal. Lett.*, 2005, **101,** 5-13.

[17] J. Luo and R. Stevens, *J. Am. Ceram. Soc.*, 1999, **82,** 1922-1924.

[18] M. A. Ecormier, K. Wilson and A. F. Lee, *J. Catal.,* 2003, **215**, 57-65.

[19] R. C. Garvie and M. F. Goss, *J. Mater. Sci.*, 1986, **21**, 1253-1257.

[20] R. C. Garvie, *J. Phys. Chem.*, 1965, **69**, 1238-1243.

[21] R. C. Garvie, *J. Phys. Chem.*, 1978, **82**, 218-224.

[22] A. Christensen and E. A. Carter, *Phys. Rev. B*, 1998, **58,** 8050-8064.

[23] C. Morterra, G. Poncelet, F. Pinna and M. Signoretto, *J. Catal.*, 1995, **157**, 109-123.

[24] W. Stichert, F. Schüth, S. Kuba and H. Knözinger, *J. Catal.*, 2001, **198**, 277-285.

[25] J. A. Moreno and G. Poncelet, *J. Catal.*, 2001, **203**, 453-465.

[26] X. Li, K. Nagaoka, R. Olindo and J. A. Lercher, *J. Catal.*, 2006, **238**, 39-45.

[27] X. Li, K. Nagaoka, L. J. Simon, J. A. Lercher, S. Wrabetz, F. C. Jentoft, C. Breitkopf, S. Matysik and H. Papp, *J. Catal.*, 2005, **230**, 214-225.

[28]F. C. Jentoft, *Oxo-Anion Modified Oxides*, in *Handbook of Heterogeneous Catalysis*, ed. G. Ertl, H. Knözinger, F. Schüth and J. Weitkamp, Wiley-VCh, 2nd edn., in press.

[29] P. Afanasiev, A. Thiollier, M. Breysse and J. L. Dubois, *Top. Catal.*, 1999, **8**, 147-160.

[30] www.Zrchem.com

[31] www.sigma-aldrich.com

[32] T. Riemer, D. Spielbauer, M. Hunger, G. A. H. Mekhemer and H. Knözigner, *J. Chem. Soc., Chem. Commun.*, 1994, **10**, 1181-1182.

[33] Z. Gao, Y. Xia, W. Hau and C. Miao, *Top. Catal.*, 1998, **6**, 101-106.

[34] M. Signoretto, M. A. Stefano, F. Pinna, S. Polizzi, C. Cerrato and C. Morterra, *Microporous Mesoporous Mater.*, 2005, **81**, 19-29.

[35] F. Garin, D. Andriamasinoro, A. Abdulsamad and J. Sommer, *J. Catal.*, 1991, **131**, 199-203.

[36] C. Y. Hsu, C. R. Heimbuch, C. T. Armes and B. C. Gates, *J. Chem. Soc., Chem. Comm.*, 1992, **22**, 1645-1646.

[37] X. Song and A. Sayari, *Catal. Rev. Sci. Eng.*, 1996, **38**, 329-412.

[38] J. B. Nicholas, J. F. Haw, L. W. Beck, T. R. Krawietz and D. B. Ferguson, *J. Am. Chem. Soc.*, 1994, **117**, 12350-12351.

[39] B. S. Umansky and K. Hall, *J. Catal.*, 1990, **124**, 97-108.

[40] L. M. Kustov, V. B. Kazansky, F. Figueras and D. Tichit, *J. Catal.*, 1994, **150**, 143-149.

[41] F. Babou, B. Bigot and P. Sautet, *J. Phys. Chem.*, 1993, **97**, 11501-11509.

[42] J. R. Sohn and H. W. Kim, *J. Mol. Catal.*, 1989, **52**, 361-374.

[43] T. Jin, M. Machida, T. Yamaguchi and K. Tanabe, *Inorg. Chem.*, 1984, **23**, 4396-4398.

[44] T. Yamaguchi, T. Jin and K. Tanabe, *J. Phys. Chem.*, 1986, **90**, 3148-3152.

[45] Y. Nagase, T. Jin, H. Hattori, T. Yamaguchi and K. Tanabe, *Bull. Chem. Soc. Jpn.*, 1985, **58**, 916-918.

[46] F. C. Jentoft, *Sulfated Zirconia Alkane Isomerisation Catalysts: A Treatise*, Thesis (Habilitationsschrift), Humboldt-Universität Berlin, 2004.

[47] M. Bensitel, O. Saur, J. C. Lavally and B. A. Morrow, *Mater. Chem. Phys.*, 1988, **19**, 147-156.

[48] C. Morterra, G. Cerrato and V. Bolis, *Catal. Today*, 1993, **17**, 505-515.

[49] K. Arata and M. Hino, *Mater. Chem. Phys.*, 1990, **26,** 213-237.

[50] T. Yamaguchi, *Appl. Catal., A*, 1990, **146**, 1-25.

[51] J. M. Parera, *Catal. Today*, 1992, **15**, 481-490.

[52] K. Arata, *Adv. Catal.*, 1990, **37**, 165-211.

[53] M. Signoretto, F. Pinna, G. Struckul, P. Chies, G. Cerrato, S. Di Ciero and C. Morterra, *J. Catal.*, 1997, **167**, 522-523.

[54] A. Clearfield, G. P. D. Serrette and A. H. Khazi-Syed, *Catal. Today*, 1994, **20,** 295-315.

[55] F. Babou, G. Coudurier and J. C. Vedrine, *J. Catal.*, 1995, **152**, 341-349.

[56] N. G. Connelly, T. Damhus, R. M. Hartshorn and A. T. Hutton, *Nomenclature of Inorganic Chemistry, IUPAC Recommendations 2005*, RSC Publishing, 2005.

[57] C. Morterra, G. Cerrato, F. Pinna and M. Signoretto, *J. Phys. Chem.*, 1994, **98**, 12373-12381.

[58] D. A. Ward and E. I. Ko., *J. Catal.*, 1994, **150**, 18-33.

[59] M. Waqif, J. Bachelier, O. Saur and J. C. Lavalley, *J. Mol. Catal.*, 1992, **72**, 127-138.

[60] V. V. Strelko, *Kinet. Catal.,* 2003, **44**, 834-839.

[61] V. Bolis, G. Magnacca, G. Cerrato and C. Morterra, *Langmuir*, 1997, **13**, 888-894.

[62] A. Hofmann and J. Sauer, *J. Phys. Chem. B*, 2004, **108**, 14652-14662.

[63] X. Li, K. Nagaoka, L. J. Simon, R. Olindo, J. A. Lercher, A. Hofmann and J. Sauer, *J. Am. Chem. Soc.*, 2005, **127**, 16159-16166.

[64] S. X. Song and R. A. Kydd, *J. Chem. Soc., Faraday Trans.*, 1998, **94**, 1333-1338.

[65] M. Risch and E. E. Wolf, *Appl. Catal., A*, 2001, **206**, 283-293.

[66] S. Y. Kim, J. G. Goodwin and D. Galloway, *Catal. Today*, 2000, **63**, 21-32.

[67] B. Li and R. D. Gonzalez, *Ind. Eng. Chem. Res.*, 1996, **35**, 3141-3148.

[68] H. K. Mishra and K. M. Parida, *Appl. Catal., A*, 2002, **224**, 179-189.

[69] C. R. Vera and J. M. Parera, *J. Catal.*, 1997, **166**, 254-262.

[70] Z. Hong, K. B. Fogash and J. A. Dumesic, *Catal. Today*, 1999, **51**, 269-288.

[71] C. R. Vera, C. L. Piech, K. Shimizu, C. A. Querini and J. M. Parera, *J. Catal.*, 1999, **187**, 39-49.

[72] F. T. T. Ng and N. Horvát, *Appl. Catal., A*, 1995, **123**, L197-L203.

[73] R. A. Comelli, C. R. Vera and J. M. Perera, *J. Catal.*, 1995, **151**, 96-101.

[74] D. Spielbauer, G. A. H. Mekhemer, E. Bosch and H. Knözinger, *Catal. Lett.*, 1996, **36**, 59-68.

[75] S. R. Vaudagna, R. A. Comelli, and N. S. Figoli, *Catal. Lett.*, 1997, **47**, 259-264.

[76] S. R. Vaudagna, R. A. Comelli, S. A. Canavese and N. S. Figoli, *J. Catal.*, 1997, **169**, 389-393.

[77] B. Li and R. D. Gonzalez, *Appl. Catal., A*, 1997, **165**, 291-300.

[78] K. B. Fogash, Z. Hong, J. M. Kobe and J. A. Dumesic, *Appl. Catal., A*, 1998, **172**, 107-116.

[79] H. Knözinger, *Top. Catal.*, 1998, **6**, 107-110.

[80] B. Li and R. D. Gonzalez, *Appl. Catal., A*, 1998, **174**, 109-119.

[81] B. Li and R. D. Gonzalez, *Catal. Today*, 1998, **46**, 55-67.

[82] R. Marcus, U. Diebold and R. D. Gonzalez, *Catal. Lett.*, 2003, **86**, 151-156.

[83] G. Resofski, M. Muhler, S. Sprenger, U. Wild and Z. Paál, *Appl. Catal., A*, 2003, **240**, 71-81.

[84] C. Li and P. C. Stair, *Catal. Lett.*, 1996, **36**, 119-123.

[85] J. Sommer, R. Jost and M. Hachoumy, *Catal. Today*, 1997, **38**, 309-319.

[86] T. K. Cheung and B. C. Gates, *Chem. Commun.*, 1996, 1937-1938.

[87] M. Marczewski, *J. Chem. Soc., Faraday Trans.,* 1986, **82**, 1687-1701.

[88] M. Marczewski, *Bull. Soc. Chim. Fr.*, 1986, 750-755.

[89] J. E. Tabora and R. J. Davis, *J. Am. Chem. Soc.,* 1996, **118,** 12240-12241.

[90] A. Ghenciu and D. Fărcaşiu, *Chem. Commun*., 1996, 169-170.

[91] D. Fărcaşiu, A. Ghenciu and J. Q. Li, *J. Catal.*, 1996, **158**, 116-127.

[92] V. Maurice, M. Salmeron and G. A. Somorjai, *Surf. Sci.*, 1990, **237**, 116-126.

[93] V. Adeeva, H. Y. Liu, B. Q. Xu and W. M. H. Sachtler, *Top. Catal.,* 1998, **6,** 61-76.

[94] H. Liu, V. Adeeva, G. D. Lei and W. M. H. Sachtler, *J. Mol. Catal. A: Chem.*, 1995, **100**, 35-48.

[95] S. Y. Kim, J. G. Goodwin and D. Fărcaşiu, *Appl. Catal.*, 2001, **207,** 281-286.

[96] T. Suzuki and T. Okuhara, *Chem. Lett.*, 2000, **5**, 470-471.

[97] H. Matsuhashi, H. Shibata, H. Nakamura and K. Arata, *Appl. Catal., A*, 1999, **187**, 99-106.

[98] J. A. Rodriquez and D. W. Goodman*, Surf. Sci. Rep.*, 1991, **14**, 1-107.

[99] J. Freund, H. Kuhlenbeck and V. Staemmler, *Rep. Prog. Phys.*, 1996, **59**, 283-347.

[100] P. L. J. Gunter, J. W. Niemantsverdriet, F. H. Ribiberteiro, G. A. Somorjai, *Catal. Rev. Sci. Eng.*, 1999, **39**, 77-168.

[101] J. W. Niemantsverdrit, A. F. P. Engelen, A. M. de Jong, W. Wieldraaijer and G. J. Kramer, *Appl. Surf. Sci.*, 1999, **144-145**, 366-374.

[102] Y. Sorek, M. Zevin, R. Reisfeld, T. Hurvits and S. Ruschin, *Chem. Mater.*, 1997, **9**, 670-676.

[103] C. W. Turner, *Am. Ceram. Soc. Bull.*, 1991, **70**, 1487-1490.

[104] M. Guglielmi, *J. Sol-Gel Sci. Tech.*, 1997, **8**, 443-449.

[105] G. C. Willis, G. B. Adams, and P. Van Rysselberghe, *Electrochim. Acta*, 1964, **9**, 79-91.

[106] M. S. El-Basiouny, A. A. Mazhar, F. El-Taib Heakal and M. A. Ameer, *J. Electroanal. Chem.*, 1983, **147**, 181-191.

[107] G. T.Rodgers, P. H. G. Draper and S. S. Wood, *Electrochim. Acta*, 1968, **13**, 251-261.

[108] P. Meisterjahn, H. W. Hoppe and J. W. Schultze, *J. Electroanal. Chem.*, 1987, **217**, 159-185.

[109] N. Khalil, A. Bowen and J. S. L. Leach, *Electrochim. Acta*, 1988, **33**, 1721-1727.

[110] E. M. Patrito and V. A. Macagno, *J. Electroanal. Chem.*, 1994, **375**, 203-211.

[111] A. S. Mogoda, M. M Hefny, S. A. Salih and H. E. El-Faiky, *Thin Solid Films*, 1994, **250**, 87-91.

[112] S. M. Abed El-Motaal, N. H. Hilal and W. A. Badaw, *Electrochim. Acta*, 1994, **39**, 2611-2617.

[113] A. Mamun, R. Schennach, J. R. Parga, M. Y. A. Mollah, M. A. Hossain and D. L. Cocke, *Electrochim. Acta*, 2001, **46**, 3343–3350.

[114] T. Pauporte and J. Finne, *J. Appl. Electrochem.*, 2006, **33**, 33–41.

[115] J. C. Banter, *J. Electrochem. Soc.*, 1967, **114**, 508-511.

[116] J. S. Leach and B. R. Pearson, *Electrochim. Acta*, 1984, **29**, 1271-1282.

[117] M. A. A. Rahim, A. A. A. Rahman and M. W. Khalil, *J. Appl. Electrochem.*, 1996, **26**, 1037-1043.

[118] H. Shin, M. Agarwel, M. R. De Guire and A. H. Heuer, *J. Am. Ceram. Soc.*, 1996, **79**, 1975-1978.

[119] M. Agarwal, M. R. De Guire and A. H. Heuer, *J. Am. Ceram. Soc.*, 1997, **80**, 2967-2981.

[120] H. Shin, M. Agarwel, M. R. De Guire and A. H. Heuer, *Acta Mater.*, 1998, **46**, 801-815.

[121] T. P. Niesen, M. R. De Guire, J. Bill, F. Aldinger, M. Rühle, A. Fischer, F. C. Jentoft and R. Schlögl, *J. Mater. Res.*, 1999, **14**, 2464-2475.

[122] A. Fischer, F. C. Jentoft, G. Weinberg, R. Schlögl, T. P. Niesen, J. Bill, F. Aldinger, M. R. De Guire and M. Rühle, *J. Mater. Res.*, 1999, **14**, 3725-3733.

[123] F. C. Jentoft, A. Fischer, G. Weinberg, U. Wild and R. Schlögl, *Stud. Surf. Sci. Catal.,* 2000, **130,** 209-214.

[124] A. Fischer, Doctorial Thesis, TU Berlin, 2001.

[125] A. D. Polli, T. Wagner, A. Fischer, G. Weinberg, F. C. Jentoft, R. Schlögl and M. Rühle, *Thin Solid Films,* 2000, **379,** 122-127.

[126] V. V. Roddatis, D. S. Su, F. C. Jentoft and R. Schlögl, *Philos. Mag. A.,* 2002, **82,** 2825-2839.

[127] V. V. Roddatis, D. S. Su, E. Beckmann, F. C. Jentoft, U. Braun, J. Kröhnert and R. Schlögl, *Surf. Coat. Technol.*, 2002, **151-152**, 63-66.

[128] H. Cölfen, H. Schnablegger, A. Fischer, F. C. Jentoft, G. Weinberg and R. Schlögl, *Langmuir,* 2002, **18,** 3500-3509.

[129] Y. Tang and M. R. De Gurie, *J. Mater. Chem.*, 2004, **14**, 1173-1179.

[130] J. Wang, S. Yang, X. Liu, S. Ren, F. Guan and M. Chen, *Appl. Surf. Sci.*, 2004, **221**, 272–280.

[131] J. Wang, X. Liu, S. Ren, F. Guan and S. Yang, *Tribology Lett.*, 2005, **18**, 429-436.

[132] G. Zhang, J. Y. Howe, D. W. Coffey, D. A. Blom, L. F. Allard and J. Cho, *Mater. Sci. Eng., C*, 2006, **26**, 1344–1350.

[133] A. P. Rizzato, C. V. Santilli and S. H. Pulcinelli, *J. Non-Cryst. Solids*, 1999, **247**, 158-163.

[134] J. M. Lin, M. C. Hsu and K. Z. Fung, *J. Power Sources*, 2006, **159**, 49–54.

[135] K. Meinel, A. Hofmann, S. Förster, R. Kulla, K. M. Schindler, H. Neddermeyer, J. Sauer and W. Widdra, *Phys. Chem. Chem. Phys.*, 2006, **8**, 1593-1600.

[136] B. C. Bunker, P. C. Rieke, B. J. Tarasevich, A. A. Campell, G. E. Fryxell, G. L. Graff, L. Song, J. Liu, J. W. Virden and G. L. McVay, *Science (Washington, D. C.)*, 1994, **264**, 48-55.

[137] S. Gorer and G. Hodes, *J. Phys. Chem.*, 1994, **98**, 5338-5346.

[138] F. C. Meldrum, J. Flath and W. Knoll, *Langmuir*, 1997, **13**, 2033-2049.

[139] C. W. Bigelow, D. L. Pickett and W. A. Zisman, *J. Colloid Interface Sci.*, 1946, **1**, 513-538.

[140] W. A. Zisman, *Adv. Chem. Ser.*, 1964, **43**, 1-51.

[141] J. D. Swalwn, D. L. Allura, J. D. Andrade, E. A. Chandross, S. Garoff, J. Israelachvili, T. J. McCarthy, R. Murray, R. F. Pease, J. F. Rabolt, K. J. Wynne and H. Yu, *Langmuir*, 1987, **3**, 932-950.

[142] A. Ulman, *Adv. Mater.*, 1990, **2**, 573-582.

[143] D. H. Charych and M. D. Bednarski, *MRS Bull.*, 1992, **17**, 61-66.

[144] A. Ulman, *An Introduction to Ultrathin Organic Films from Langmuir-Blodgett to Self Assembly*, Academic Press, New York, 1991.

[145] S. Ahrland, D. Karipides and B. Norén, *Acta Chem. Scand.*, 1963, **17**, 411-424.

[146] R. E. Connick and W. H. McVey, *J. Am. Chem. Soc.*, 1949, **71**, 3182-3191.

[147] E. Matijević, *Acc. Chem. Res.*, 1981, **14**, 22-29.

[148] A. Clearfield, *Rev. Pure Appl. Chem.*, 1964, **14**, 91-108.

[149] B. A. Lister and L. A. MacDonald, *J. Chem. Soc*., 1952, 4315-4330.

[150] R. Ruer, *Z. Anorg. Chem.*, 1904, **42**, 87-99.

[151] F. G. Baglin and D. Breger, *Inorg. Nucl. Chem. Lett.*, 1976, **12**, 173-177.

[152] O. Hauser, *Z. Anorg. Allg. Chem.*, 1905, **45**, 185-204.

[153] W. Kern, *J. Electrochem. Soc.*, 1990, **137**, 1887-1892.

[154] J. F. Moulder, W. F. Stickle, P. E. Sobol and K. D. Bomben, *Handbook of X-ray Photoelectron Spectroscopy*, Perkin Elmer Physical Electrons Division, 1992.

[155] C. D. Wagner, L. E. Davis, M. V. Zeller, J. A. Taylor, R. M. Raymond and L. H. Gale, *Surf. Interface Anal.*, 1981, **3**, 211–225.

[156] *Inorganic Crystal Structure Database (ICSD)*, http://icsd.fkf.mpg.de

[157] N. M. Rodriguez, P. E. Anderson, A. Wootsch, U. Wild, R. Schlögl, and Z. Páal, *J. Catal.*, 2001, **197**, 365-377.

[158] M. P. Seah and W. A. Dench, *Surf. Interf. Anal.*, 1979, **1**, 2-11.

[159] R. Srinivasan, R. A. Keogh, D. R. Milburn and B. H. Davis, *J. Catal.*, 1995, **153**, 123-130.

[160] J. Singer and D. T. Cromer, *Acta Cryst.*, 1959, **12**, 719-723.

[161] I. Molodetsky, A. Navrotsky, M. J. Paskowitz, V. J. Leppert and S. H. Risbud, *J. Non-Cryst. Solids*, 2000, **262**, 106-113.

[162] C. Breitkopf, H. Papp, X. Li, R. Olindo, J. A. Lercher, R. Lloyd, S. Wrabetz, F. C. Jentoft, K. Meinel, S. Förster, K. M. Schindler, H. Neddermeyer, W. Widdra, A. Hofmann and J. Sauer, *Phys. Chem. Chem. Phys.*, 2007, **9**, 3600-3618.

[163] H. Matsuhashi, H. Motoi and K. Arata, *Catal. Lett.*, 1994, **26**, 325-328.

[164] R. Srinivasan, R. A. Keogh, A. Ghenciu, D. Farcasiu and B. H. Davis, *J. Catal.*, 1996, **158**, 502–510.

[165] H. Suja, C. S. Deepa, K. Sreeja Rani and S. Sugunan, *Appl. Catal., A*, 2002, **230**, 233-243.

[166] R. W. Stevens, S. S. C. Chuang and B. H. Davis, *Appl. Catal.*, A, 2003, **252**, 57-74.

[167] R. W. Stevens, S. S. C. Chuang and B. H. Davis, *Thermochim. Acta*, 2003, **407**, 61–71.

[168] S. Furuta, H. Matsuhashi and K. Arata, *Appl. Catal., A*, 2004, **269**, 187–191.

[169] N. A. Comelli, E. N. Ponzi and M. I. Ponzi, *Chem. Eng. J.*, 2006, **117**, 93–99.

[170] S. T. Hussain, M. Mazhar, S. Gul, K. T. Chuang, and A. R. Sanger, *Bull. Korean Chem. Soc.*, 2006, **27**, 1844-1850.

[171] T. Okuhara, T. Nishimura, H. Watanabe and M. Misono, *J. Mol. Catal.*, 1992, **74**, 247-256.

[172] X. Song and A. Sayari, *Appl. Catal., A*, 1994, **110**, 121-136.

[173] A. Corma, V. Formes, M. I. Juan-Rajadell, J. M. Lopez Nieto, *Appl. Catal., A*, 1994, **116**, 151-163.

[174] A. Corma, M. I. Juan-Rajadell, J. M. Lopez-Nieto, A. Martinez and C. Marthez, *Appl. Catal., A*, 1994, **111**, 175-189.

[175] J. E. Tabora and R. J. Davis, *J. Chem. Soc. Faraday Trans.*, 1995, **91**, 1825-1833.

[176] M. A. Coelho, D. E. Resasco, E. C. Sikabwe and R. L. White, *Catal. Lett.*, 1995, **32**, 253-262.

[177] R. Barthos, F. Lonyi, J. Engelhardt and J. Valyon, *Top. Catal.*, 2000, **10**, 79–87.

[178] N. Katada, J. Endo, K. Notsu, N. Yasunobu, N. Naito and M. Niwa, *J. Phys. Chem. B*, 2000, **104**, 10321-10328.

[179] H. K. Mishra, A. K. Dalai, K. M. Parida and S. K. Bej, *Appl. Catal.*, A, 2001, **217**, 263-273.

[180] R. Barthos, F. Lonyi, G. Onyestyak and J. Valyon, *Solid State Ionics*, 2001, **141-142**, 253-258.

[181] A. Trunschke, J. Deutsch, D. Müller, H. Lieske, V. Quaschning and E. Kemnitz, *Catal. Lett.*, 2002, **83**, 271-279.

[182] R. Sakthivel, H. A. Prescott, J. Deutsch, H. Lieske and E. Kemnitz, *Appl. Catal., A*, 2003, **253**, 237–247.

[183] F. Omota, A. C. Dimian and A. Bliek, *Chem. Eng. Sci.*, 2003, **58**, 3175-3185.

[184] M. Niwa, Y. Habuta, K. Okumura and N. Katada, *Catal. Today*, 2003, **87**, 213–218.

[185] H. K. Mishra, A. K. Dalai, D. D. Das, K. M. Parida and N. C. Pradhan, *J. Colloid Interface Sci.*, 2004, **272**, 378–383.

[186] N. Li, A. Wang, X. Wang, M. Zheng, R. Cheng and T. Zhang, *Appl. Catal., B*, 2004, **48**, 259–265.

[187] G. D. Yadav and A. D. Murkute, *J. Catal.*, 2004, **224**, 218–223.

[188] N. Li, A. Wang, M. Zheng, X. Wang, R. Cheng and T. Zhang, *J. Catal.*, 2004, **225**, 307–315.

[189] N. Katada and M. Niwa, *Catal. Surv. Asia*, 2004, **8**, 161-170.

[190] W. Wang, J. H. Wang, C. L. Chen, N. P. Xu and C. Y. Mou, *Catal. Today*, 2004, **97**, 307–313.

[191] S. Parambadath, M. Chidambaram and A. P. Singh, *Catal. Today*, 2004, **97**, 233–240.

[192] B. M. Reddy, P. M. Sreekanth and V. R. Reddy, *J. Mol. Catal. A:Chem.*, 2005, **225**, 71–78.

[193] B. M. Reddy, P. M. Sreekanth and P. Lakshmanan, *J. Mol. Catal. A:Chem*, 2005, **237**, 93–100.

[194] K. Föttinger, E. Halwax and H. Vinek, *Appl. Catal., A*, 2006, **301**, 115–122.

[195] A. V. Ivanov, S. V. Lysenko, S. V. Baranova, A. V. Sungurov, T. N. Zangelov and E. A. Karakhanov, *Microporous Mesoporous Mater.*, 2006, **91**, 254–260.

[196] W. H. Chen, H. H. Ko, A. Sakthivel, S. J. Huang, S. H. Liu, A. Y. Lo, T. C. Tsai and S. B. Liu, *Catal. Today*, 2006, **116**, 111–120.

[197] C. H. Lin and C. Y. Hsu, *J. Chem. Soc., Chem. Commun.*, 1992, 1479-1480.

[198] A. Jatia, C. Chang, J. D. MacLeod, T. Okubo and M. E. Davis, *Catal. Lett.*, 1993, **25**, 21-28.

[199] K. T. Wan, C. B. Khouw, and M. E. Davis, *J. Catal.*, 1996, **158**, 311–326.

[200] T. A. Peters, N. E. Benes, A. Holmen and J. T. F. Keurentjes, *Appl. Catal., A*, 2006, **297**, 182–188.

[201] D. R. Milburn, K. Saito, R. A. Keogh and B. H. Davis, *Appl. Catal., A*, 2001, **215**, 191-197.

[202] A. Adeeva, J. W. de Hann, J. Jänchen, G. D. Lei, V. Schünemann, L. M. van de Ven, W. M. H. Sachtler and R. A. van Santen, *J. Catal.*, 1995, **151**, 364-372.

[203] N. Li, A. Wang, Z. Liu, X. Wang, M. Zheng, Y. Huang and T. Zhang, *Appl. Catal., B*, 2006, **62**, 292–298.

[204] E. C. Sikabwe and R. L. White, *Catal. Lett.*, 1997, **44**, 177-183.

[205] H. Matsuhashi and K. Arata, *Catal. Surv. Asia*, 2006, **10**, 1-7.

[206] T. Shishido and H. Hattori, *Appl. Catal., A*, 1996, **146**, 157-164.

[207] G. K. Chuah, S. Jaenicke and T. H. Xu, *Surf. Interface Anal.*, 1999, **28**, 131-134.

[208] C. Su, J. Li, D. He, Z. Cheng and Q. Zhu, *Appl. Catal., A*, 2000, **202**, 81-89.

[209] J. M. Dominguez, J. L. Hernandez and G. Sandoval, *Appl. Catal., A*, 2000, **197**, 119-130.

[210] K. Pokrovski, K. T. Jung, and A. T. Bell, *Langmuir*, 2001, **17**, 4297-4303.

[211] D. He, Y. Ding, H. Yin, T. Wang, H. Luo and C. Li, *Catal. Lett.*, 2002, **84**, 89-93.

[212] W. Weiss, M. Ritter, D. Zscherpel, M. Swoboda and R. Schlögl, *J. Vac. Sci. Technol. A*, 1998, **16**, 21-29.

[213] http://webbook.nist.gov/

[214] P. Stoltze, *Prog. Surf. Sci.*, 2000, **65**, 65-150.

[215] W. A. Brown, R. Kose and D. A. King, *Chem Rev.*, 1998, **98**, 797-832.

[216] W. Ranke and Y. Joseph, *Phys. Chem. Chem. Phys.*, 2002, **4**, 2483–2498.

[217] K. Christmann, *Introduction to Surface Physical Chemistry*, Steinkopff Verlag, Darmstadt, 1991.

[218] W. Weiss and W. Ranke, *Prog. Surf. Sci.*, 2002, **70**, 1-151.

[219] S. Fölsch, A. Stock and M. Henzler, *Surf. Sci*., 1992, **264**, 65-72.

[220] M. Henzler, A. Stock and M. Böl, in *Adsorption on Ordered Surfaces of Ionic Solids and Thin Films*, ed. E. Umbach and H. J. Freund, Springer, Berlin, 1993, vol. 33., pp. 15-23.

[221] W. Ranke, *Surf. Sci.*, 1995, **342**, 281-292.

[222] W. Ranke and W. Weiss, *Surf. Sci.*, 1998, **414**, 236-253.

[223] W. Ranke and W. Weiss, *Surf. Sci.*, 2000, **465**, 317-330.

[224] Y. Joseph, W. Ranke and W. Weiss, *J. Phys. Chem. B*, 2000, **104**, 3224-3236.

[225] M. R. González, K. B. Fogash, J. M. Kobe and J. A. Dumesic, *Catal. Today*, 1997, **33**, 303-312.

[226] R. C. Weast, *Handbook of Chemistry and Physics*, 58th edn., CRC Press, Cleveland, 1977.

[227] C. Breitkopf, *J. Mol. Catal. A: Chem.*, 2005, **226**, 269–278.

[228] X. Li, K. Nagaoka, L. J. Simon, R. Olindo and J. A. Lercher, *J. Catal.*, 2005, **232**, 456-466.

[229] P. J. Timans, *J. Appl. Phys.*, 1993, **74**, 6353-6364.

[230] P. Kramer and L.J. van Ruyven, *Appl. Phys. Lett.*, 1972, **20**, 420-422.

[231] M. H. Hecht, *Phys. Rev. B*, 1990, **41**, 7918-7921.

[232] S. Chang, I. M. Vitomirov, L. J. Brillson, D. F. Rioux, P. D. Kirchner, G. D. Pettit, J.M. Woodall and M. H. Hecht, *Phys. Rev. B*, 1990, **41**, 12299-12302.

[233] K. Kimura, S. Katsumata, Y. Achiba, T. Yamazaki, S. Iwata, *Handbook of He I Photoelectron Spectra of Fundamental Organic Molecules*, Japan Scientific Societies Press, Tokyo and Halsted Press, New York, 1981.

[234] T. Arnold, S. Channa, S. M. Clarke, R. E. Cook and J. Z. Larese, *Phys. Rev. B*, 2006, **74**, 085421.

[235] D. Briggs and T. Grant, *Surface Analysis by Auger and X-ray Photoelectron Spectroscopy*, IM Publications, West Sussex and Surface Spectra Limited, Manchester, 2003.

[236] L. Sanche, *Nucl. Instrum. Methods Phys. Res., Sect. B*, 2003, **208**, 4-10.

[237] S. E. Hoory and J. M. Prausnitz, *Trans. Faraday Soc.*, 1967, **63**, 455-460.

[238] G. C. Chirnside and C. G. Pope, *J. Phys. Chem.*, 1964, **68**, 2377-2379.

[239] S. Ross, J. K. Salens and J. Olivier, *J Phys. Chem.*, 1962, **66**, 696-700.

[240] Z. Wu, S. N. Ehrlich, B. Matthies, K. W. Herwig, P. Dai, U. G. Volkmann, F. Y. Hansen and H. Taub, *Chem. Phys. Lett.*, 2001, **348**, 168-174.

[241] J. M. Hilding and E. A. Grulke, *J. Phys. Chem. B*, 2004, **108**, 13688-13695.

[242] S. Wrabetz and F. C. Jentoft, unpublished work.

[243] D. Briggs and M. P. Seah, *Practical Surface Analysis*, John Wiley and Sons, Chichester, 2nd edn., 1990, vol. 1, pp. 168-173 and 244-248.

[244] B. S. Klose, Doctorial thesis, TU Berlin, 2005.

[245] D. R. Milburn, R. A. Keogh, R. Srinivasan and B. H. Davis, *Appl. Catal., A*, 1996, **147**, 109-125.

[246] S. Ardizzone, M. G. Cattania and P. Lugo, *Electrochim. Acta*, 1994, **39**, 1509-1517.

[247] K. Ebitani, J. Konishi, T. Tanaka and H. Hattori, *J. Catal.*, 1992, **135**, 60-67.

[248] J. M. Manoli, C. Potvin, M. Muhler, U. Wild, G. Resofszki, T. Buchholz and Z. Paál, *J. Catal.*, 1998, **178**, 338-351.

[249] C. Morant, J. M. Sanz, L. Galán, L. Soriano and F. Rueda, *Surf. Sci.*, 1989, **218**, 331-345.

[250] Z. Paál, U. Wild, M. Muhler, J.-M. Manoli, C. Potvin, T. Buchholz, S. Sprenger and G. Resofszki, *Appl. Catal., A*, 1999, **188**, 257-266.

[251] M. D. Appay, J. M. Manoli, C. Potvin, M. Muhler, U. Wild, O. Poznyakova and Z. Paál, *J. Catal.*, 2004, **222**, 419-428.

[252] S. Chang and R. Doong, *Chem. Mater.*, 2005, **17**, 4837-4844.

[253] H. Bluhm, M. Hävecker, A. Knop-Gericke, E. Kleimenov, R. Schlögl, D. Teschner, V. I. Bukhtiyarov, D. F. Ogletree and M. Salmeron, *J. Phys. Chem. B,* 2004, **108**, 14340-14347.

[254] G. Tzolova-Müller and F. C. Jentoft, unpublished results.

[255] J. J. Yeh and I. Lindau, *Atomic and Nuclear Data Tables*, 1985, **32**, 1-155.

[256] P. E. Batson, *Phys. Rev. B: Condens. Matter,* 1993, **48**, 2608-2610.

[257] J. Stöhr, *NEXAFS Spectroscopy*, Springer, Berlin, 1992.

[258] M. P. Seah and S. J. Spencer, *Surf. Interface Anal.*, 2002, **33**, 640–652.

[259] A. P. Hitchcock and I. Ishii, *J. Electron Spectrosc. Relat. Phenom.*, 1987, **42**, 11–26.

[260] A. P. Hitchcock, S. Beaulieu, T. Steel, J. Stöhr and F. Stette, *J. Chem. Phys.*, 1984, **80**, 3927–3935.

[261] G. Comelli, J. Stöhr, C. J. Robinson and W. Jark, *Phys. Rev. B: Condens. Matter*, 1988, **38**, 7511–7519.

[262] A. P. Hitchcock and D. C. Mancini, *J. Electron Spectrosc.*, 1994, **67**, 1-132.

[263] O. Guise, H. Marbach, J. Levy, J. Ahner and J. T. Yates, *Surf. Sci.*, 2004, **571**, 128-138.

[264] G. Centi, F. Cavani and F. Trifirò, *Selective Oxidation by Heterogeneous Catalysis*, Kluwer Academic/Plenum Publishers, New York, 2001, pp. 446-454.

[265] L. Wang, Y. Tian, H. Ding and J. Li, *Eur. Polym. J.*, 2006, **42**, 2921–2930.

[266] X. Wallart, C. H. de Villeneuve and P. Allongue, *J. Am. Chem. Soc.*, 2005, **127**, 7871-7878.

[267] H. Jensen, A. Soloviev, Z. Lib and E. G. Søgaard, *Appl. Surf. Sci.*, 2005, **246**, 239–249.

[268] V. van Elsbergen, C. Weijtens and J. Zaumseil, *Appl. Surf. Sci.*, 2004, **234**, 120–125.

[269] N. Saito, S. H. Lee, N. Maeda, R. Ohta, H. Sugimura and O. Takai, *J. Vac. Sci. Technol. A*, 2004, **22**, 1425-1427.

[270] R. Tomita, S. Urano and S. Kohiki, *J. Polym. Sci., Part A: Polym. Chem.*, 2002, **40**, 2917–2926.

[271] M. Atreya, S. Li, E. T. Kang, K. G. Neoh, Z. H. Ma and K. L. Tan, *J. Vac. Sci. Technol. A*, 1999, **17**, 853-861.

[272] S. Affrossman and S. M. MacDonald, *Langmuir*, 1996, **12**, 2090-2095.

[273] J. Silvestre-Albero, M. Borasio, G. Rupprechter and H. J. Freund, *Catal. Commun.*, 2007, **8**, 292-298.

[274] G. Beamson and D. Briggs, *High Resolution XPS of Organic Polymers*, *The Scienta ESCA300 Database*, Wiley, Chichester, 1992.

[275] X. Wang and M. Lieberman, *Langmuir*, 2003, **19**, 7346-7353.

[276] T. Ishida, N. Choi, W. Mizutani, H. Tokumoto, I. Kojima, H. Azehara, H. Hokari, U. Akiba and M. Fujihira, *Langmuir*, 1999, **15**, 6799-6806.

[277] C. D. Wagner, A. V. Naumkin, A. Kraut-Vass, J. W. Allison, C. J. Powell and J. R. Rumble, *NIST X-ray Photoelectron Spectroscopy Database, NIST Standard Reference Database 20*, version 3.4 (Web Version), 2006, http://srdata.nist.gov/xps/

[278] B. S. Klose, F. C. Jentoft, R. Schlögl, I. R. Subbotina and V. B. Kazansky, *Langmuir*, 2005, **21**, 10564-10572.

[279] E. Kristensen, PhD dissertation, Uppsla University, 1996.

[280] M. Wirde, U. Gelius, T. Dunbar and D. L. Allara, *Nucl. Instrum. Methods Phys. Res., Sect. B*, 1997, **131**, 245-251.

[281] K. Bandyopadhyay, K. Vijayamohanan, M. Venkataramanan and T. Pradeep, *Langmuir*, 1999, **15**, 5314-5322.

[282] I. Kartio, K. Laajalehto and E. Suoninen, *Colloids Surf., A,* 1999, **154**, 97–101.

[283] K. Heister, M. Zharnikov, M. Grunze, L. S. O. Johansson and A. Ulman, *Langmuir*, 2001, **17**, 8-11.

[284] B. S. Klose, F. C. Jentoft and R. Schlögl, *J. Catal.*, 2005, **233**, 68-80.

[285] C. D. Wagner, D. A. Zatko and R. H. Raymond, *Anal. Chem.*, 1980, **52**, 1445.

[286] R. Ahmad, J. Melsheimer, F. C. Jentoft and R. Schlögl, *J. Catal.*, 2003, **218**, 365-374.

[287] P. L. J. Gunter, J. W. Niemantsverdriet, F. H. Riberio and G. A. Somorjai, *Catal. Rev.-Sci. Eng.*, 1997, **39**, 77-168.

[288] C. T. Campbell, *Adv. Catal.*, 1989, **36**, 1-54.

[289] O. R. Kahn, E. E. Petersen and G. A. Somorjai, *J. Catal.*, 1974, **34**, 294-306.

[290] E. W. Kuipers, I. H. Vinkenburg and H. Oosterbeek, *J. Catal.*, 1995, **152**, 137-146.

[291] X. Xu and D. W. Goodman, *Appl. Phys. Lett.*, 1992, **61**, 774-776.

[292] S. Ladas, H. Poppa and M. Boudart, *Surf. Sci.*, 1981, **102**, 151-171.

[293] A. Baffa, C. Lin, A. T. Bell and G. A. Somorjai, *J. Catal.*, 1994, **149**, 149-158.

[294] C. T. Campbell and M. T. Paffett, *Surf. Sci.*, 1984, **139**, 396-416.

[295] D. W. Blakely, E. I. Kozak, B. A. Sexton and G. A. Somorjai, *J. Vac. Sci. Technol.*, 1976, **13**, 1091-1096.

[296] D. W. Goodman, R. D. Kelley, T. E. Madey and J. T. Yates, *J. Catal.*, 1980, **63**, 226-234.

[297] H. J. Krebs, H. P. Bonzel and G. Gafner, *Surf. Sci.*, 1979, **88**, 269-283.

[298] C. T. Campbell and K. A. Daube, *J. Catal.*, 1987, **104**, 109-119.

[299] X. Li, Doctorial Thesis, Technischen Universität München, 2004.

[300] C. Morterra, G. Cerrato, C. Emanuel and V. Bolis, *J. Catal.*, 1993, **142**, 249-367.

[301] C. Morterra, V. Bolis, G. Cerrato and G. Magnacca, *Surf. Sci.*, 1994, **307-309**, 1206-1213.

[302] E. Escalona Platero, M. Peñarroya Mentruit, C. Otero Areán and A. Zecchina, *J. Catal.*, 1996, **162**, 268-276.

[303] Y. Xia, W. Hua and Z. Gao, *Appl. Catal., A.*, 1999, **185**, 293-300.

[304] R. L. Marcus, R. D. Gonzalez, E. L. Kugler and A. Auroux, *Chem. Eng. Comm.*, 2003, **190**, 1601-1619.

[305] K. Biró, F. Figueras and S. Békássy, *Appl. Catal., A*, 2002, **229**, 235-243.

[306] D. Prasetyoko, Z. Ramli, S. Endud and H. Nur, *J. Mol. Catal. A*, 2005, **241**, 118-125.

[307] P. Afanasiev, C. Geantet and M. Breysse, *J. Mater. Chem.*, 1994, **4**, 1653-1657.

[308] A. S. Dias, S. Lima, M. Pillinger and A. A. Valente, *Catal. Lett.*, 2007, **114**, 151-160.

[309] A. V. Lavrenov, E. V. Perelevskii, V. P. Finevich, V. I. Zaikovskii, E. A. Paukshtis, V. K. Duplyakin and S. S. Bal'zhinimaev, *Russ. J. Appl. Chem.*, 2003, **76**, 550-557.

[310] H. K. Mishra, A. K Dalai, D. D. Das, K. M Parida and N. C. Pradhan, *J. Colloid Interface Sci.*, 2004, **272**, 378-383.

[311] A. Hahn, T. Ressler, R. E. Jentoft and F. C. Jentoft, *Chem. Commun.*, 2001, 537-538.

[312] A. M. C. Davies, *Spectroscopy Europe*, 2007, **19**, 32-33.

[313] B.S. Klose, F.C. Jentoft, R. Schlögl, A. Hofmann and J. Sauer, XXXIX Jahrestreffen Deutscher Katalytiker, Weimar, 15-17 March, 2006.

[314] R. Srinivasan and B. H. Davis, *J. Colloid Interface Sci.*, 1993, **156**, 400-405.

[315] M. Sorrentino, L. Steinbrecher and F. Hazel, *J. Colloid Interface. Sci.*, 1969, **31**, 307-316.

[316] A. Keshavaraja, N. E. Jacob and A. V. Ramaswamy, *Thermochim. Acta*, 1995, **254**, 267-275.

[317] J. Livage, K. Doi and C. Mazières, *J. Am. Ceram. Soc.*, 1968, **51**, 349-353.

[318] A. Hahn, R. E. Jentoft, T. Ressler, G. Weinberg, R. Schlögl and F. C. Jentoft, *J. Catal.*, 2005, **236**, 324-334.

[319] S. Chokkaram, R. Sirnivasan, D. R. Milburn and B. H. Davis, *J. Colloid. Interface Sci.*, 1994, **165**, 160-168.

[320] A. F. Holleman and E. Wiberg, *Lehrbuch der Anorganischen Chemie*, Walter de Gruyter, Berlin, New York, 1985 pp. 519-524.

[321] *Gmelins Handbuch der anorganischen Chemie, S 9, B2: Schwefelsauerstoffsaeuren*, Verlag Chemie, 1960, pp. 822-825 and 874-875.